This dissertation has been microfilmed exactly as received

64-11,760

MILLER, Frank Lee, 1930-
EXCITATION OF HELIUM ATOMS BY ELECTRON IMPACT.

The University of Oklahoma, Ph.D., 1964
Physics, electronics and electricity

University Microfilms, Inc., Ann Arbor, Michigan

Downloaded from SHAREOK. Persistent Handle URL: https://hdl.handle.net/11244/1784

THE UNIVERSITY OF OKLAHOMA

GRADUATE COLLEGE

EXCITATION OF HELIUM ATOMS BY ELECTRON IMPACT

A DISSERTATION

SUBMITTED TO THE GRADUATE FACULTY

in partial fulfillment of the requirements for the

degree of

DOCTOR OF PHILOSPHY

BY

FRANK LEE MILLER

Norman, Oklahoma

1964

EXCITATION OF HELIUM ATOMS BY ELECTRON IMPACT

APPROVED BY

Chun C. Lin

Robert M. St. John

J. Rud Nielsen

R. F. Fowler

Arthur Bernhart

DISSERTATION COMMITTEE

ACKNOWLEDGEMENTS

The author wishes to express his appreciation to the people whose aid greatly facilitated this work: Dr. Chun C. Lin who suggested the problem and whose most helpful direction furthered its completion; Dr. Robert M. St. John who supervised the data collection and processing; Mr. R. J. Anderson, Mr. R. W. Kassik, and Mr. R. Sims who helped with the experimental work; and Mr. T. W. Nee who assisted in processing the data. Special thanks are given to the author's wife, Jackie, who has waited patiently for the "unveiling" of these words and who helped with the preparation of this manuscript.

TABLE OF CONTENTS

Page

LIST OF TABLES v

LIST OF ILLUSTRATIONS vii

Chapter

I. INTRODUCTION 1

II. MEASUREMENT OF APPARENT CROSS SECTIONS 8

III. CALCULATION OF ABSOLUTE EXCITATION CROSS SECTIONS 28

IV. TRANSFER OF EXCITATION 69

V. SECONDARY PEAKS IN CERTAIN EXCITATION FUNCTIONS AT HIGH PRESSURE 75

VI. COMPARISON WITH OTHER EXPERIMENTAL WORK 83

VII. COMPARISON WITH THEORY 91

VIII. CONCLUSIONS 100

LIST OF REFERENCES 102

LIST OF TABLES

Table		Page
I.	Peak Apparent Cross Sections	26
II.	Polarization Corrections and Corrected Apparent Cross Sections	27
III.	Peak Apparent and Actual Cross Sections and Electron Energies	32
IV.	3^1S Excitation Function Data	33
V.	4^1S Excitation Function Data	34
VI.	5^1S Excitation Function Data	35
VII.	6^1S Excitation Function Data	36
VIII.	3^1P Excitation Function Data	37
IX.	4^1P Excitation Function Data	38
X.	3^1D Excitation Function Data	39
XI.	4^1D Excitation Function Data	40
XII.	5^1D Excitation Function Data	41
XIII.	6^1D Excitation Function Data	42
XIV.	3^3S Excitation Function Data	43
XV.	4^3S Excitation Function Data	44
XVI.	5^3S Excitation Function Data	45
XVII.	3^3P Excitation Function Data	46
XVIII.	3^3D Excitation Function Data	47
XIX.	4^3D Excitation Function Data	48
XX.	5^3D Excitation Function Data	49

Table		Page
XXI.	6^3D Excitation Function Data	50
XXII.	Measured and Calculated 3^3D Population Rates	73
XXIII.	Comparison of Experimental Apparent Cross Sections	84
XXIV.	Shape Comparison of Experimental Apparent Excitation Functions	88
XXV.	Shape Comparison of Experimental Apparent Excitation Functions	89
XXVI.	Comparison of Observed and Calculated Cross Sections	92

LIST OF ILLUSTRATIONS

Figure		Page
1.	Physical Arrangement of the Detection System.....	10
2.	Planck's Law and Linear Approximation.....	14
3.	Monochromator Relative Transmissivity.....	15
4.	Standard Lamp Optical System.....	17
5.	$I_{PM}(cc)/Ip$ vs log p for 5016A (3^1P--2^1S).....	21
6.	$I_{PM}(cc)/Ip$ vs log p for 3965A (4^1P--2^1S).....	22
7.	$I_{PM}(cc)/Ip$ vs log p for 3889A (3^3P--2^3S).....	23
8.	Eighteen Apparent Excitation Functions.....	25
9.	$Q'(3^1S)$ and $Q(3^1S)$ vs Electron Energy.....	51
10.	$Q'(4^1S)$ and $Q(4^1S)$ vs Electron Energy.....	52
11.	$Q'(5^1S)$ and $Q(5^1S)$ vs Electron Energy.....	53
12.	$Q'(6^1S)$ and $Q(6^1S)$ vs Electron Energy.....	54
13.	$Q'(3^1P)$ and $Q(3^1P)$ vs Electron Energy.....	55
14.	$Q'(4^1P)$ and $Q(4^1P)$ vs Electron Energy.....	56
15.	$Q'(3^1D)$ and $Q(3^1D)$ vs Electron Energy.....	57
16.	$Q'(4^1D)$ and $Q(4^1D)$ vs Electron Energy.....	58
17.	$Q'(5^1D)$ and $Q(5^1D)$ vs Electron Energy.....	59
18.	$Q'(6^1D)$ and $Q(6^1D)$ vs Electron Energy.....	60
19.	$Q'(3^3S)$ and $Q(3^3S)$ vs Electron Energy.....	61
20.	$Q'(4^3S)$ and $Q(4^3S)$ vs Electron Energy.....	62
21.	$Q'(5^3S)$ and $Q(5^3S)$ vs Electron Energy.....	63
22.	$Q'(3^3P)$ and $Q(3^3P)$ vs Electron Energy.....	64

Figure Page

23. $Q'(3^3D)$ and $Q(3^3D)$ vs Electron Energy..... 65

24. $Q'(4^3D)$ and $Q(4^3D)$ vs Electron Energy..... 66

25. $Q'(5^3D)$ and $Q(5^3D)$ vs Electron Energy..... 67

26. $Q'(6^3D)$ and $Q(6^3D)$ vs Electron Energy..... 68

27. 3^3D Excitation Function at Various Pressures..... 70

28. Measured and Calculated 3^3D Population Rate..... 74

29. 3^3P Excitation Function at Various Pressures..... 76

30. 4^1S Excitation Function at Various Pressures..... 77

31. 4^3S Excitation Function at Various Pressures..... 78

32. 3^3P Excitation Function at Various Pressures..... 82

33. Experimental and Theoretical $Q(3^1S)$ vs Electron Energy..... 94

34. Experimental and Theoretical $Q(3^1P)$ and $Q(4^1P)$ vs Electron Energy..... 95

EXCITATION OF HELIUM ATOMS BY ELECTRON IMPACT

CHAPTER I

INTRODUCTION

If an atomic gas is bombarded with a collimated beam of monoenergetic electrons, some of the atoms are excited to various higher energy states. This is evidenced by the emission of radiation characteristic of those states as they undergo transitions to lower states. The description of the interaction of electrons with the atoms can be made quantitative by means of the concept of cross sections. If the gas at a given pressure is exposed to the action of electrons, the rate at which any particular reaction (such as atomic excitation) occurs per unit volume is proportional to the number of electrons per unit area per unit time impinging on the gas times the number of atoms per unit volume. The proportionality constant is called the cross section. In other words the cross section for a specified reaction is defined as the average number of individual processes occurring per target atom with an incident beam of one electron per unit area. The cross section for a given reaction is a property of the target atom, of the incident electron, and their relative velocity. The probability of an atom being excited to a particular state is proportional to the electron excitation cross section for that state.

Such a cross section expressed as a function of electron energy is called the electron excitation function.

A particular excited state (jth state) of an atom may be populated and depopulated in many ways. It may be populated by electron impact with a ground state atom (direct excitation), transitions of atoms from higher excited states to the jth state (cascading), collision of an excited atom with a ground state atom (transfer gain), electron impact with an excited atom (collision of the second kind), collision of two excited atoms, and collision with an impurity atom. Depopulation of an excited state may occur by spontaneous transition to lower excited states (radiative loss), collision with a ground state atom (transfer loss), collision with the walls of the chamber, electron impact (collision of the second kind), collision with an excited atom, and collision with an impurity atom.

For this experiment helium was selected as the atomic gas. The advantages of helium are several. It is readily obtainable in a relatively pure form. It is a monatomic gas thereby avoiding considertions of molecular energy levels. The chemical inertness of helium allows a heated filament to be used in producing an electron beam. The relatively simple atomic structure results in the discrete emission spectrum being composed of wavelengths separated sufficiently that an extremely high decree of spectroscopic resolution is not vital. In

addition, theoretical calculations have been made of the excitation functions of helium so that experimental results can be compared with theory.

If the purest helium obtainable is used in a collision chamber that has previously been evacuated to a pressure of 10^{-6} mm of mercury or less, the impurity concentration will be sufficiently low that the contributions to both population and depopulation by collisions with impurity atoms are negligible. The short lifetimes of the excited states and their small excitation cross sections result in excited state populations that are negligible compared to ground state populations. As a result the contribution of collisions of the second kind and collisions between excited atoms to population and depopulation are negligible. With the exception of the metastable states of helium (2^1S and 2^3S), for which this is the primary method of depopulation, collisions with the walls make a negligible contribution to depopulation at low pressures.

Thus, the steady state equation in which population rate per unit volume equals depopulation rate per unit volume may be written as:

Direct excitation rate + Cascading rate + Transfer gain rate =

Radiation loss rate + Transfer loss rate

One additional method of population can play an important role. Light emitted by helium atoms undergoing spontaneous transitions from

^1P states to the 1^1S ground state may be absorbed by other ground state atoms before it escapes from the collision chamber. This phenomenon is known as imprisonment of resonance radiation. It has the overall effect of reducing the rate at which ^1P states are depopulated. Imprisonment phenomena can be handled in the analysis of data either by modifying the transition probabilities per unit time [1] or by operating at pressures below which imprisonment is negligible (approximately 5×10^{-4}mm).

Several authors have reported theoretical and experimental investigations of helium excitation functions. [1-11] A lack of agreement between theoretical and experimental excitation functions and the paucity of data available evidences a need for improved information about these functions and the processes involved.

In the past several years work has been done on excitation functions at the University of Oklahoma. The experimental system which has been developed to measure excitation functions consists of three basic parts: the collision chamber, [2] the detection system, and the data processing and recording system. [12] The collision chamber is contained in a 65 mm pyrex cylinder which is connected at each end to an oil diffusion pump and a mechanical fore pump. The vacuum system contains an ionization gage and a McLeod gage for measuring the pressure in the system, and a dosing system for introducing varying amounts of gas. The

fact that the collision chamber container can be evacuated at either end facilitates removal of impurities from the system through a combination of pumping and flushing out with helium.

The collision chamber section consists of a hollow cylindrical cathode 3 mm in diameter with one end made of emitting material. Electrons emitted from the cathode are accelerated and focused by a system of accelerating and collimating electrodes. The result is a monenergetic beam of electrons (of any chosen energy between 0 and 500 eV) 2 mm in diameter which passes through the collision chamber proper to a collecting electrode. The collision chamber itself is a metal cylinder with a hole in one end to admit the electron beam. The other end consists of a fine wire screen to allow electrons to pass through to the collecting electrode. In one side there is a small window to permit viewing of the light emitted by excited atoms in the path of the electron beam. The collision chamber constitutes a Faraday cage. In this field free region the electrons suffer energy losses only through the process of atomic collision.

The detection system consists basically of a Jarrell-Ash 1/2 meter monochromator with Ebert mounting and a photomultiplier tube. A lens focuses a portion of the light from a specific volume of the collision chamber on the entrance slit of the monochromator. Light from the exit slit of the monochromator is directed and focused on the photomultiplier

cathode by a prism and a lens. Reduction of noise and stray light signals is accomplished by square wave modulation either by mechanical chopping or by applying a square wave potential to the accelerating electrode.

The data processing and recording system has been described in detail by St. John et al.[12] In this system a tuned amplifier converts the square wave output of the photomultiplier tube into a sinusoidal signal which is then rectified by a phase sensitive detector. The dc voltage output of this detector is then fed into an analog divider where it is divided by a signal proportional to the electron beam current. This quotient is applied to the vertical deflection plates of an oscilloscope. The electron accelerating voltage is applied to the horizontal deflection plates of the oscilloscope. The trace thus produced represents a plot of photomultiplier current divided by collision chamber current vs electron energy and is recorded photographically. Following a procedure in which the light detection system is calibrated by means of a standard lamp absolute values of the curve are obtained from direct readings of the photomultiplier current and electron beam current at a convenient electron energy.

The ratio of photomultiplier current to collision chamber current is proportional to a quantity called apparent cross section. This is the excitation cross section obtained by assuming that atomic excited states are populated exclusively by direct excitation and that the light emitted

by these atoms upon undergoing spontaneous transitions to lower states is unpolarized and radiated isotropically. Corrections which must be applied to convert the apparent cross sections to absolute cross sections will be discussed in subsequent chapters.

This system provides rapid, sensitive production of excitation functions. It is capable of producing a voltage proportional to the apparent excitation cross section as a continuous function of electron energy. It is invaluable in determination of actual cross sections from low pressure apparent excitation functions and of transfer cross sections for transfer occurring at higher pressure.

CHAPTER II

MEASUREMENT OF APPARENT CROSS SECTIONS

At pressures sufficiently low so that transfer effects are negligible one can define an apparent cross section, $Q''(j)$, for a particular state (j) by the equation

Apparent direct excitation rate = Apparent radiative loss rate

or
$$Q''(j)NI/eS = N'(j)A(j) \qquad (1)$$

In this equation N is the density of ground state atoms, I is the electron beam current, S is the cross sectional area of the electron beam, e is the electronic charge, and A(j) is the total probability per unit time for transition from the jth state to all the lower states. $N'(j)$ is the apparent density of atoms in the jth state, i. e., the density one would expect if the radiated light were isotropic and had the same intensity in all directions as in the direction of observation.

In order to measure the apparent cross section, the intensity of light of the wavelength characteristic of a transition from the jth state emitted from a known volume of the collision chamber is measured. This makes a determination of $N'(j)A(j)$ possible. Results of theoretical calculations are avilable for the value of A(j).[1] Electron beam current, I, is easily measured. Electron beam cross-sectional area is readily determined from the geometry of the collimating grids in the electron gun.

The electronic charge is a known constant. The density of the ground state atoms, N, is determined by measuring the pressure and temperature of the gas in the collision chamber and using the relationshp $N = p/kT$. Here, p is the pressure, k is Boltzmann's constant, and T is the absolute temperature of the gas.

Figure 1 shows the physical arrangement of the optical section of the equipment. A portion of the light from the collision chamber (C) is passed through a lens to the entrance slit of the monochromator (M). From the exit slit of the monochromator it passes through a prism and another lens to a photomultiplier tube (PM). The monochromator permits examination of a single spectral line of helium with a resolution of ± 16 angstrom units, with entrance and exit slits set at widths of 1 mm each. The entrance window of the optical system determines the length of the beam (ℓ) that is viewed. The beam diameter is less than the entrance window. The solid angle (Ω_{CC}) through which light from the viewed portion of the beam is collected is equal to the area of the entrance pupil (A') divided by the optical distance from the entrance pupil to the beam. The area of the entrance pupil was measured by inserting a small aperture stop of known area (A) in the light beam and measuring the ratio of photomultiplier current to collision chamber current $(I_{PM}/I)_1$. The ratio of photomultiplier current to collision chamber current was measured with the small aperture removed $(I_{PM}/I)_o$. The effective area of the entrance

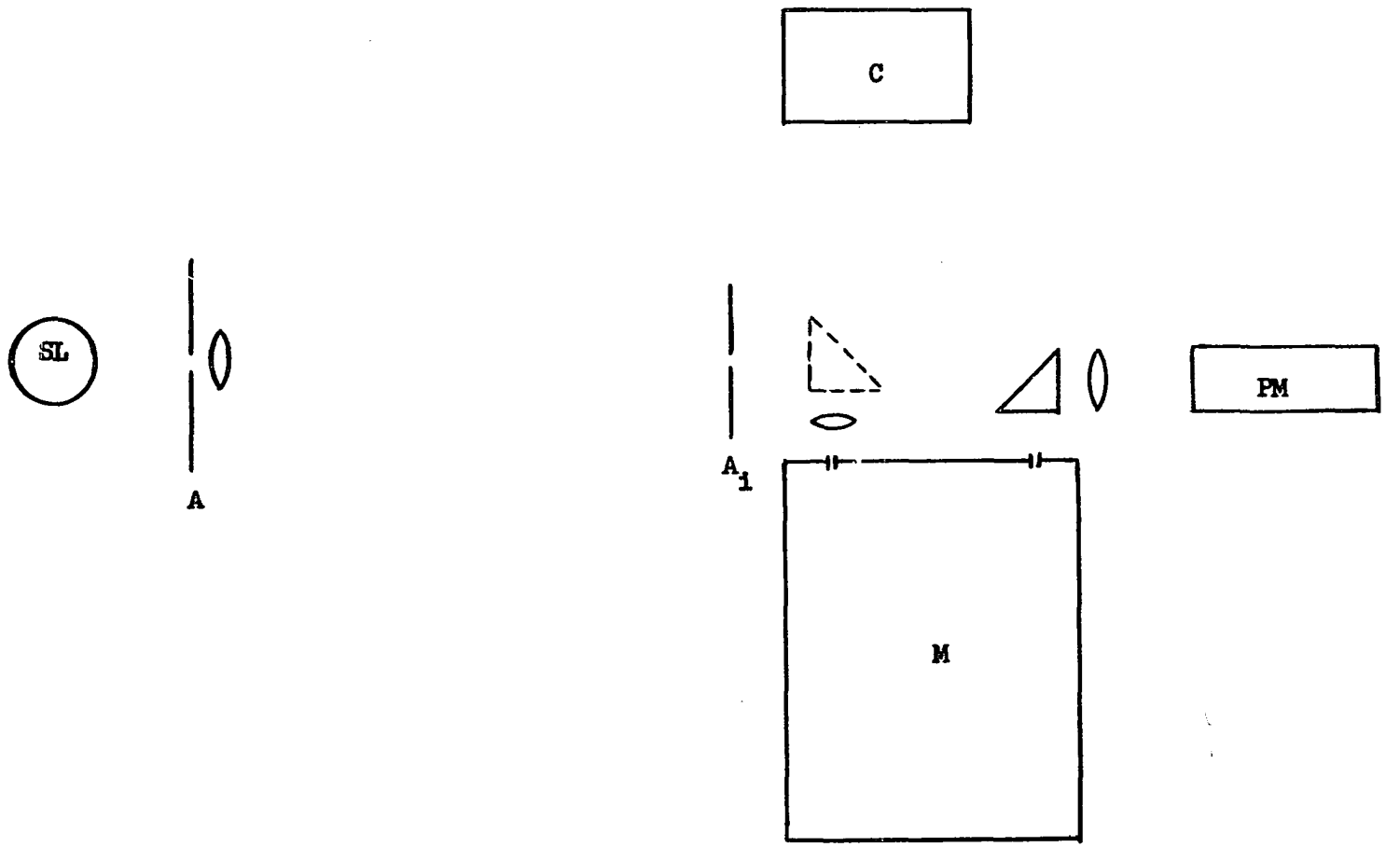


FIGURE 1.-PHYSICAL ARRANGEMENT OF THE DETECTION SYSTEM

pupil of the optical system is then determined from the equation

$$A' = A \frac{(I_{PM}/I)_o}{(I_{PM}/I)_1}$$

This method of calculating Ω_{cc} avoids possible error introduced by the fact that rays from the ends of the extended light source may be inclined to the optic axis of the system sufficiently to cause them to be prevented by stops in the monochromator from reaching the photomultiplier tube.

If $\ell S = V$ is the viewed volume of the collision chamber traversed by the beam, equation (1) may be rewritten as

$$Q''(j)NIV/eS = N'(j)A(j)V$$

or

$$Q''(j)NI\ell/e = N'(j)A(j)V$$

It is customary to introduce the branching ratio, $B = A(j)/A(jk)$, where $A(jk)$ is the transition probability per unit time from the jth state to the kth state. This is done so that $A(j)$ can be written as $A(jk)B$, since the monochromator restricts investigation to a particular transition (j to k). Thus we have

$$Q''(j)NI\ell/eB = N'(j)A(jk)V$$

The right hand side of this equation is the apparent total number of photons of wavelength characteristic of the j to k transition emitted from the volume V per unit time. If the relative transmissivity of the monochromator and associated optical elements for that wavelength is q, and

that of the collision chamber wall T_{cc}, then we have

$$N'(j)A(jk)V(\Omega_{cc}/4\pi)qT_{cc} = C(\lambda)I_{PM}(cc)$$

In this equation $I_{PM}(cc)$ is photomultiplier current associated with light from the collision chamber and $C(\lambda)$ is the photon efficiency of the tube.

Since

$$N'(j)A(jk)V = C(\lambda)I_{PM}(cc)4\pi/\Omega_{cc}qT_{cc} = Q''(j)NI\ell/eB$$

and

$$N = p/kT$$

it follows that

$$Q''(j) = \frac{4\pi kTeB}{\Omega_{cc}qT_{cc}} \frac{C(\lambda)I_{PM}(cc)}{Ip} \qquad (2)$$

In order to determine $C(\lambda)$, light from a standard lamp (SL in Fig. 1) was examined with the same monochromator setting. The lamp was a tungsten ribbon filament pyrometer supplied and standardized by the General Electric Company. The lamp was operated at three temperatures in the range from 1400 to 1700 degrees Kelvin and its emission calculated within a small wavelength interval for the wavelength of each transition observed. Emissivity tables for tungsten determined by Larrabee[13] were used. The sensitivity of the detection system was determined with the three lamp temperatures. The maximum deviation of the sensitivity from the mean value at a given wavelength was generally less than 5%.

If $\Psi_{\lambda}^{B}T$ is the radiant energy density of wavelength λ emitted by a black body at an absolute temperature T, then for the wavelengths and

filament temperatures used in this work, a good approximation of $\Psi^B_{\lambda T}$ is given by Wien's Law,[14]

$$\Psi^B_{\lambda T} = (8\pi ch/\lambda^5)\exp(-ch/\lambda kT)$$

Since we are investigating wavelengths in the region shown in Fig. 2a, we can approximate $\Psi^B_{\lambda T}$ as a linear function of λ for small wavelength intervals ($\pm$ 20 angstroms or less) as shown in Fig. 2b. Then we have

$$\Psi^B_{\lambda T} = \Psi^B_{\lambda_o T} + xs/\Psi^B_{\lambda_o T} \qquad (3)$$

where $x = \lambda - \lambda_o$ and s is the slope of the curve.

The intensity of radiation normal to the surface of a flat black body (I_N) is given by

$$I_N = \Psi c/2\pi$$

However, $\Psi^B_{\lambda T}$ in Eq. (3) is that for an isothermal enclosure for which Ψ is twice that in front of a flat surface.[14] Therefore the intensity for a black body is given by

$$I^B_{\lambda TN} = \Psi^B_{\lambda T} c/4\pi$$

and the intensity of a non-black body with emissivity $\epsilon_{\lambda T}$ is given by

$$I_{\lambda TN} = I^B_{\lambda TN}\epsilon_{\lambda T}$$

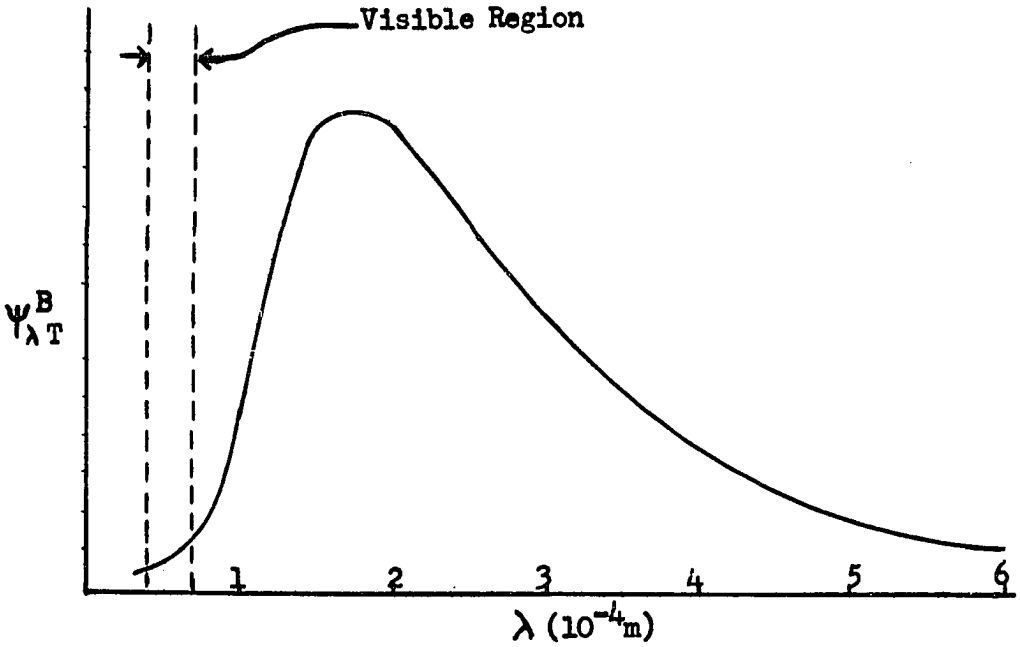
If we define $R_{\lambda TN}$ as the rate of emission of photons from a flat non-black body per unit area per unit wavelength per unit solid angle, then we have

$$R_{\lambda TN} = I_{\lambda TN}/h\nu = I_{\lambda TN}\lambda/hc = I_{\lambda TN}(\lambda_o + x)/hc = I_{\lambda TN}\lambda_o(1 + x/\lambda_o)/hc$$

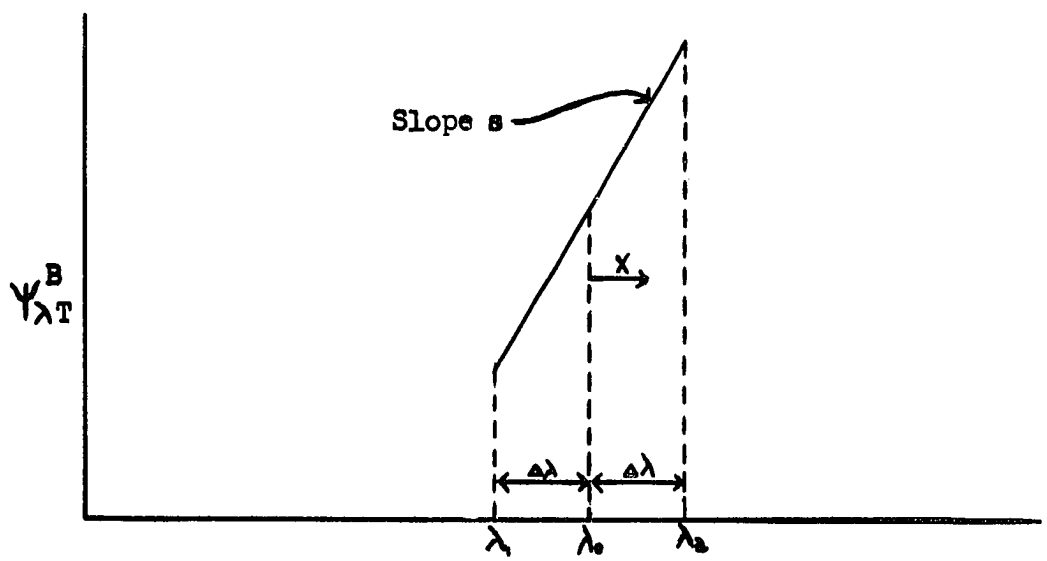
Since the monochromator will transmit all wavelengths between $\lambda_o - \Delta\lambda$ and $\lambda_o + \Delta\lambda$ as shown in Fig. 3, the relative transmissivity of the monochromator must be taken into account by defining

$$R'_{\lambda TN} = R_{\lambda TN} T_{rel}$$

where T_{rel} is written as $1 + x/\Delta\lambda$ for $-\Delta\lambda \leq x \leq 0$ and as $1 - x/\Delta\lambda$ for $0 \leq x \leq \Delta\lambda$. Then we have

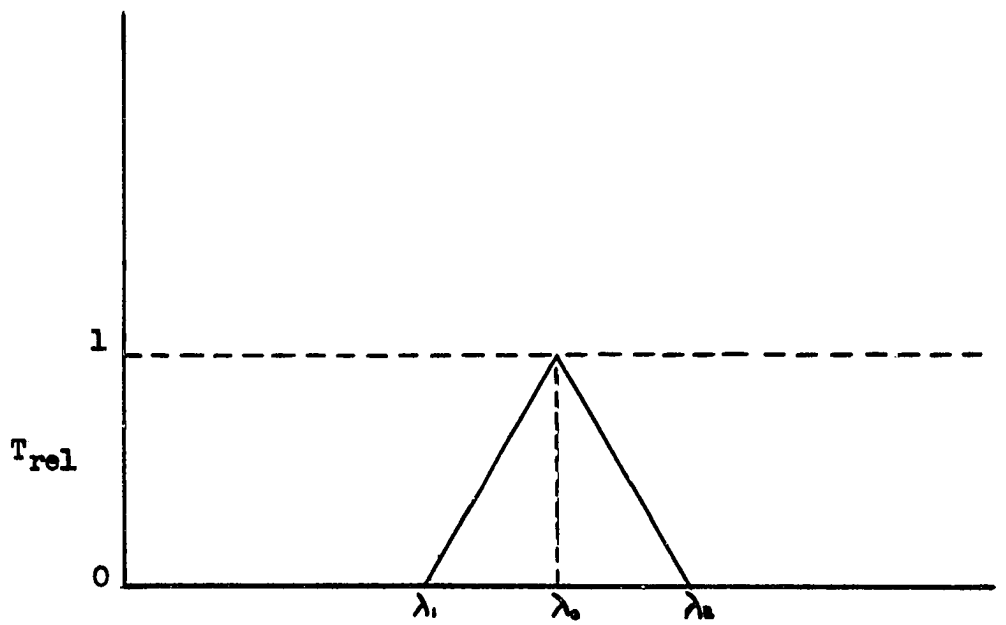


a. Black body energy density vs wavelength ($T \cong 1600^{\circ}K$)



b. Linear approximation of portion of curve in a.

FIGURE 2.--PLANCK'S LAW AND LINEAR APPROXIMATION



$\Delta\lambda = \lambda_2 - \lambda_0 = \lambda_0 - \lambda_1 = W \times 16A$
(W = slit width in mm)

FIGURE 3.--MONOCHROMATOR RELATIVE TRANSMISSIVITY

$$R'_{\lambda TN} = (\psi^B_{\lambda_o T} c \epsilon_{\lambda T} \lambda_o / 4\pi hc)(1 + xs/\psi^B_{\lambda_o T})(1 + x/\lambda_o)(1 \pm x/\Delta\lambda)$$

Where the double sign ($\pm$) is indicated in the above equation, (+) should be used when $x < 0$ and (-) when $x > 0$. Expanding and integrating $R'_{\lambda TN}$ from λ_1 to λ_2 one obtains

$$R_{\lambda_2 - \lambda_1} = \int_{\lambda_1}^{\lambda_2} R'_{\lambda TN} d\lambda = (\psi^B_{\lambda_o T} \epsilon_{\lambda_o T} \lambda_o \Delta\lambda / 4\pi h)(1 + s\Delta\lambda^2 / 6\psi^B_{\lambda_o T} \lambda_o)$$

This rather cumbersome expression has been calculated for a variety of values of λ_o and T on an IBM 650 computer.

Letting R_{SL} be the rate of emission of photons which pass through a slot the size of the electron beam (area = A_i) and strike the photomultiplier, one finds

$$R_{SL} = R_{\lambda_2 - \lambda_1} q T_{LP} \Omega_{SL} A_o$$

In this equation T_{LP} is the transmissivity of the optical elements peculiar to the standard lamp, A_o is the area of the standard lamp filament viewed by the optical system and Ω_{SL} is the solid angle through which light from A_o is collected by the optical system. Figure 4 shows the physical arrangement of the portion of the optical system used for the standard lamp. A lens located a distance d_o from the standard lamp filament (SL) focuses light from the filament on a masking slit (A_i) a distance of d_i away. A circular aperture of variable diameter (d) located a distance d'_o from the filament determines Ω_{SL}. The area of the masking slit A_i may be written as ℓh_i where ℓ is the same as the viewed length of the beam in the collision chamber and h_i is the same as the beam diameter. From Fig. 4 it is seen that

$$\Omega_{SL} = d^2 / 4 d'^2_o$$

and that

$$A_o = A_i d_o^2 / d_i^2 = \ell h_i d_o^2 / d_i^2$$

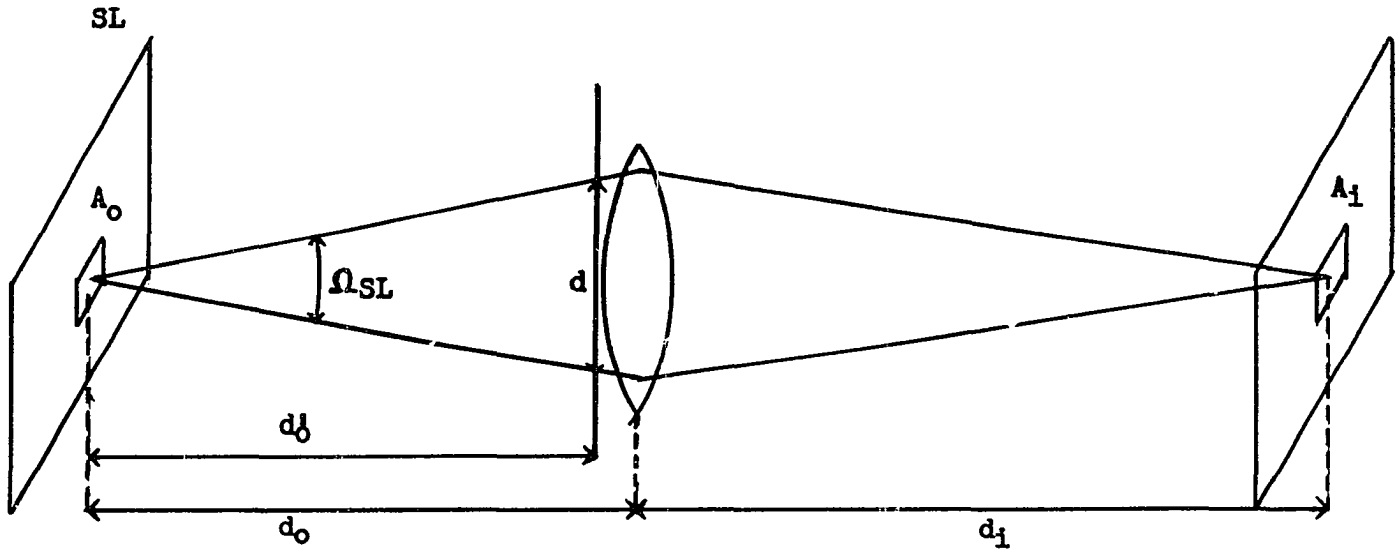


FIGURE 4.--STANDARD LAMP OPTICAL SYSTEM

The quantity R_{SL} may now be written as

$$R_{SL} = R_{\lambda_2-\lambda_1} q T_{LP} (\pi d^2/4 d_o'^2)(\ell h_i d_o^2/d_i^2)$$

or as

$$R_{SL} = C(\lambda) I_{PM}(SL)$$

where $I_{PM}(SL)$ is the photomultiplier current produced by light from the standard lamp for a monochromator setting of λ_o. Equating the two expressions for R_{SL} and solving for $C(\lambda)$ one obtains

$$C(\lambda) = \frac{\pi \ell h_i d_o^2 q T_{LP}}{4 d_o'^2 d_i^2} \frac{d^2 R_{\lambda_2-\lambda_1}}{I_{PM}(SL)}$$

Substituting this value of $C(\lambda)$ in Eq. (2) results in an absolute value of apparent cross section, $Q''(j)$, which may be written as

$$Q''(j) = \frac{\pi^2 h_i d_o^2 T_{LP} kTe}{\Omega_{cc} T_{cc} d_o'^2 d_i^2} B \frac{d^2 R_{\lambda_2-\lambda_1}}{I_{PM}(SL)} \frac{I_{PM}(cc)}{Ip} \qquad (4)$$

In this work the following values of the various constants in Eq. (4) were used

h_i = .2 cm

d_o = 18.2 cm

T = 300°K

Ω_{cc} = 6.44 x 10^{-4} steradians

d_o' = 17.2 cm

d_i = 206 cm

The transmissivities T_{LP} and T_{cc} represent those quantities peculiar to the standard lamp and collision chamber portions of the optical system respectively. A 4% loss was assumed at each non-coated air-glass interface. Since there were four such interfaces in the standard lamp portion of the system and two in the collision chamber portion, the resulting value of T_{LP}/T_{cc} is .92. Using the above

values, Eq. (4) may be written as

$$Q''(j) = 3.70 \times 10^{-31} \text{cm}^2 \text{ coul(mm of mercury)} B \frac{d^2 R_{\lambda_2-\lambda_1}}{I_{PM}(SL)} \frac{I_{PM}(cc)}{Ip} \quad (5)$$

If d is measured in cm, all currents in μa, and p in mm of mercury, $Q''(j)$ has units of cm^2.

To determine $Q''(j)$, the collision chamber is filled with helium at the desired pressure and the monochromator adjusted for the wavelength characteristic of the desired j to k transition. The automatic processing and data recording system produces a trace on a Tektronix oscilloscope as the electron energy is varied continuously. This trace is photographed with a Tektronix C-12 camera with a Polaroid back. The ordinate of the curve is proportional to the quantity $I_{PM}(cc)/I$ and the abscissa to the electron energy. The electron energy is then set to some convenient value, usually the peak of the excitation function, readings taken on microammeters of $I_{PM}(cc)$ and I, and the ratio $I_{PM}(cc)/Ip$ is calculated.

A coated prism is next placed in front of the entrance lens to the monochromator, $I_{PM}(SL)$ is measured for several settings of d and standard lamp filament temperature (which determines $R_{\lambda_2-\lambda_1}$), and the average value of $d^2R_{\lambda_2-\lambda_1}/I_{PM}(SL)$ calculated. With these quantities and the known branching ratio $B = A(j)/A(jk)$, $Q''(j)$ is easily determined by use of equation (5) for the selected electron energy. From the photographed excitation function, scaling factors may be measured and $Q''(j)$ calculated for any electron energy.

To discover the dependence of $Q''(j)$ on pressure, the peak value of $Q''(j)$ is calculated as described above for several pressures. $Q''(j)$

is then plotted against pressure as shown in Figs. 5, 6, and 7. The apparent cross sections should be independent of pressure unless transfer and/or imprisonment are occurring. These pressure curves are particularly useful in determining maximum pressures that may be used without the advent of imprisonment or transfer. The slight decrease of $Q''(3^3P)$ with increased pressure will be discussed in Chapter V.

The apparent cross section, $Q''(j)$ has not taken into account the polarization of the radiation from the collision chamber. The degree of polarization of the emitted light varies with electron energy, pressure, and direction of the emitted light relative to the electron beam. In this work all light examined was emitted perpendicular to the electron beam. In arriving at Eq. (5), isotropic emission of unpolarized light was assumed. Since the radiation generally is not isotropic, nor unpolarized, a polarization correction factor, $f_p(\theta, j)$, is introduced so that $I_{PM}(cc)f_p(\theta, j)$ is proportional to the angular average of the light intensity and thus allows the determination of the entire light flux emitted from the collision chamber.

The polarization correction factor is[15]

$$f_p(\theta, j) = \frac{1}{3}\,\frac{300-P(j)}{100-P(j)\cos^2\theta}$$

where $P(j)$ is the percentage polarization. For our viewing angle of 90 degrees, the polarization correction factor is

$$f_p(90^o, j) = 1-P(j)/300$$

Values of $P(j)$ have been measured by McFarland and Soltysik[9] for varying pressure and electron energy for several of the transitions

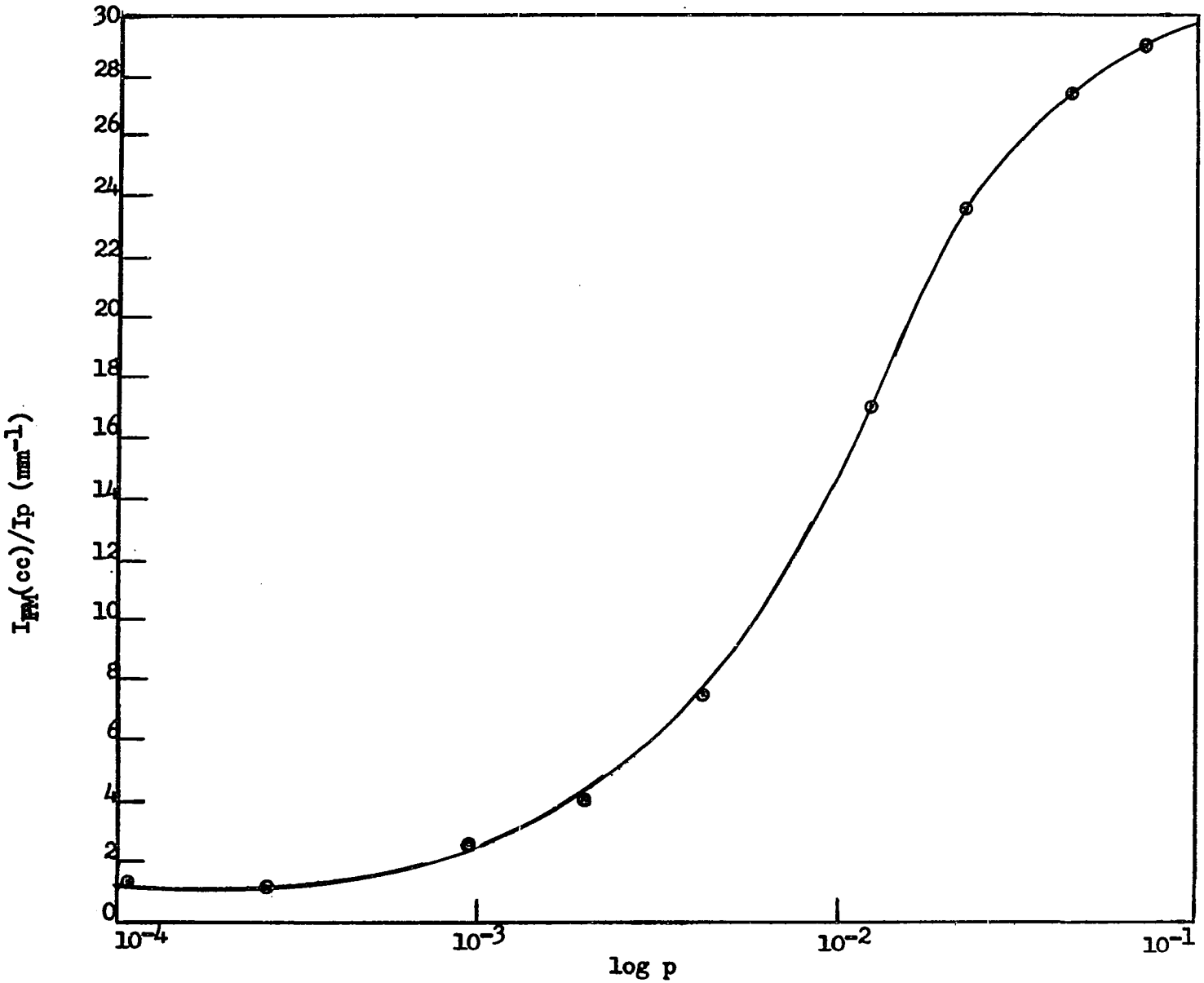


FIGURE 5.—$I_{PM}(cc)/Ip$ VS LOG p FOR 5016A (3^1P—2^1S)

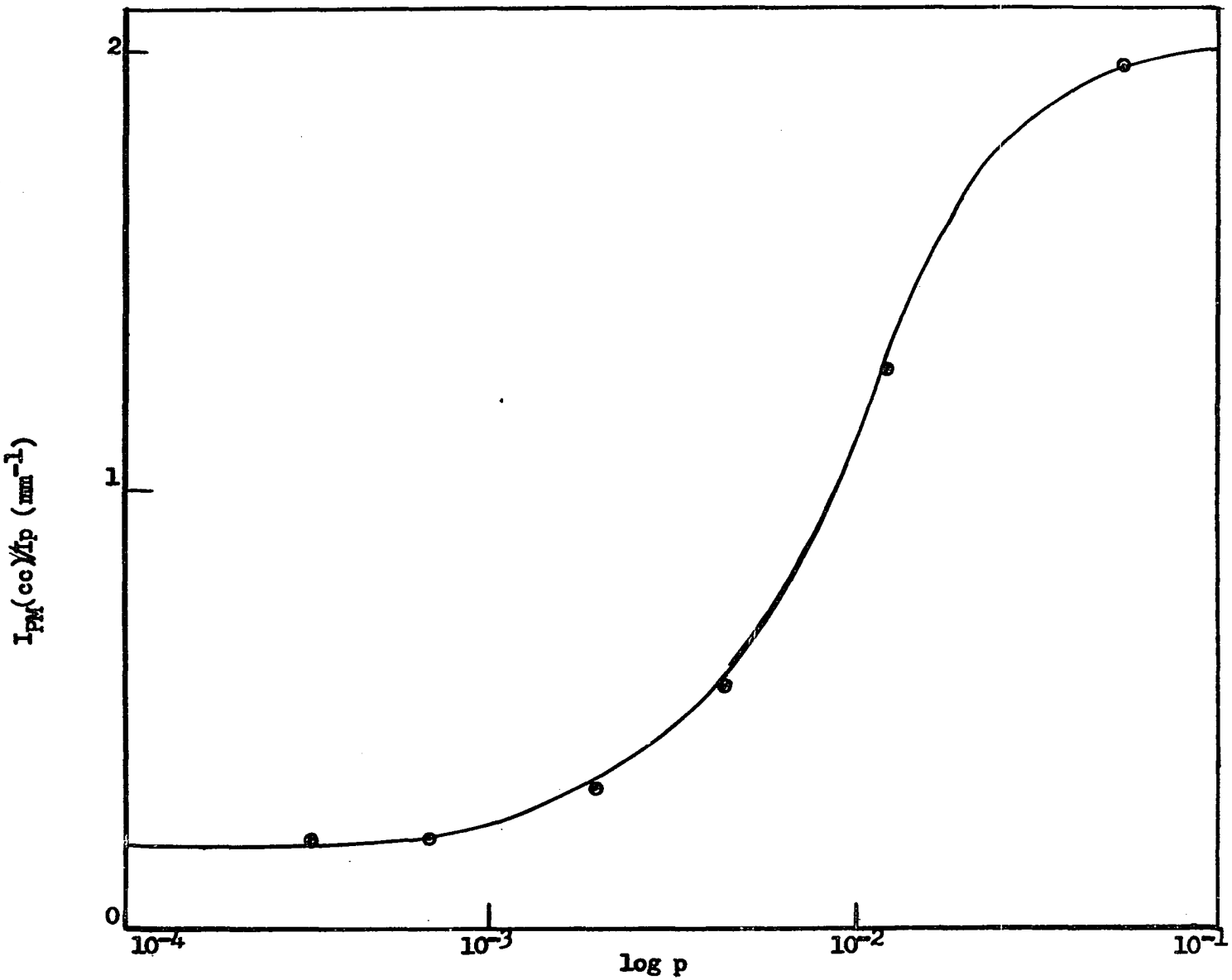


FIGURE 6.—$I_{PM}(cc)/Ip$ VS LOG p FOR 3965A ($4^1P—2^1S$)

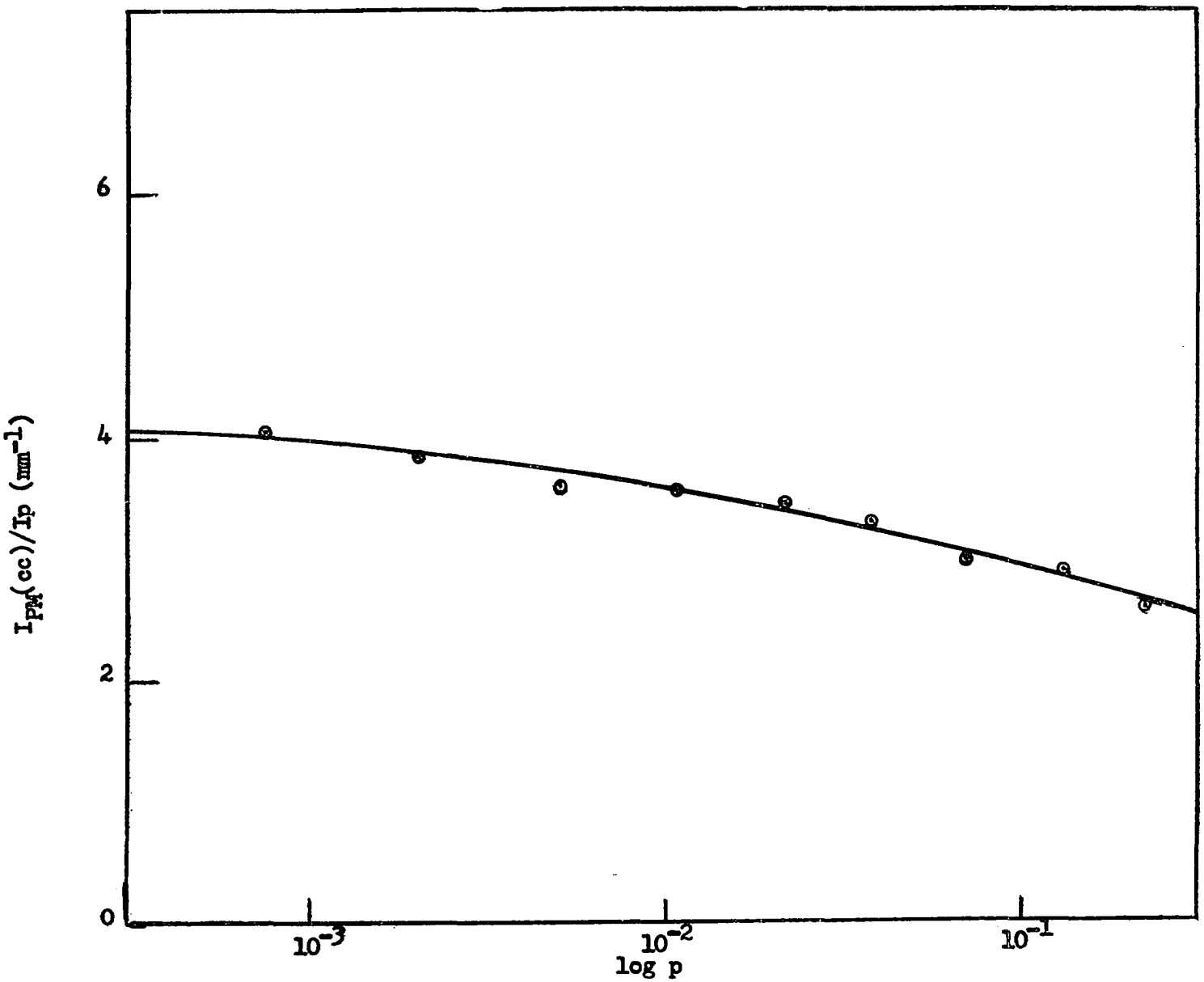


FIGURE 7.—$I_{PM}(cc)/Ip$ VS LOG p FOR 3889A ($3^3P—2^3S$)

observed in this work and are used for making the polarization corrections reported here. Since the amount of polarization correction is generally rather small, the values of $P(j)$ given by McFarland and Soltysik were used whenever available and extrapolations of these values were used for the transitions that were not reported.

If we define $Q'(j)$ as the cross section corrected for polarization, it can be written as

$$Q'(j) = f_p(90^o, j)Q''(j)$$

The correction factor $f_p(90^o, j)$ applied to $Q''(j)$ actually is a correction to the apparent density of excited atoms $N'(j)$ and converts it to $N(j)$, the actual density of atoms in the jth state. This can best be seen from Eq. (1). Thus,

$$N(j) = f_p(90^o, j)N'(j)$$

The maximum percentage by which Q' varied from Q'' was 0 for ^1S levels, 4 to 7% for ^1P levels, 13 to 17% for ^1D levels, 0 for ^3S levels, 5% for the 3^3P level, and 4 to 5% for the ^3D levels. The higher levels showed less polarization than the low levels and thus received smaller corrections. This situation thus minimized the errors involved in the extrapolation procedure used in procuring the $Q'(j)$ curve from the $Q''(j)$ curve.

The apparent excitation functions for the 18 energy levels of helium investigated in this work are shown in Fig. 8. The maximum or peak values of $Q''(j)$ together with the quantities used to calculate them are listed in Table I. The percent polarization for maximum $Q''(j)$, the polarization correction factor, and the peak apparent cross sections corrected for polarization are shown in Table II.

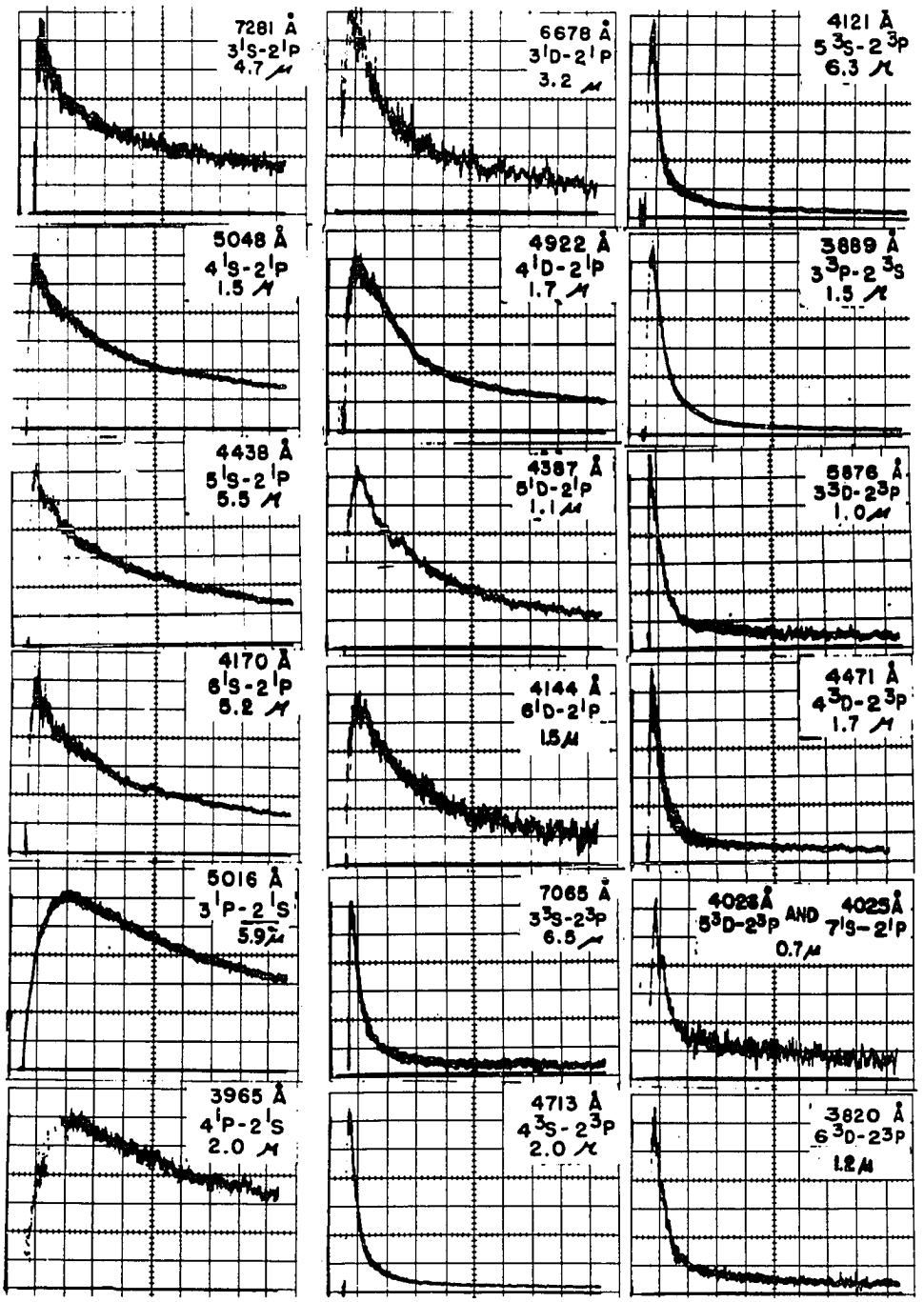


FIGURE 8.--EIGHTEEN APPARENT EXCITATION FUNCTIONS

TABLE I

PEAK APPARENT CROSS SECTIONS

Level	λ (A)	p (μ)	Electron Energy (eV)	$I_{PM}(cc)^{-1}/Ip$ $(mm)^{-1}$	$\frac{d^2R_{\lambda_2-\lambda_1}}{I_{PM}(SL)}$ $(10^{11}\ \mu coul)^{-1}$	B	$Q''(j)$ $(10^{-20}cm^2)$
3^1S*	7281	21.0	40	0.0054	3950	1.00	49
4^1S	5047	1.5	43	1.72	2.25	1.69	24
5^1S	4438	5.5	45	4.3	2.74	2.12	9.2
6^1S	4170	5.2	45	1.25	4.38	2.36	4.8
3^1P	5016	0.01	100	1.00	2.18	43.6	350
4^1P	3965	2.0	100	0.20	5.76	37.3	159
3^1D*	6678	3.2	46	0.0085	2140	1.00	42
4^1D	4922	1.7	53	1.53	2.27	1.37	17.6
5^1D	4388	1.1	53	5.4	2.92	1.54	9.0
6^1D	4144	1.5	53	1.67	4.69	1.63	4.7
3^3S*	7065	6.5	35	0.015	3125	1.00	107
4^3S	4714	2.0	35	2.4	2.32	1.69	35
5^3S	4122	6.3	35	3.1	5.12	2.09	12.3
3^3P	3889	1.5	37	3.85	6.12	1.11	97
3^3D	5876	1.0	35	1.27	6.67	1.00	31
4^3D	4471	1.7	35	0.96	2.66	1.27	12.0
5^3D	4026	0.7	38	0.18	6.62	1.39	6.2
6^3D	3820	1.2	35	0.87	7.59	1.58	3.9

* These levels were measured with a different photomultiplier tube. In order to take into account differences in calibration, an adjustment factor of 0.62 was used.

TABLE II

POLARIZATION CORRECTIONS AND CORRECTED APPARENT CROSS SECTIONS

Level	$Q''(j)_{max}$ (10^{-20} cm^2)	P(j) %	$fp(90^\circ, j)$	$Q'(j)_{max}$ (10^{-20} cm^2)
3^1S	49	0	1	49
4^1S	24	0	1	24
5^1S	9.2	0	1	9.2
6^1S	4.8	0	1	4.8
3^1P	350	13	0.956	337
4^1P	159	6	0.979	156
3^1D	42	41	0.864	36
4^1D	17.6	42	0.859	15.1
5^1D	9.0	36	0.879	7.9
6^1D	4.7	36	0.879	4.2
3^3S	107	0	1	107
4^3S	35	0	1	35
5^3S	12.3	0	1	12.3
3^3P	97	9.5	0.968	94
3^3D	31	12.5	0.958	30
4^3D	12.0.	14	0.953	11.4
5^3D	6.2	10.5	0.965	5.9
6^3D	3.9	11.5	0.962	3.7

CHAPTER III

CALCULATION OF ABSOLUTE EXCITATION CROSS SECTIONS

The absolute excitation cross section depends solely upon the direct excitation of atoms to the state in question. The steady state population rate equation for some state (j)

Direct excitation rate + Cascading rate = Radiative loss rate

may be written as

$$Q(j)NI/eS + \sum_i N(i)A(ij) = N(j)A(j) \qquad (6)$$

In this equation Q(j) is the absolute excitation cross section, N(i) is the density of the ith state atoms, and A(ij) is the transition probability per unit time of atoms from the ith to the jth states.

Equation (1) upon application of the polarization correction factor may be written as

$$Q'(j)NI/eS = N(j)A(j)$$

From this equation it is seen that

$$N(i) = Q'(i)NI/A(i)eS$$

Equation (6) may now be written as

$$Q(j)NI/eS + \sum_i Q'(i)NIA(ij)/eSA(i) = Q'(j)NI/eS$$

or

$$Q(j) = Q'(j) - \sum_i Q'(i)A(ij)/A(i)$$

Thus with a knowledge of the apparent excitation cross sections corrected for polarization and the theoretical transition probabilities one can calculate the contribution of cascading and arrive at a value of Q(j). In some cases the values of Q'(i) are not known. For these

cases it is assumed that the shape of the high n value excitation functions was the same as those of the low n functions having the same orbital quantum number L. The magnitudes of the high level Q'(i) functions were assumed to vary as $n^{-\alpha}$ where α is a parameter determined from the measured amplitudes of the lower states. Theoretical transition probabilities have been compiled for $n \leq 8$.[1] An extrapolation procedure again was used to find the values for higher states.

The actual percentage of correction applied to an excitation function for cascading effects varied with electron energy due to differences between the shape of the excitation function of the cascading levels and the shape of the excitation function being corrected. The variation in the cascading correction was not so prominent for the triplet functions due to the similarity among triplet apparent excitation functions. The maximum cascade contribution to the 3^1S level was 15% and occurred at an electron energy of 300 eV. Cascade corrections of a similar percentage were obtained for the higher ^1S levels. The 3^1P level sustained a 14% correction at 35 eV and a 4% correction at 100 eV. The 4^1P level received somewhat smaller percentage corrections and distinctly less absolute corrections. The ^1D functions suffered maximum correction at 450 eV; they were in the range of 5 to 8%.

The cascade corrections sustained by triplet functions were nearly constant as a function of voltage. The 3^3S, 4^3S, and 5^3S functions of Q' were 20 to 30% due to cascade. The Q' curve of 3^3P was 30% due to cascade. The cascade correction for the ^3D functions

varied from 10 to 19%.

Fortunately, the errors which might be introduced by the extrapolation processes necessarily are small since the cascading from high states is small. That part of the population of a state coming from levels involved in the extrapolation processes was 7% for the 3^1S state. The amounts falling to other low level states by this process were as follows: 3^1P, 1%; 3^1D, 4%; 3^3S, 3%; 3^3P, 4%; 3^3D, 1%. Measurements of the ^3P family were limited to n = 3. The fall.off of cross section with n was determined from the paper of Gabriel and Heddle which supplied cross section data for the 3, 4, and 5 states.

There are additional uncertainties associated with the cascading from the F states. These were approximated by using the calculated values of $Q(4^1F)$ and $Q(4^3F)$[16] with an n^{-3} dependence for higher F states. The cascading from the G to F states was neglected since the populations of the G states are expected to be very small on account of the rapid decrease of direct excitation cross section with increasing values of L. Under these assumptions we have calculated N(nF) and found that the F to D cascading contributes less than 1% of the total populations of the ^1D and ^3D states. This result remains essentially the same when the singlet-triplet mixing of the F states is taken into consideration.[5]

The excitation function obtained at 4025-6A represents the sum of two line functions. These are 4026A (5^3D to 2^3P) and 4025A (7^1S to 2^1P). One can obtain an excellent approximation to the excitation function of the 7^1S level by extrapolation from the 3, 4, 5, and 6

levels of that family. Application of the appropriate branching ratio yields the function of the 4025A line, with a maximum value of $1.1 \times 10^{-20} cm^2$. This when subtracted from the function representing the sum of the two excitation processes, yields the 4026A function which in turn yields the 5^3D apparent excitation function.

Table III lists the maximum values of $Q''(j)$, $Q'(j)$, and $Q(j)$ for each state examined together with the electron energy corresponding to the peak values. Tables IV through XXI list $Q''(j)$, $Q'(j)$, cascading contributions, and $Q(j)$ for various electron energies for these states. Figures 9 through 26 show the electron excitation functions $Q'(j)$ and $Q(j)$ for these states.

TABLE III

PEAK APPARENT AND ACTUAL CROSS SECTIONS AND ELECTRON ENERGIES

Level	Electron Energy (eV)	$Q''(j)$ $(10^{-20}cm^2)$	$Q'(j)$ $(10^{-20}cm^2)$	$Q(j)$ $(10^{-20}cm^2)$
3^1S	40	49	49	49
4^1S	43	24	24	23.7
5^1S	45	9.2	9.2	8.8
6^1S	45	4.8	4.8	4.4
3^1P	100	350	337	322
4^1P	100	159	156	152
3^1D	46	42	36	35
4^1D	53	17.6	15.1	14.9
5^1D	53	9.0	7.9	7.8
6^1D	53	4.7	4.2	4.1
3^3S	35	107	107	89
4^3S	35	35	35	26
5^3S	35	12.3	12.3	9.5
3^3P	37	97	94	67
3^3D	35	31	30	25
4^3D	35	12.0	11.4	9.2
5^3D	38	6.2	5.9	5.1
6^3D	35	3.9	3.7	3.1

TABLE IV

3^1S EXCITATION FUNCTION DATA

Electron Energy (eV)	$Q''(j)$ $(10^{-20}cm^2)$	$Q'(j)$ $(10^{-20}cm^2)$	^1P Cascade $(10^{-20}cm^2)$	$Q(j)$ $(10^{-20}cm^2)$
30	16.64	16.64	1.09	15.55
35	44.38	44.38	1.46	42.92
40	49.00	49.00	1.76	47.24
50	44.38	44.38	2.48	41.90
60	40.68	40.68	2.96	37.72
80	35.32	35.32	3.48	31.84
100	31.90	31.90	3.64	28.26
150	25.89	25.89	3.46	22.43
200	21.73	21.73	3.19	18.54
250	19.42	19.42	2.90	16.52
300	17.94	17.94	2.67	15.27
350	16.64	16.64	2.42	14.22
400	15.72	15.72	2.23	13.49
450	14.79	14.79	2.10	12.69

TABLE V

4^1S EXCITATION FUNCTION DATA

Electron Energy (eV)	$Q''(j)$ $(10^{-20}cm^2)$	$Q'(j)$ $(10^{-20}cm^2)$	^1P Cascade $(10^{-20}cm^2)$	$Q(j)$ $(10^{-20}cm^2)$
30	8.20	8.20	0.27	7.93
35	19.89	19.89	0.36	19.53
40	23.37	23.37	0.43	22.94
43	24.20	24.20	0.48	23.72
45	22.76	22.76	0.54	22.22
50	21.73	21.73	0.61	21.12
60	19.68	19.68	0.73	18.95
80	17.22	17.22	0.86	16.36
100	15.58	15.58	0.89	14.69
150	12.30	12.30	0.85	11.45
200	10.25	10.25	0.78	9.47
250	9.02	9.02	0.71	8.31
300	8.20	8.20	0.65	7.55
350	7.38	7.38	0.59	6.79
400	6.56	6.56	0.55	6.01
450	5.86	5.86	0.52	5.34

TABLE VI

$5\,^1S$ EXCITATION FUNCTION DATA

Electron Energy (eV)	$Q''(j)$ $(10^{-20}cm^2)$	$Q'(j)$ $(10^{-20}cm^2)$	^1P Cascade $(10^{-20}cm^2)$	$Q(j)$ $(10^{-20}cm^2)$
30	3.19	3.19	0.21	2.98
35	6.53	6.53	0.28	6.25
40	8.28	8.28	0.34	7.94
45	9.24	9.24	0.42	8.82
50	8.76	8.76	0.48	8.28
60	7.93	7.93	0.57	7.36
80	7.01	7.01	0.67	6.34
100	6.37	6.37	0.71	5.66
150	5.15	5.15	0.67	4.48
200	4.30	4.30	0.62	3.68
250	3.66	3.66	0.56	3.10
300	3.19	3.19	0.52	2.67
350	2.74	2.74	0.47	2.27
400	2.39	2.39	0.43	1.96
450	2.07	2.07	0.41	1.66

TABLE VII

6^1S EXCITATION FUNCTION DATA

Electron Energy (eV)	$Q''(j)$ ($10^{-20}cm^2$)	$Q'(j)$ ($10^{-20}cm^2$)	^1P Cascade ($10^{-20}cm^2$)	$Q(j)$ ($10^{-20}cm^2$)
30	1.65	1.65	0.17	1.48
35	3.22	3.22	0.23	2.99
40	4.46	4.46	0.28	4.18
45	4.79	4.79	0.35	4.44
50	4.54	4.54	0.39	4.15
60	4.13	4.13	0.47	3.66
80	3.55	3.55	0.55	3.00
100	3.14	3.14	0.58	2.56
150	2.48	2.48	0.55	1.93
200	2.06	2.06	0.51	1.55
250	1.82	1.82	0.46	1.36
300	1.57	1.57	0.42	1.15
350	1.40	1.40	0.38	1.02
400	1.24	1.24	0.35	0.89
450	1.07	1.07	0.33	0.74

TABLE VIII

3^1P EXCITATION FUNCTION DATA

Electron Energy (eV)	Q''(j) ($10^{-20}cm^2$)	Q'(j) ($10^{-20}cm^2$)	^1S Cascade ($10^{-20}cm^2$)	^1D Cascade ($10^{-20}cm^2$)	Q(j) ($10^{-20}cm^2$)
30	105.6	101.2	4.75	5.14	91.3
35	143.7	134.8	11.52	7.24	116.1
40	182.0	168.6	13.54	7.93	147.1
45	217.1	201.4	13.19	8.35	179.9
50	246.4	229.2	12.59	8.38	208.2
60	293.3	274.0	11.41	7.45	255.1
80	340.3	321.9	9.98	6.12	305.8
100	352.0	336.5	9.03	5.20	322.3
120	346.1	332.3	8.18	4.43	319.7
150	328.5	319.7	7.13	3.73	308.8
200	299.2	295.3	5.94	2.80	286.6
250	269.9	268.5	5.23	2.40	260.9
300	246.4	246.4	4.75	1.99	239.7
350	222.9	223.6	4.28	1.79	217.5
400	205.3	206.2	3.80	1.66	200.7
450	193.6	194.6	3.40	1.52	189.7

TABLE IX

4^1P EXCITATION FUNCTION DATA

Electron Energy (eV)	Q''(j) ($10^{-20}cm^2$)	Q'(j) ($10^{-20}cm^2$)	^1S Cascade ($10^{-20}cm^2$)	^1D Cascade ($10^{-20}cm^2$)	Q(j) ($10^{-20}cm^2$)
30	32.9	32.8	1.01	1.26	30.5
35	56.3	54.2	2.45	1.77	50.0
40	74.0	71.1	2.88	1.94	66.2
45	90.0	86.4	2.80	2.04	81.6
50	101.4	97.4	2.68	2.05	92.6
60	120.6	116.2	2.42	1.82	111.9
80	145.3	141.2	2.12	1.50	137.6
90	156.3	152.5	2.02	1.38	149.1
100	159.0	155.7	1.92	1.27	152.5
105	159.0	156.0	1.87	1.22	152.9
120	156.1	153.8	1.74	1.08	150.9
150	150.8	149.4	1.52	0.91	147.0
200	138.4	138.3	1.26	0.69	136.4
250	126.1	126.6	1.11	0.59	124.9
300	115.1	115.8	1.01	0.49	114.3
350	104.2	104.9	0.91	0.44	103.6
400	96.0	96.7	0.81	0.41	95.5
450	90.5	91.2	0.72	0.37	90.1

TABLE X

3^1D EXCITATION FUNCTION DATA

Electron Energy (eV)	Q''(j) ($10^{-20}cm^2$)	Q'(j) ($10^{-20}cm^2$)	^1P Cascade ($10^{-20}cm^2$)	^1F Cascade ($10^{-20}cm^2$)	Q(j) ($10^{-20}cm^2$)
30	24.71	21.99	0.27	0.028	21.69
40	39.54	33.93	0.44	0.077	33.41
46	41.70	36.03	0.55	0.086	35.39
50	41.08	35.86	0.61	0.088	35.16
60	36.08	31.86	0.73	0.086	31.04
70	32.12	28.68	0.81	0.082	27.79
100	24.09	22.24	0.90	0.068	21.27
150	16.68	15.96	0.86	0.045	15.05
200	12.36	11.99	0.79	0.034	11.17
250	10.50	10.26	0.72	0.029	9.51
300	8.65	8.52	0.66	0.025	7.83
350	7.72	7.67	0.60	0.023	7.05
400	7.10	7.10	0.55	0.021	6.53
450	6.49	6.49	0.52	0.021	5.95

TABLE XI

4^1D EXCITATION FUNCTION DATA

Electron Energy (eV)	Q''(j) ($10^{-20}cm^2$)	Q'(j) ($10^{-20}cm^2$)	^1P Cascade ($10^{-20}cm^2$)	^1F Cascade ($10^{-20}cm^2$)	Q(j) ($10^{-20}cm^2$)
30	1.84	1.54	0.080	0.017	1.44
35	11.32	9.40	0.107	0.040	9.25
40	15.30	12.74	0.129	0.046	12.56
45	16.68	14.06	0.159	0.052	13.85
50	17.44	14.88	0.181	0.053	14.65
53	17.60	15.12	0.185	0.054	14.88
60	17.29	15.01	0.217	0.052	14.74
80	15.61	13.85	0.254	0.047	13.55
100	13.16	11.88	0.266	0.041	11.57
150	8.42	7.86	0.253	0.027	7.58
200	6.12	5.86	0.233	0.020	5.61
250	4.90	4.77	0.212	0.018	4.54
300	4.28	4.21	0.195	0.015	4.00
350	3.98	3.93	0.177	0.014	3.74
400	3.67	3.64	0.163	0.013	3.46
450	3.37	3.34	0.154	0.012	3.17

TABLE XII

5^1D EXCITATION FUNCTION DATA

Electron Energy (eV)	Q''(j) ($10^{-20}cm^2$)	Q'(j) ($10^{-20}cm^2$)	^1P Cascade ($10^{-20}cm^2$)	^1F Cascade ($10^{-20}cm^2$)	Q(j) ($10^{-20}cm^2$)
30	0.94	0.82	0.054	0.012	0.75
35	5.79	4.99	0.072	0.028	4.89
40	7.83	6.79	0.087	0.033	6.67
45	8.53	7.42	0.107	0.036	7.28
50	8.92	7.81	0.122	0.037	7.65
53	9.00	7.91	0.125	0.037	7.75
60	8.84	7.84	0.146	0.036	7.66
80	7.90	7.24	0.171	0.033	7.04
100	6.73	6.21	0.179	0.028	6.00
150	4.30	4.09	0.170	0.019	3.90
200	3.13	3.00	0.157	0.014	2.83
250	2.50	2.44	0.143	0.012	2.28
300	2.19	2.15	0.131	0.010	2.01
350	2.03	2.00	0.119	0.010	1.87
400	1.88	1.85	0.110	0.009	1.73
450	1.72	1.69	0.103	0.008	1.58

TABLE XIII

$6\,^1D$ EXCITATION FUNCTION DATA

Electron Energy (eV)	Q''(j) ($10^{-20}cm^2$)	Q'(j) ($10^{-20}cm^2$)	^1P Cascade ($10^{-20}cm^2$)	^1F Cascade ($10^{-20}cm^2$)	Q(j) ($10^{-20}cm^2$)
30	0.49	0.43	0.016	0.002	0.41
35	3.04	2.62	0.021	0.002	2.60
40	4.10	3.55	0.025	0.002	3.52
45	4.47	3.89	0.031	0.002	3.86
50	4.68	4.10	0.035	0.002	4.06
53	4.72	4.15	0.036	0.002	4.11
60	4.66	4.12	0.042	0.002	4.08
80	4.19	3.80	0.050	0.002	3.75
100	3.53	3.26	0.052	0.002	3.21
150	2.26	2.15	0.049	0.002	2.10
200	1.64	1.57	0.046	0.002	1.52
250	1.31	1.28	0.041	0.002	1.24
300	1.15	1.13	0.038	0.002	1.09
350	1.07	1.05	0.035	0.002	1.01
400	0.99	0.97	0.032	0.002	0.94
450	0.90	0.89	0.030	0.002	0.86

TABLE XIV

3^3S EXCITATION FUNCTION DATA

Electron Energy (eV)	Q''(j) ($10^{-20}cm^2$)	Q'(j) ($10^{-20}cm^2$)	^3P Cascade ($10^{-20}cm^2$)	Q(j) ($10^{-20}cm^2$)
25	16.05	16.05	2.99	13.06
30	69.55	69.55	12.83	56.72
35	107.0	107.0	18.98	88.92
40	87.38	87.38	18.84	68.54
45	67.77	67.77	16.81	50.96
50	55.28	55.28	14.64	40.64
60	32.10	32.10	10.56	21.54
70	23.18	23.18	7.11	16.07
80	16.90	16.90	5.01	11.89
90	13.37	13.37	4.06	9.31
100	11.06	11.06	3.43	7.63
150	6.60	6.60	1.60	5.00
200	5.35	5.35	1.21	4.14
250	4.99	4.99	1.06	3.93
300	4.81	4.81	1.01	3.80
350	4.64	4.64	0.95	3.69
400	4.46	4.46	0.87	3.59
450	4.28	4.28	0.81	3.47

TABLE XV

4^3S EXCITATION FUNCTION DATA

Electron Energy (eV)	$Q''(j)$ ($10^{-20}cm^2$)	$Q'(j)$ ($10^{-20}cm^2$)	^3P Cascade ($10^{-20}cm^2$)	$Q(j)$ ($10^{-20}cm^2$)
25	5.22	5.22	1.35	3.87
30	22.62	22.62	5.77	16.85
35	34.80	34.80	8.54	26.26
40	28.42	28.42	8.48	19.94
45	22.04	22.04	7.56	14.48
50	17.98	17.98	6.59	11.39
60	10.44	10.44	4.75	5.69
70	7.54	7.54	3.20	4.34
80	5.50	5.50	2.25	3.25
90	4.35	4.35	1.83	2.52
100	3.60	3.60	1.54	2.06
150	2.15	2.15	0.72	1.43
200	1.74	1.74	0.55	1.19
250	1.62	1.62	0.48	1.14
300	1.57	1.57	0.45	1.12
350	1.51	1.51	0.43	1.08
400	1.45	1.45	0.39	1.06
450	1.39	1.39	0.36	1.03

TABLE XVI

5^3S EXCITATION FUNCTION DATA

Electron Energy (eV)	Q''(j) ($10^{-20}cm^2$)	Q'(j) ($10^{-20}cm^2$)	^3P Cascade ($10^{-20}cm^2$)	Q(j) ($10^{-20}cm^2$)
25	1.85	1.85	0.45	1.40
30	8.00	8.00	1.91	6.09
35	12.3	12.3	2.83	9.47
40	10.05	10.05	2.81	7.24
45	7.79	7.79	2.50	5.29
50	6.36	6.36	2.18	4.18
60	3.69	3.69	1.57	2.12
70	2.67	2.67	1.06	1.61
80	1.85	1.85	0.75	1.10
90	1.54	1.54	0.60	0.94
100	1.27	1.27	0.51	0.76
150	0.76	0.76	0.24	0.52
200	0.62	0.62	0.18	0.44
250	0.57	0.57	0.16	0.41
300	0.55	0.55	0.15	0.40
350	0.53	0.53	0.14	0.39
400	0.51	0.51	0.13	0.38
450	0.49	0.49	0.12	0.38

TABLE XVII

3^3P EXCITATION FUNCTION DATA

Electron Energy (eV)	Q''(j) ($10^{-20}cm^2$)	Q'(j) ($10^{-20}cm^2$)	^3D Cascade ($10^{-20}cm^2$)	^3S Cascade ($10^{-20}cm^2$)	Q(j) ($10^{-20}cm^2$)
25	14.52	14.36	0.96	3.30	10.10
30	62.92	61.66	4.12	14.30	43.24
35	93.90	91.18	6.30	22.01	62.87
37	96.80	93.70	5.94	20.54	67.22
40	93.90	90.52	5.39	17.98	67.15
45	84.22	80.77	4.62	13.94	62.19
50	73.57	70.33	3.81	11.37	55.15
60	53.24	50.74	2.49	6.60	41.65
70	35.82	34.14	1.80	4.77	27.57
80	25.17	24.06	1.46	3.30	19.30
90	20.33	19.50	1.15	2.75	15.60
100	17.13	16.48	0.95	2.27	13.26
150	7.84	7.66	0.69	1.36	5.61
200	5.90	5.83	0.62	1.10	4.11
250	5.13	5.08	0.57	1.03	3.48
300	4.84	4.84	0.53	0.99	3.32
350	4.55	4.56	0.49	0.95	3.12
400	4.16	4.17	0.46	0.92	2.79
450	3.87	3.88	0.43	0.88	2.57

TABLE XVIII

3^3D EXCITATION FUNCTION DATA

Electron Energy (eV)	Q''(j) ($10^{-20}cm^2$)	Q'(j) ($10^{-20}cm^2$)	^3F Cascade ($10^{-20}cm^2$)	^3P Cascade ($10^{-20}cm^2$)	Q(j) ($10^{-20}cm^2$)
25	4.71	4.52	0.00	0.78	3.74
30	20.41	19.57	0.05	3.33	16.19
35	31.40	30.08	0.10	4.92	25.06
40	26.85	25.75	0.10	4.89	20.76
45	22.92	22.00	0.10	4.36	17.54
50	18.84	18.09	0.09	3.80	14.20
60	12.25	11.81	0.08	2.74	8.99
70	8.79	8.53	0.08	1.84	6.61
80	6.90	6.74	0.07	1.30	5.37
90	5.56	5.44	0.07	1.05	4.32
100	4.55	4.47	0.06	0.89	3.52
150	3.30	3.27	0.04	0.41	2.82
200	2.95	2.94	0.03	0.31	2.60
250	2.73	2.72	0.03	0.27	2.42
300	2.54	2.53	0.03	0.26	2.24
350	2.32	2.32	0.03	0.25	2.04
400	2.17	2.17	0.02	0.22	1.93
450	2.04	2.04	0.02	0.21	1.81

TABLE XIX

4^3D EXCITATION FUNCTION DATA

Electron Energy (eV)	Q''(j) ($10^{-20}cm^2$)	Q'(j) ($10^{-20}cm^2$)	^3F Cascade ($10^{-20}cm^2$)	^3P Cascade ($10^{-20}cm^2$)	Q(j) ($10^{-20}cm^2$)
25	1.80	1.74	0.00	0.34	1.40
30	7.80	7.49	0.02	1.46	6.01
35	12.00	11.44	0.04	2.16	9.24
40	10.26	9.79	0.04	2.14	7.61
45	8.76	8.39	0.04	1.91	6.44
50	7.20	6.92	0.03	1.67	5.22
60	4.68	4.53	0.03	1.20	3.30
70	3.36	3.27	0.03	0.81	2.43
80	2.70	2.65	0.02	0.57	2.06
90	2.12	2.09	0.02	0.46	1.61
100	1.74	1.72	0.02	0.39	1.31
150	1.26	1.25	0.01	0.18	1.06
200	1.13	1.13	0.01	0.14	0.98
250	1.04	1.04	0.01	0.12	0.91
300	0.97	0.97	0.01	0.11	0.85
350	0.89	0.89	0.01	0.11	0.77
400	0.83	0.83	0.01	0.10	0.72
450	0.78	0.78	0.01	0.09	0.68

TABLE XX

5^3D EXCITATION FUNCTION DATA

Electron Energy (eV)	Q''(j) ($10^{-20}cm^2$)	Q'(j) ($10^{-20}cm^2$)	^3F Cascade ($10^{-20}cm^2$)	^3P Cascade ($10^{-20}cm^2$)	Q(j) ($10^{-20}cm^2$)
25	0.81	0.78	0	0.14	0.64
30	3.98	3.82	0	0.59	3.23
35	6.08	5.85	0	0.88	4.97
38	6.16	5.94	0	0.87	5.07
40	5.70	5.50	0	0.87	4.63
45	4.72	4.57	0	0.78	3.79
50	4.04	3.92	0	0.68	3.24
60	2.80	2.74	0	0.49	2.25
70	1.89	1.86	0	0.34	1.52
80	1.24	1.22	0	0.24	1.00
90	1.05	1.04	0	0.19	0.85
100	0.92	0.91	0	0.16	0.75
150	0.76	0.76	0	0.07	0.69
200	0.71	0.71	0	0.06	0.65
250	0.67	0.67	0	0.05	0.62
300	0.60	0.60	0	0.05	0.55
350	0.54	0.54	0	0.04	0.50
400	0.47	0.47	0	0.04	0.43
450	0.40	0.40	0	0.04	0.36

TABLE XXI

6^3D EXCITATION FUNCTION DATA

Electron Energy (eV)	Q''(j) ($10^{-20}cm^2$)	Q'(j) ($10^{-20}cm^2$)	^3F Cascade ($10^{-20}cm^2$)	^3P Cascade ($10^{-20}cm^2$)	Q(j) ($10^{-20}cm^2$)
25	0.58	0.57	0	0.09	0.48
30	2.51	2.41	0	0.40	2.01
35	3.86	3.71	0	0.59	3.12
40	3.30	3.18	0	0.59	2.59
45	2.82	2.73	0	0.52	2.21
50	2.32	2.25	0	0.46	1.79
60	1.51	1.48	0	0.33	1.15
70	1.08	1.06	0	0.22	0.84
80	0.87	0.86	0	0.16	0.70
90	0.68	0.67	0	0.13	0.54
100	0.56	0.56	0	0.11	0.45
150	0.41	0.41	0	0.05	0.36
200	0.36	0.36	0	0.04	0.32
250	0.34	0.34	0	0.03	0.31
300	0.31	0.31	0	0.03	0.28
350	0.29	0.29	0	0.03	0.26
400	0.27	0.27	0	0.03	0.24
450	0.25	0.25	0	0.03	0.22

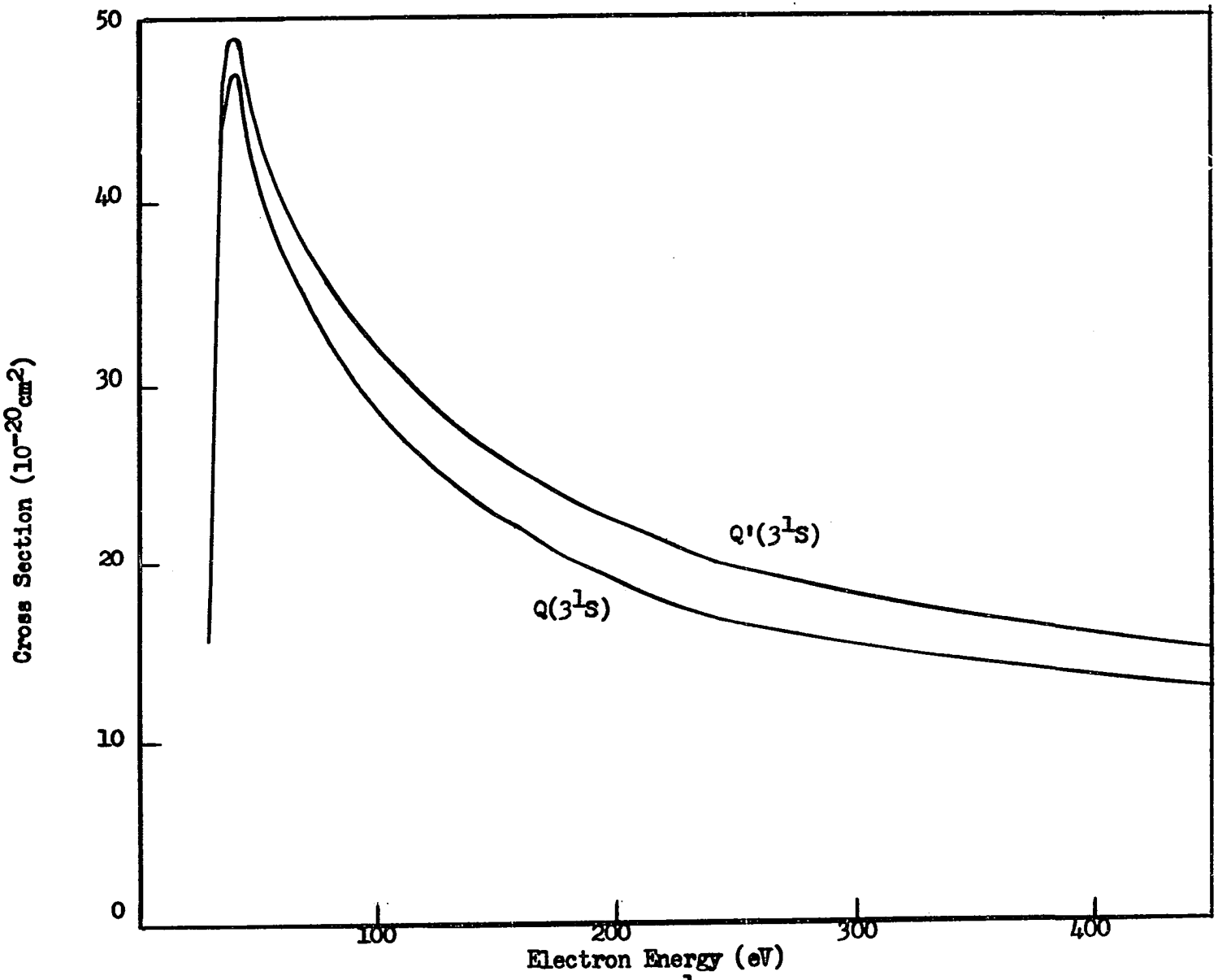


FIGURE 9.--Q'(3^1S) AND Q(3^1S) VS ELECTRON ENERGY

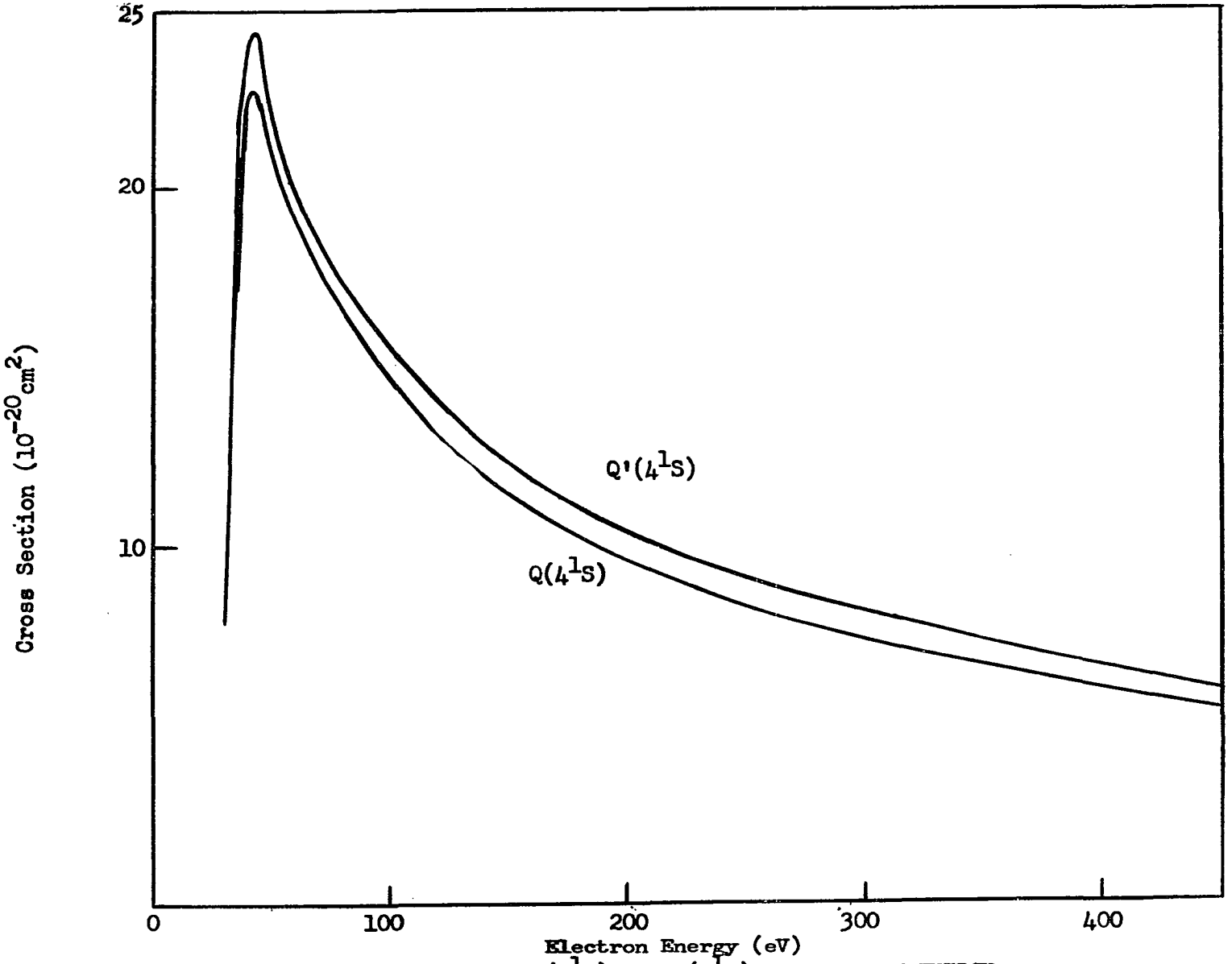


FIGURE 10.--Q'(4^1S) AND Q(4^1S) VS ELECTRON ENERGY

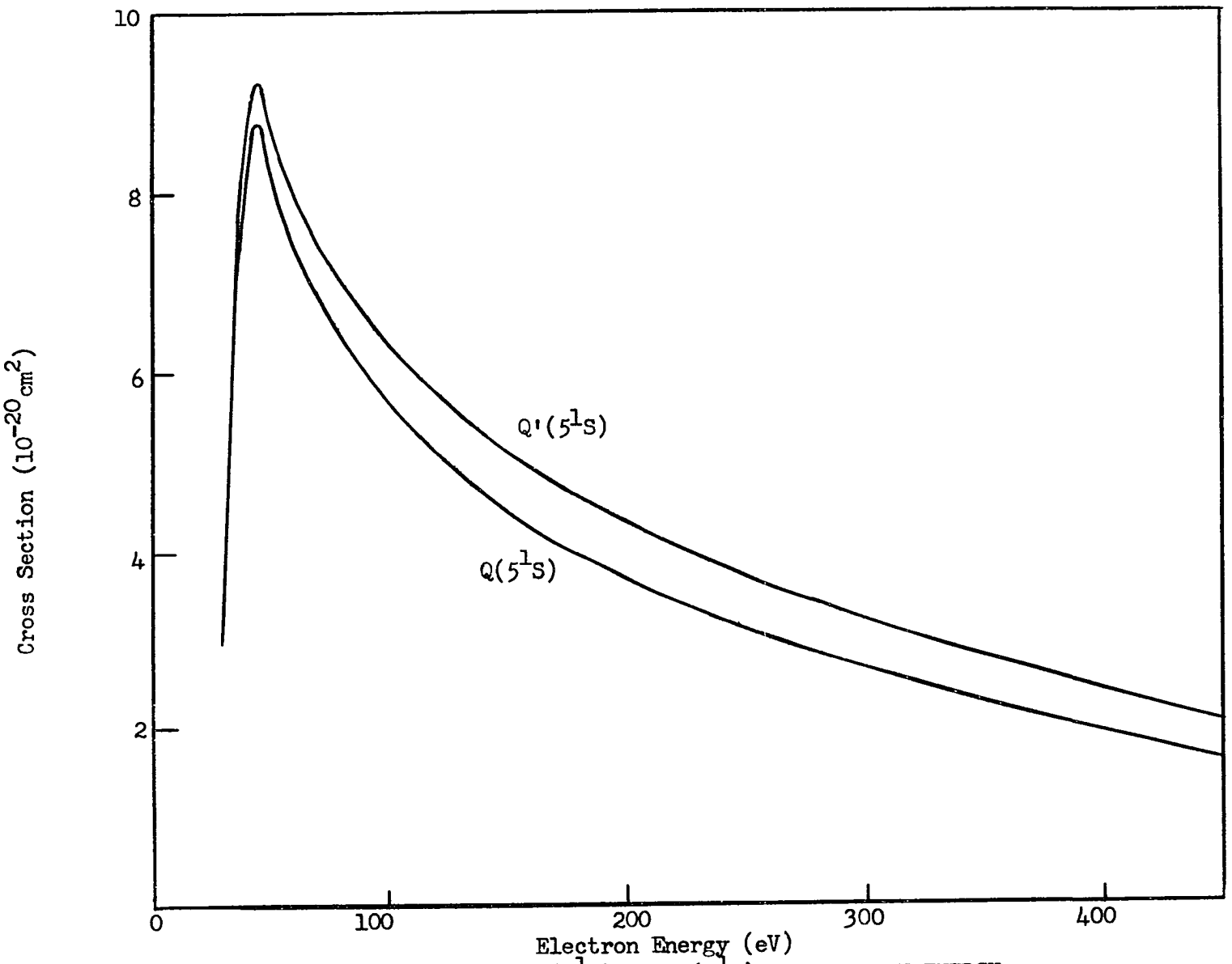


FIGURE 11.-- Q'(5^1S) AND Q(5^1S) VS ELECTRON ENERGY

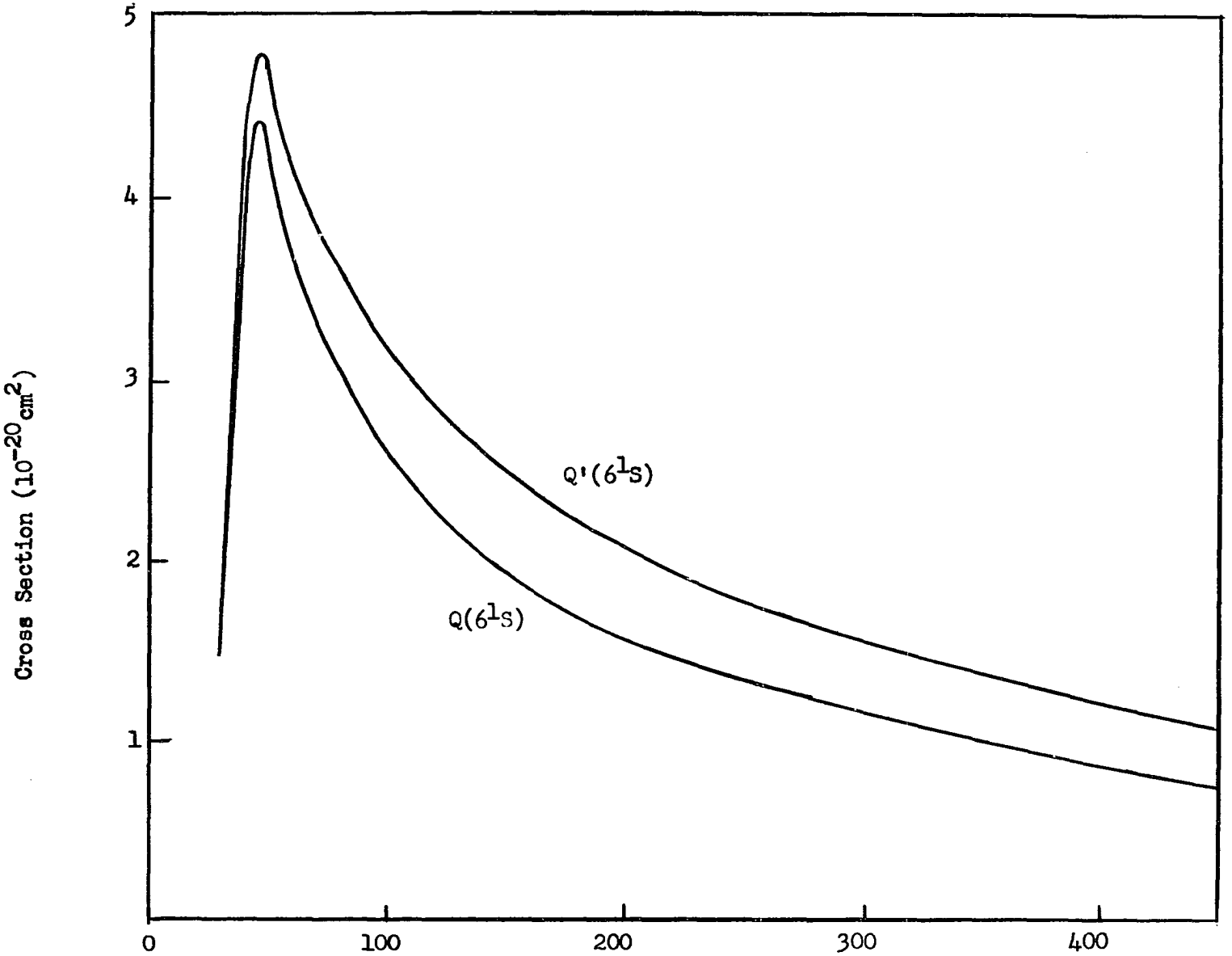


FIGURE 12.—Q'(6^1S) AND Q(6^1S) VS ELECTRON ENERGY

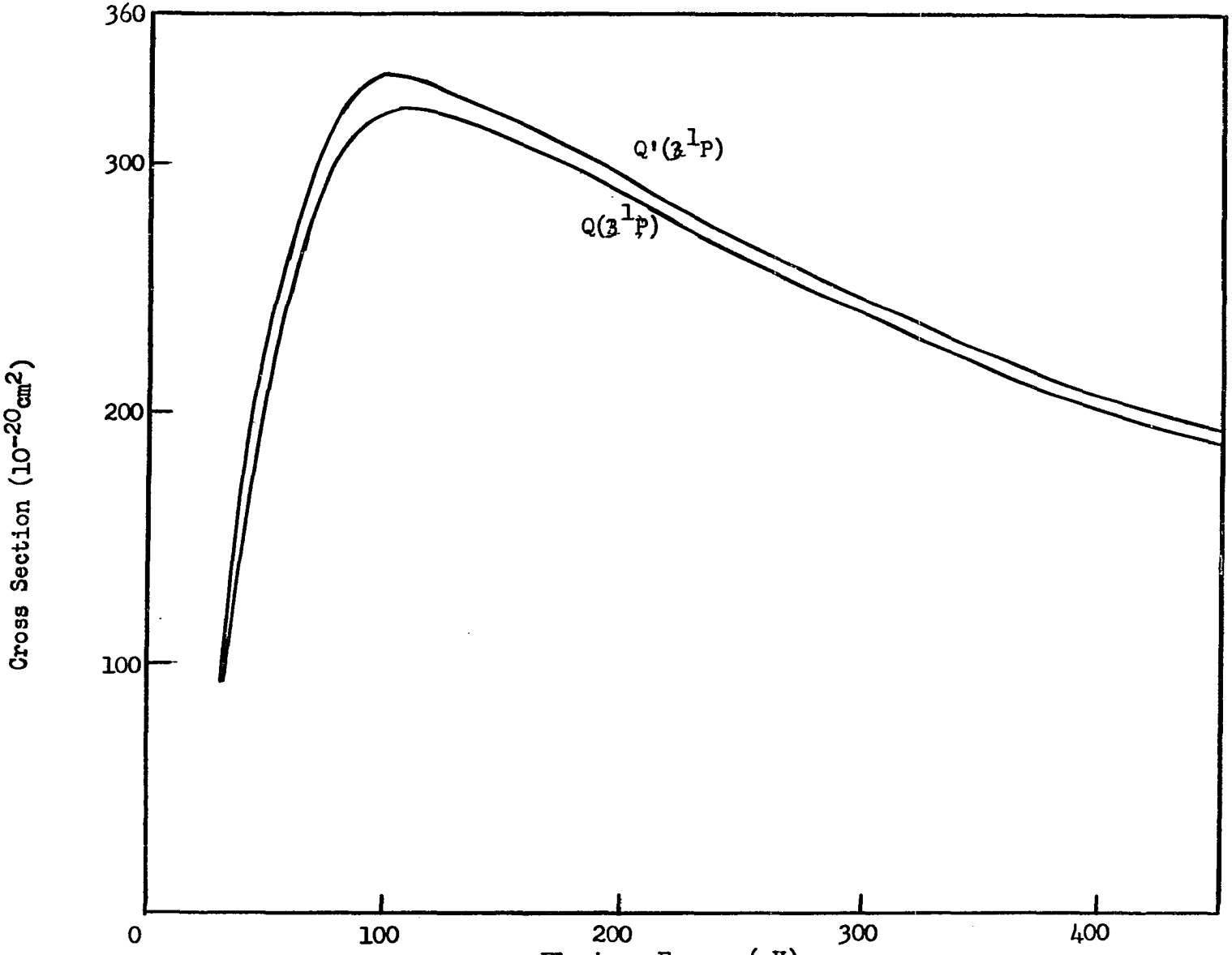


FIGURE 13.--$Q'(3^1P)$ AND $Q(3^1P)$ VS ELECTRON ENERGY

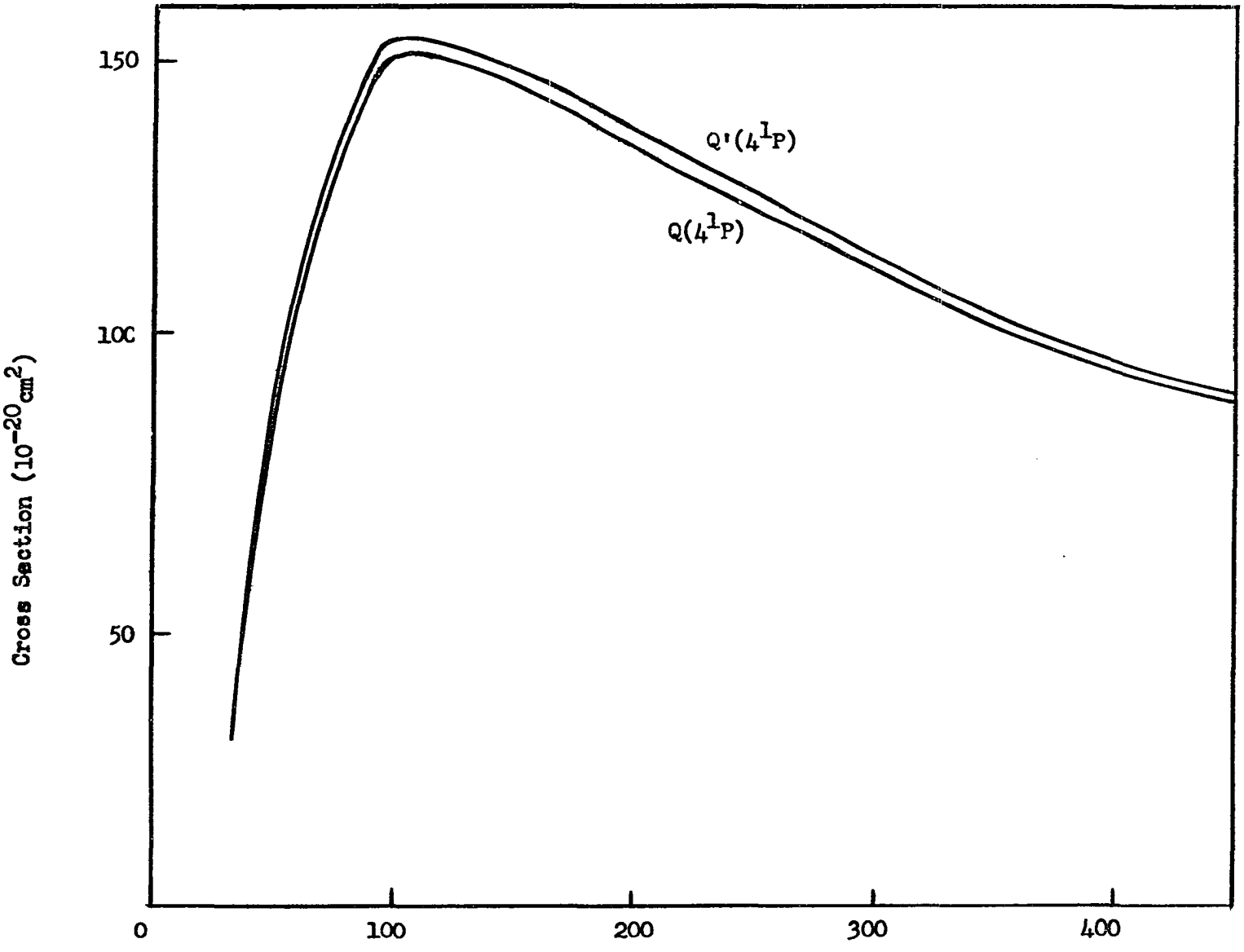


FIGURE 14.--Q'(4^1P) AND Q(4^1P) VS ELECTRON ENERGY

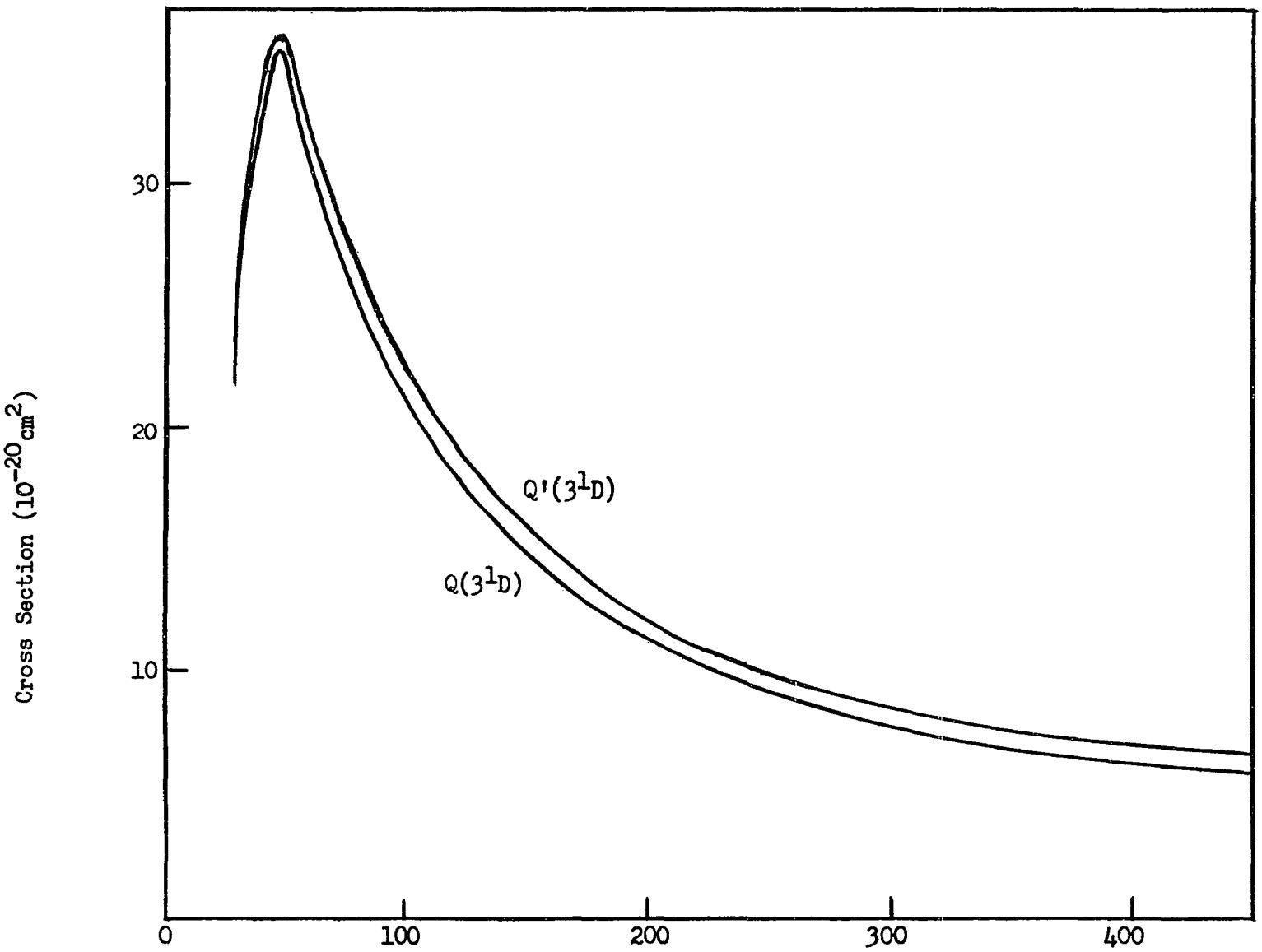


FIGURE 15.--Q'(3^1D) AND Q(3^1D) VS ELECTRON ENERGY

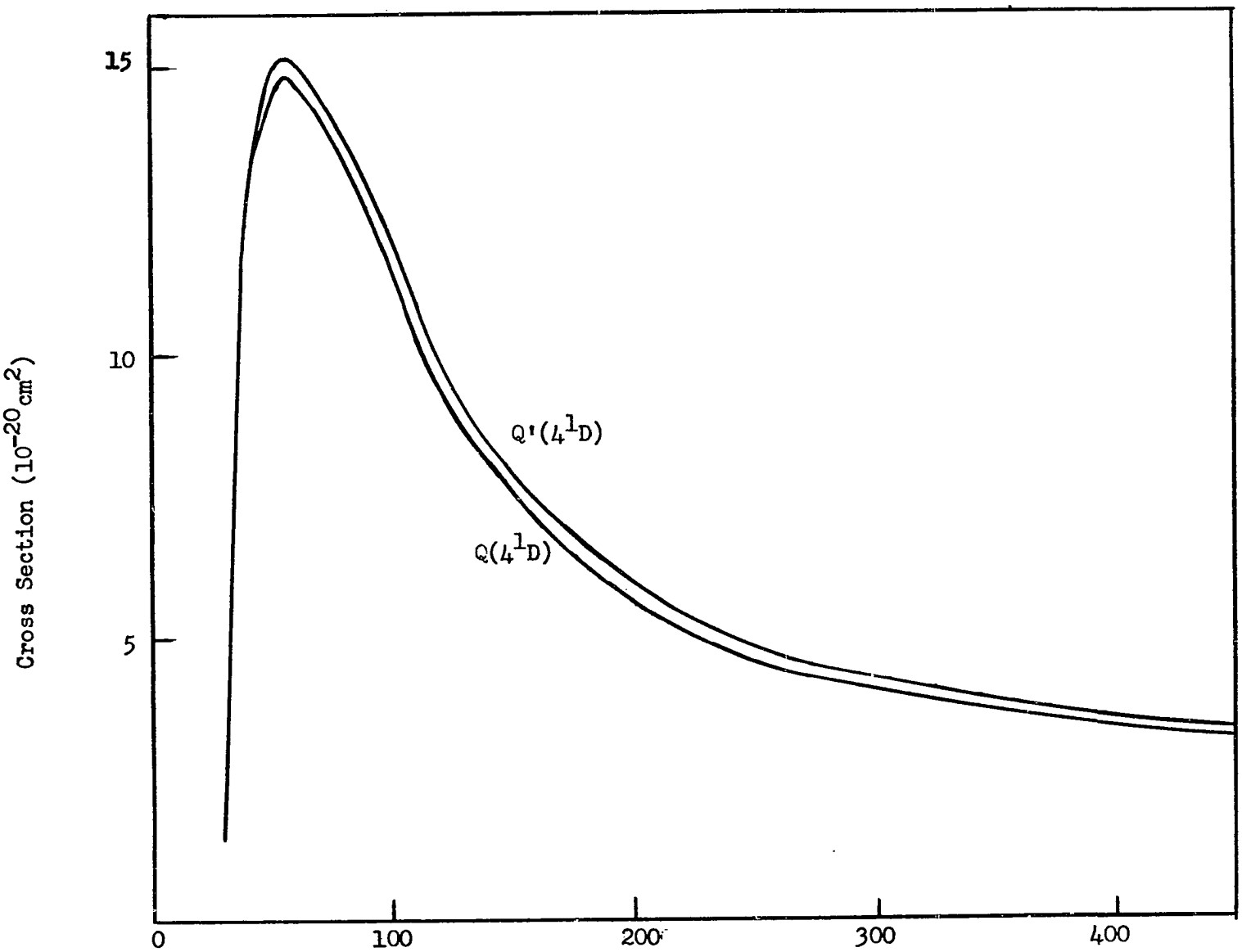


FIGURE 16.—Q'(4^1D) AND Q(4^1D) VS ELECTRON ENERGY

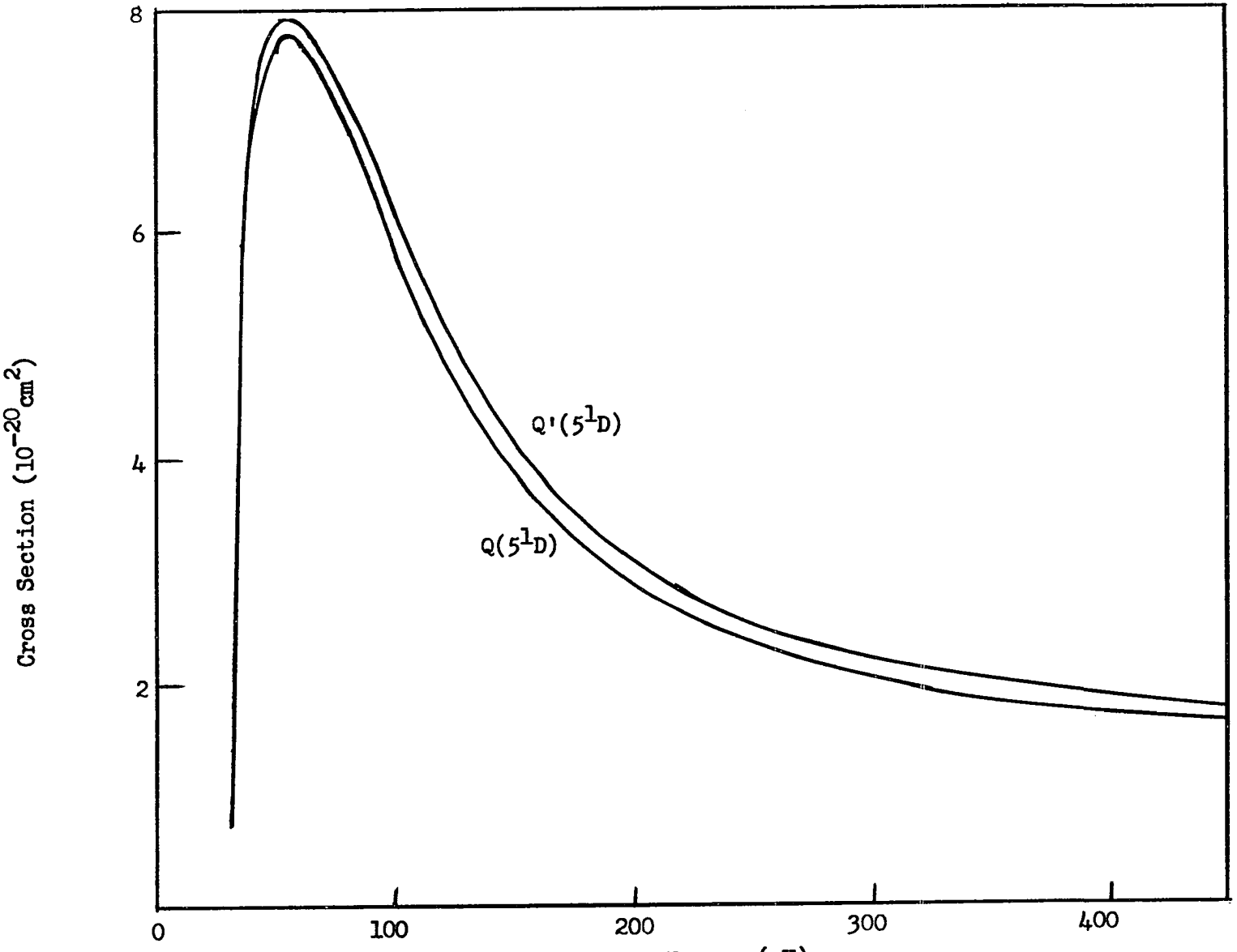


FIGURE 17.--Q'(5^1D) AND Q(5^1D) VS ELECTRON ENERGY

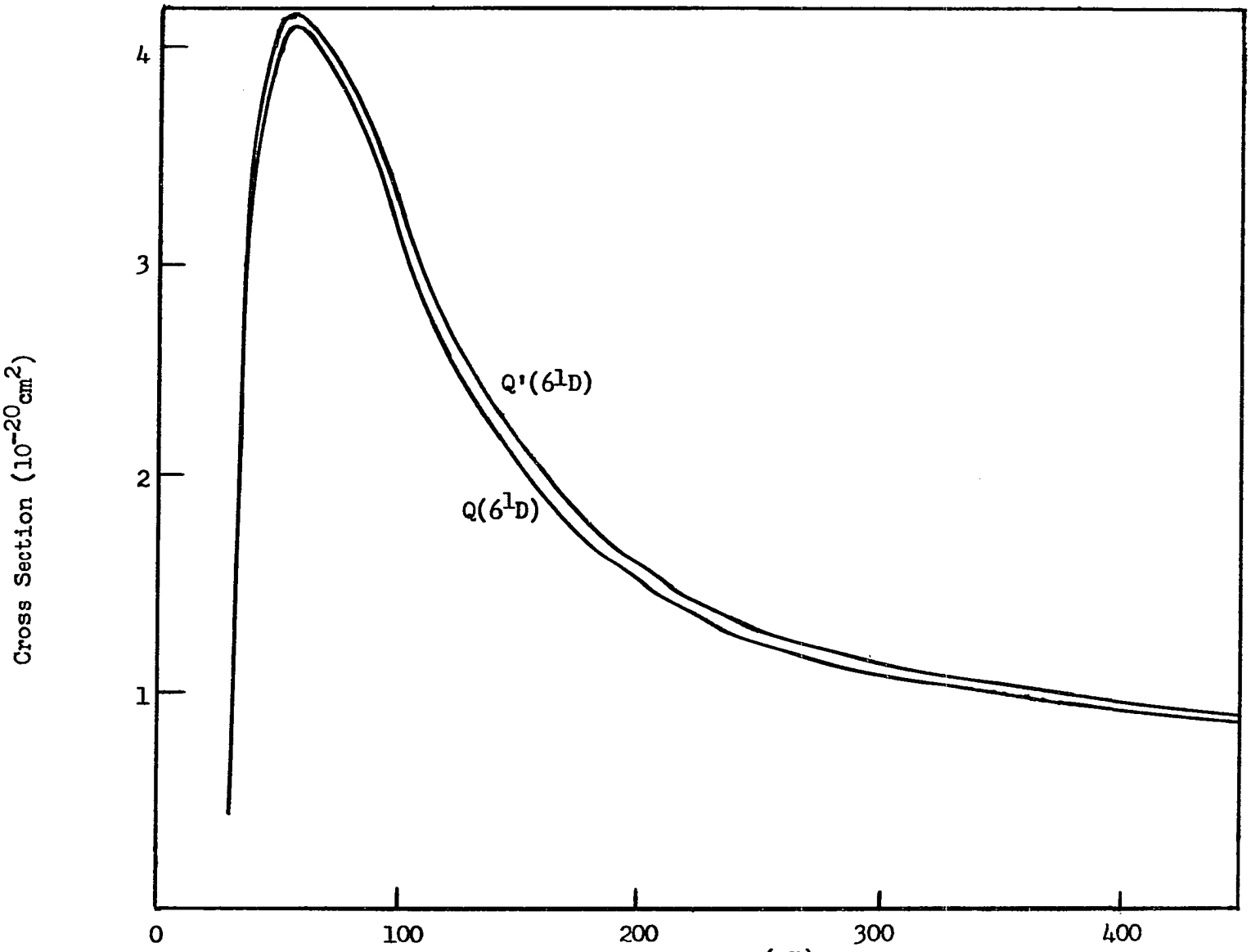


FIGURE 18.--Q'(6^1D) AND Q(6^1D) VS ELECTRON ENERGY

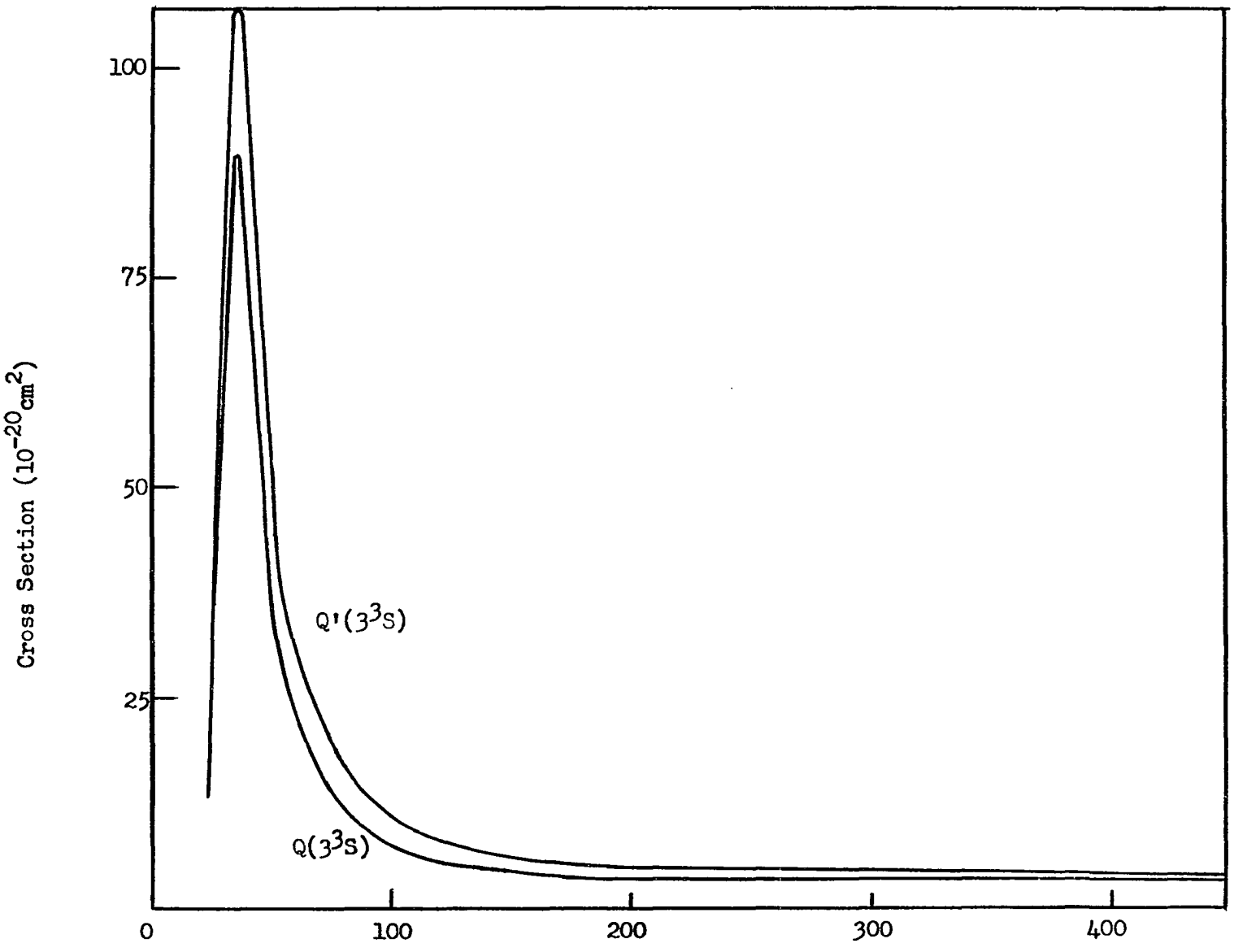


FIGURE 19.--Q'(3^3S) AND Q(3^3S) VS ELECTRON ENERGY

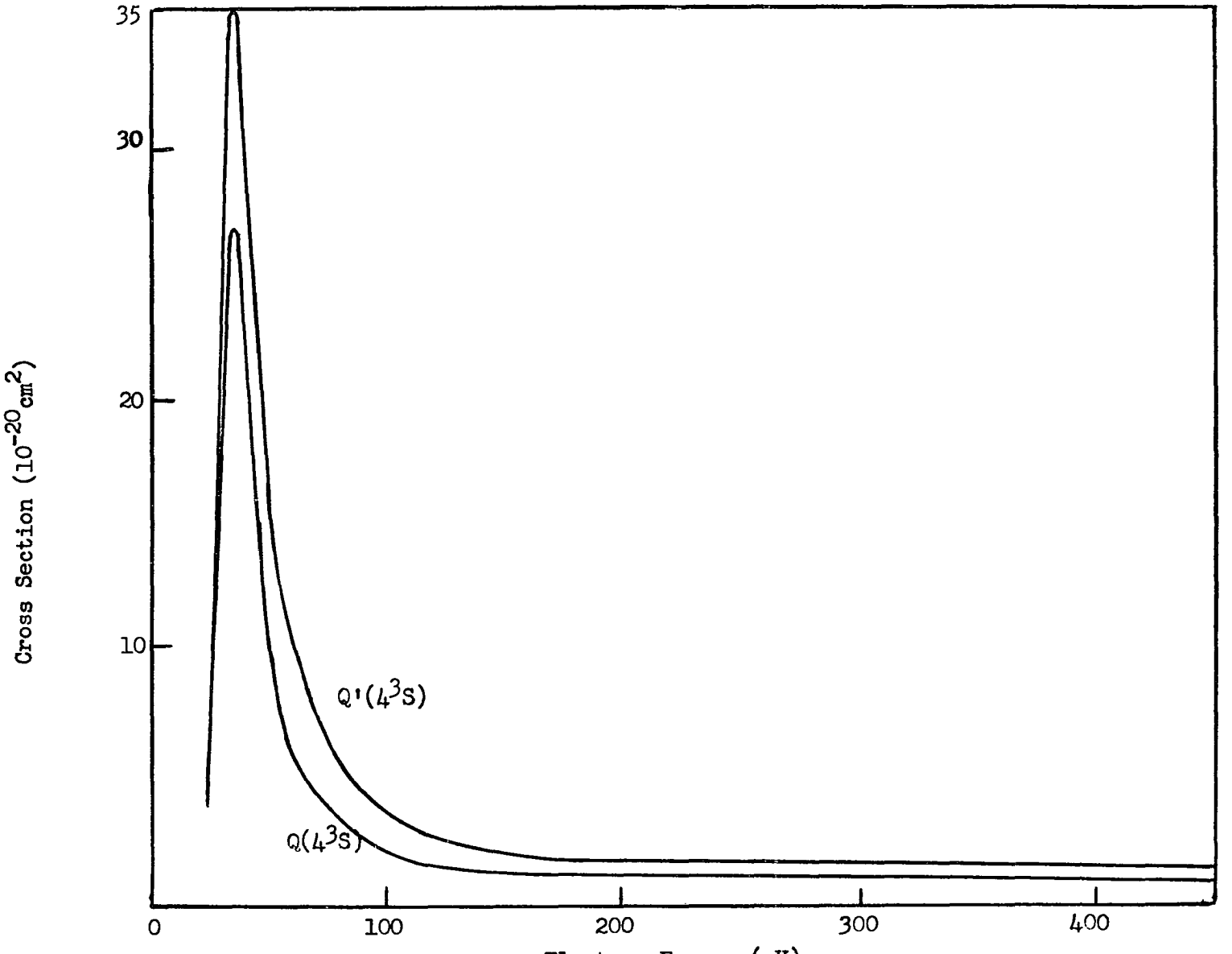


FIGURE 20.--Q'(4^3S) AND Q(4^3S) VS ELECTRON ENERGY

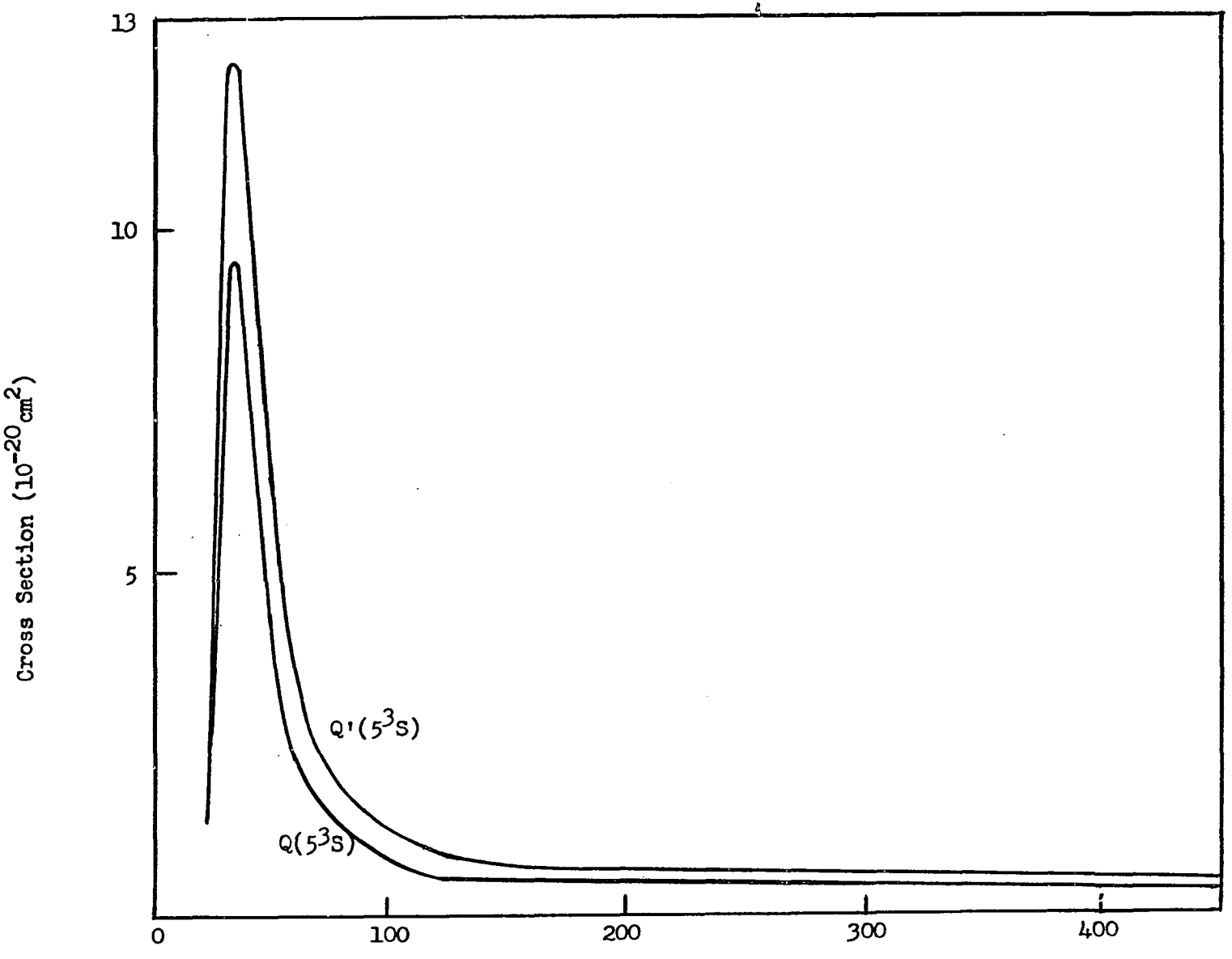


FIGURE 21.—Q'(5^3S) AND Q(5^3S) VS ELECTRON ENERGY

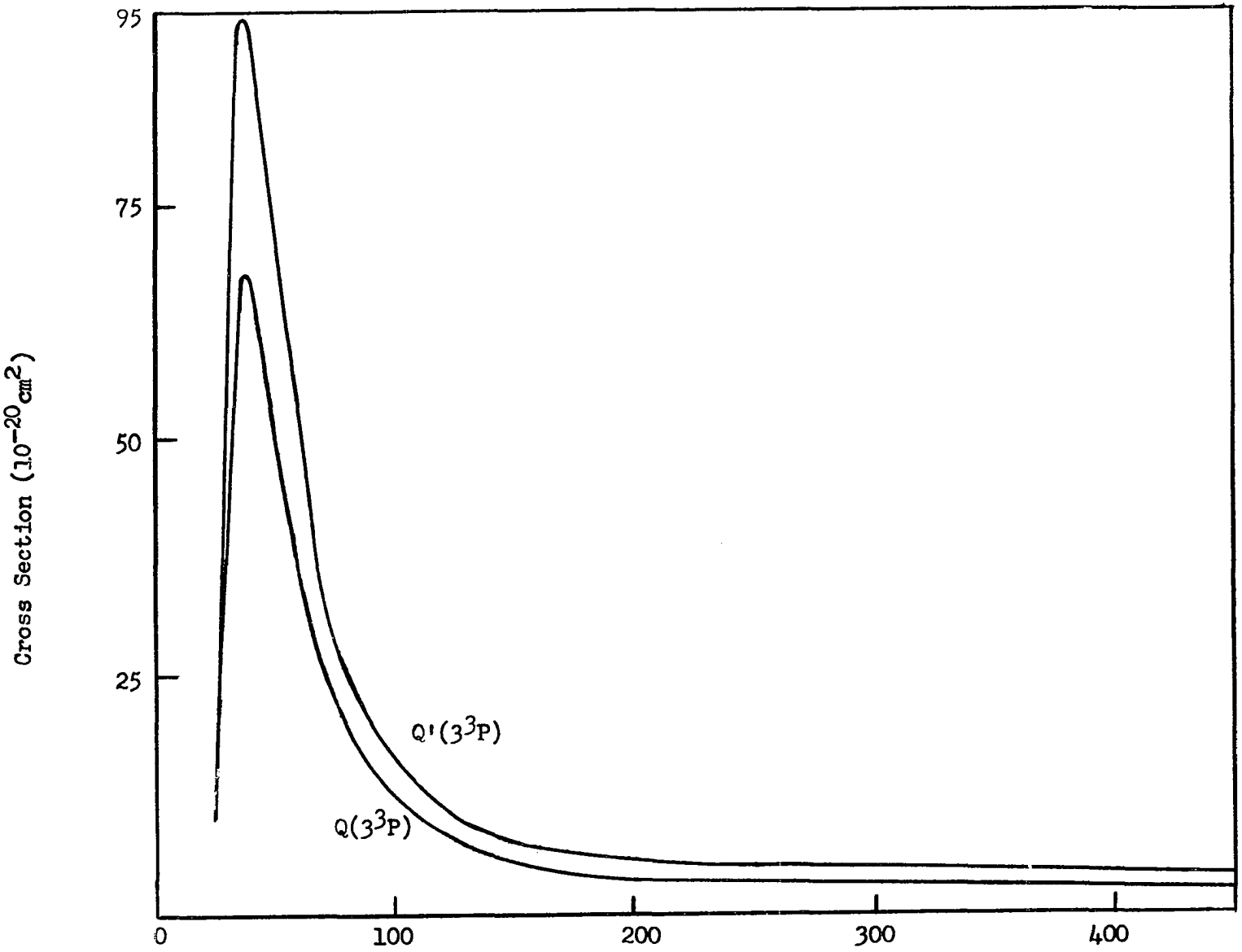


FIGURE 22.--Q'(3^3P) AND Q(3^3P) VS ELECTRON ENERGY

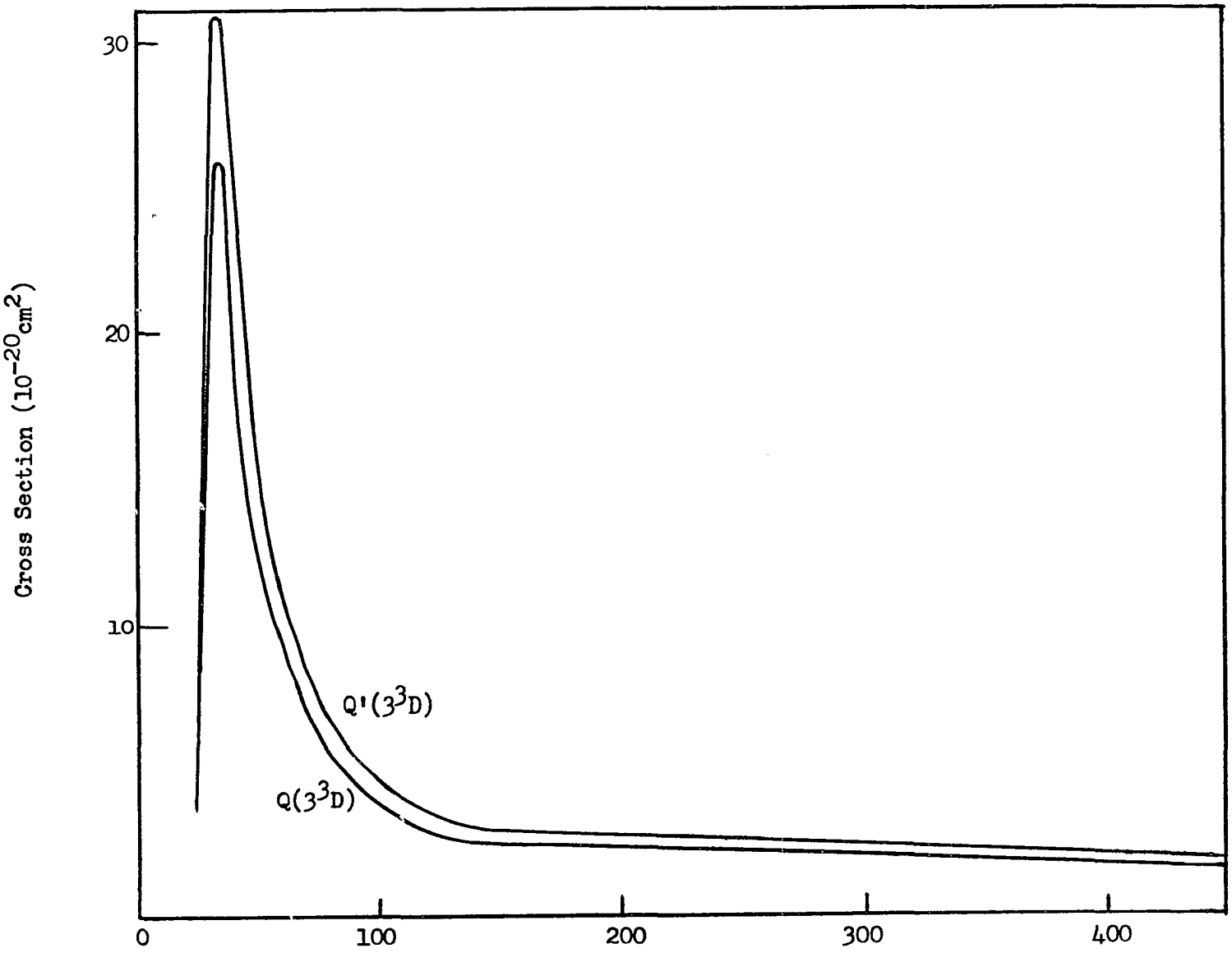


FIGURE 23.--Q'(3^3D) AND Q(3^3D) VS ELECTRON ENERGY

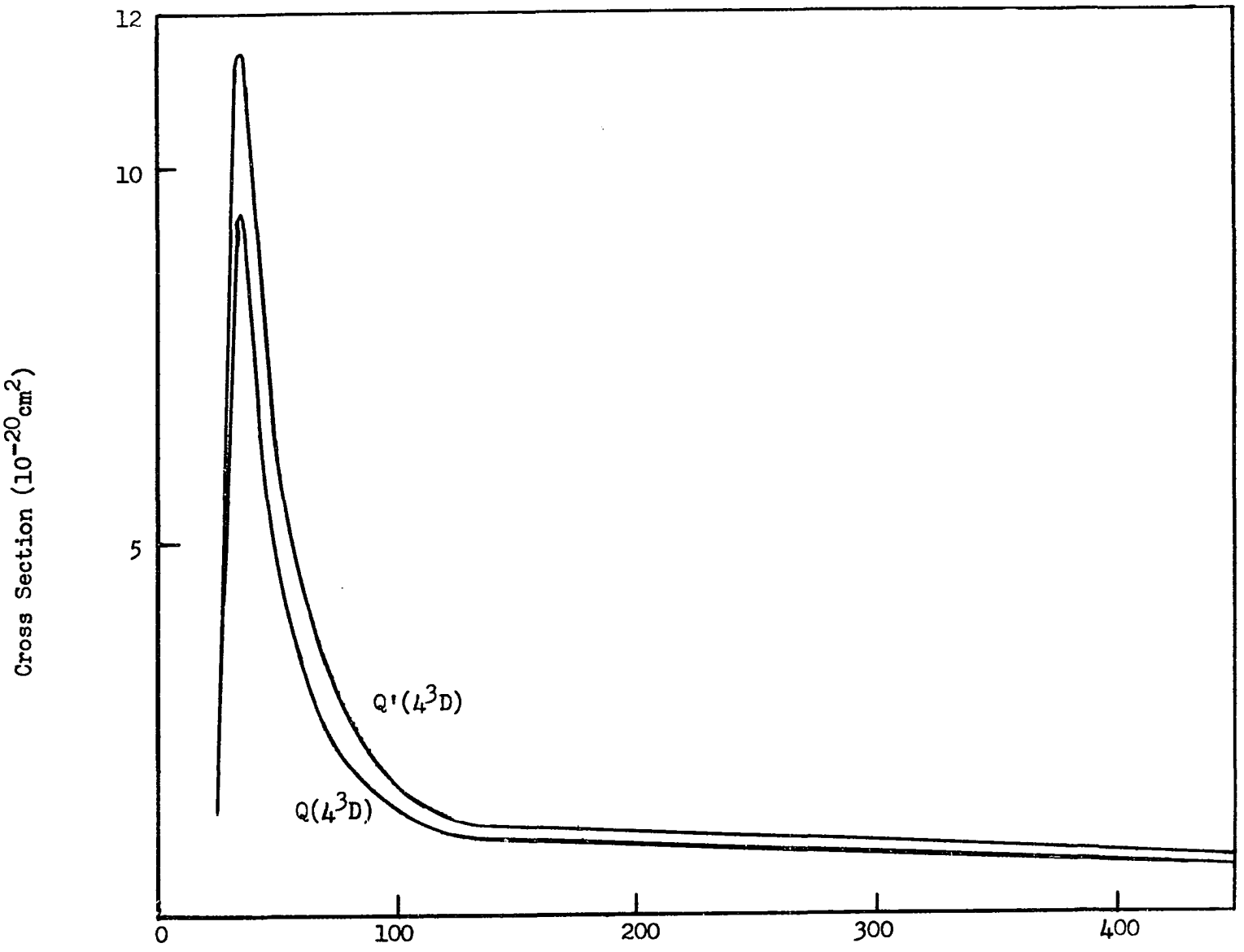


FIGURE 24.--Q'(4^3D) AND Q(4^3D) VS ELECTRON ENERGY

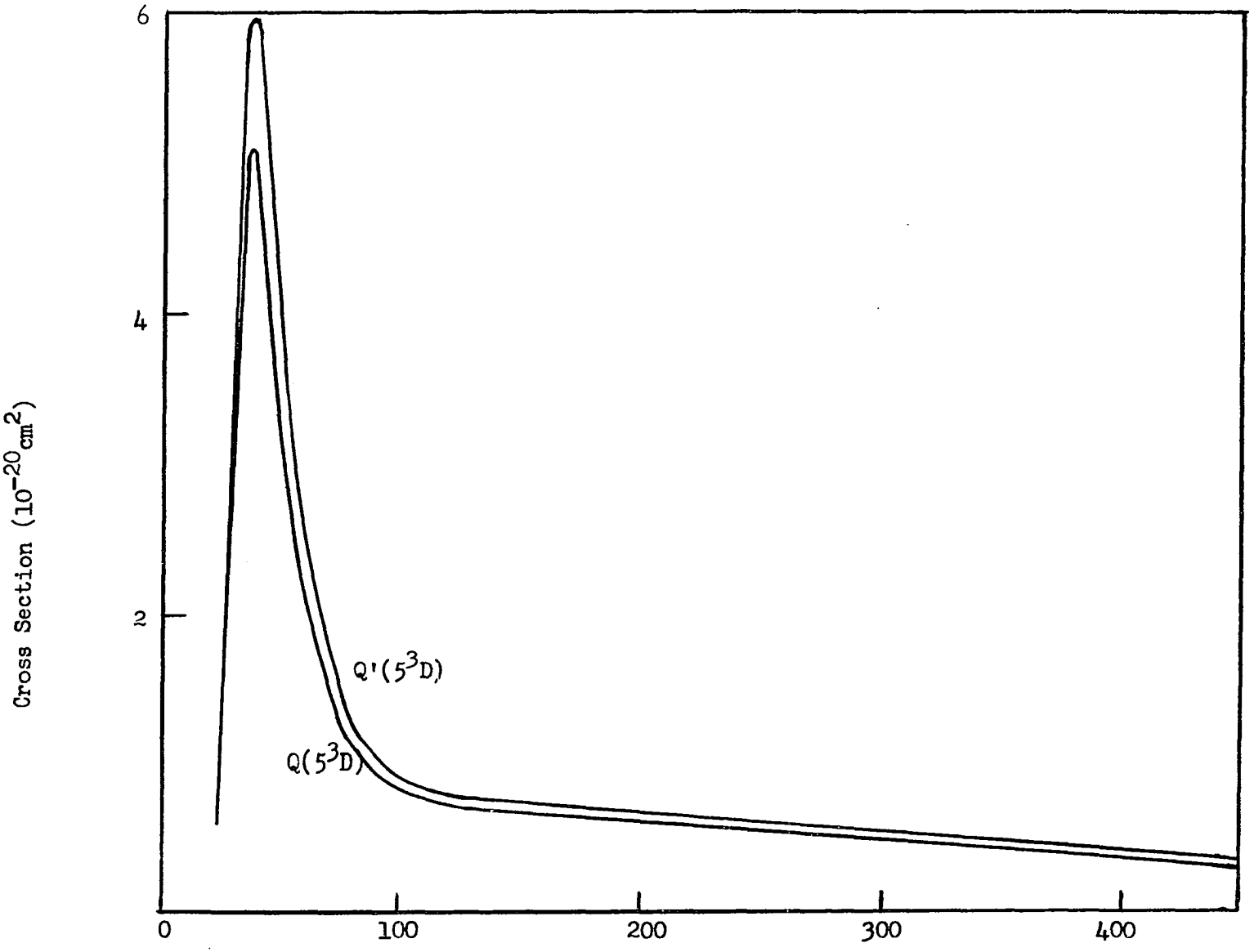


FIGURE 25.--Q'(5^3D) AND Q(5^3D) VS ELECTRON ENERGY

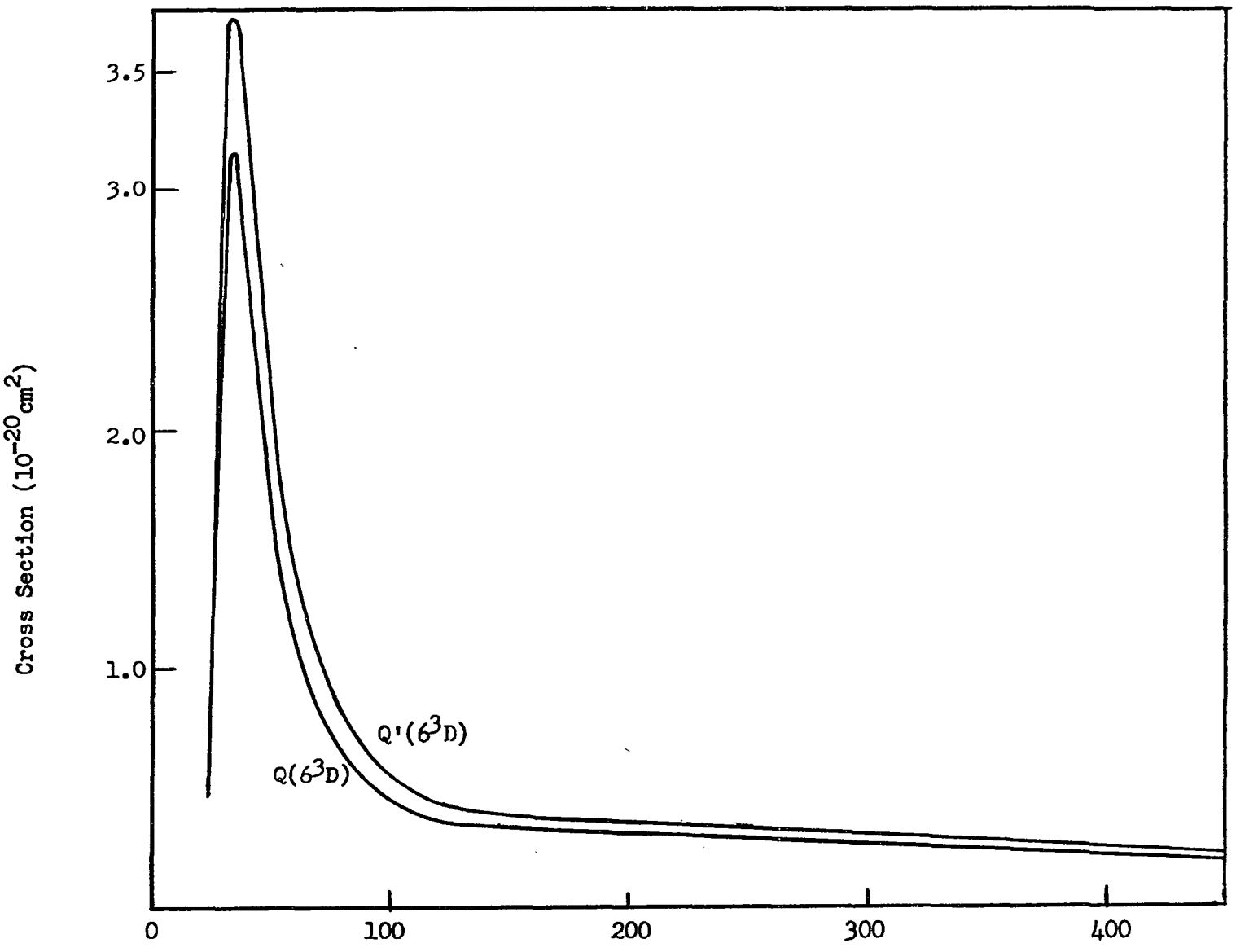


FIGURE 26.--Q'(6^3D) AND Q(6^3D) VS ELECTRON ENERGY

CHAPTER IV

TRANSFER OF EXCITATION

Since the excitation cross section of helium is independent of pressure for the primary process of direct excitation, one would expect the excitation functions to be identical at all pressures. This, however, is not the case. The n^1P excitation functions change little in relative shape but do increase in magnitude with increased pressure. This can be sucessfully accounted for by the previously mentioned process of imprisonment. A plot of $Q(n^1P)$ vs pressure shows various regions of imprisonment; none, partial and complete. See Figs. 5 and 6.

The n^3D excitation functions also show a change with increased pressure, both in magnitude and shape. See Fig. 27. The similarity in shape of the secondary peak that appears in n^3D at sufficiently high pressure and the n^1P excitation function leads to the belief that it might be due to a transfer of excitation from n^1P to n^3D by a mechanism similar to the following

$$He(1^1S) + He(n^1P) \longrightarrow He(n^3D) + He(1^1S)$$

Some investigators have assumed a transfer of this type[17] even though the Wigner spin conservation rule[18] is violated. St. John and Fowler[3] have proposed an alternative mechanism. Namely, that transfer of excitation occurs at high n levels, where LS coupling, and therefore the Wigner spin rule, is not so strong, by the following process

$$He(1^1S) + He(n^1P) \longrightarrow He(nF) + He(1^1S)$$

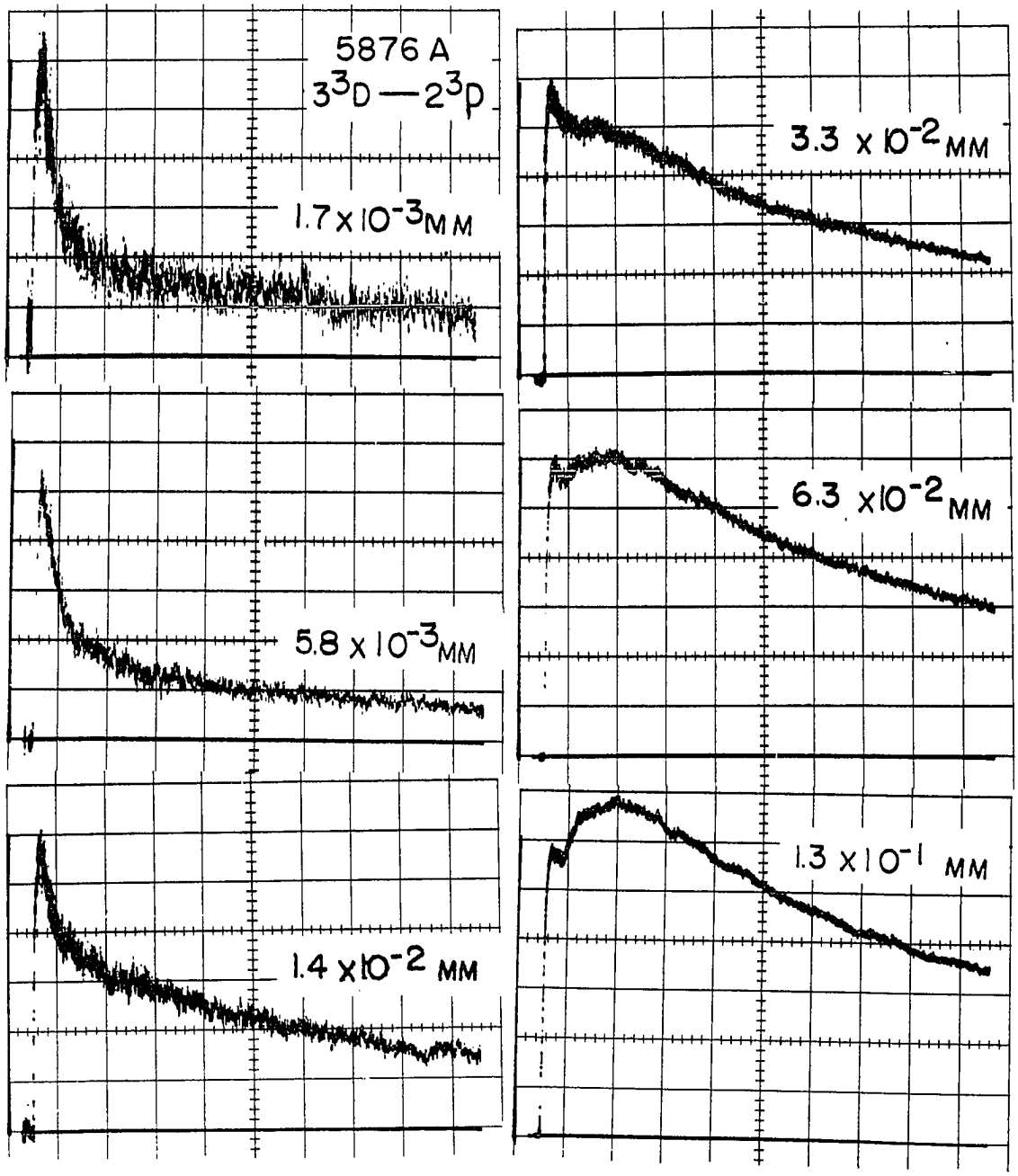


FIGURE 27.--3^3D EXCITATION FUNCTION AT VARIOUS PRESSURES

For high n values the n^1F and n^3F are expected to be mixed. Thus, the nF states can cascade to both the n^1D and n^3D states. The latter produces the observed excitation functions for n^3D.

St. John and Fowler[3] have shown that by this process the population of the triplet F states, $N(n^3F)$, is given by the expression

$$N(n^3F) = \frac{[Q'(n^1P) + Q'(n^3F)]\, INb/eSA(n^1P) + Q(n^3F)I/Q_t eS\bar{c}}{1 + bA(n^3F)/A(n^1P) + A(n^3F)/NQ_t\bar{c}}$$

where the symbols have the same meaning as used before in this dissertation with the addition of b, the ratio of the statistical weights of the n^3F and n^1P states; Q_t, the cross section for transfer of excitation; and $\bar{c}$, the mean relative speed of the helium atoms.

Then Q_t was calculated by the subtraction of the population rate due to direct excitation, available from low pressure data, and the population rate due to cascading from the n^3P levels from the observed n^3D population rate at high pressure and a given electron energy. This difference must be the population rate due to cascading from the n^3F levels. For example, consider

$$N(3^3D)A(3^3D) - Q(3^3D)NI/eS - \sum_{n=4}^{\infty} N(n^3P)A(n^3P \text{--} 3^3D) = \sum_{n=4}^{\infty} N(n^3F)A(n^3F \text{--} 3^3D)$$

The left hand side of the above equation consists of experimentally determinable quantities. Trial values of Q_t are then used to determine the right hand side. The value of Q_t which best satisfies the equation is found by a simple but tedious trial and error method.

The work of St. John and Fowler was done only for one electron energy, 100 eV. In order to more fully test the theory it was desired to determine Q_t by the above method for several electron energies over the range of the excitation function. Table XXII gives the values

for various electron energies of direct excitation rate, cascading rate from n^3P states, cascading rate from n^3F states including transfer, total excitation rate and experimentally observed total excitation rate. All quantities have been divided by collision chamber current and pressure in order to be able to compare results which are independent of these quantities.

A graphical comparison of experimental and theoretical excitation rates is shown in Fig. 28. Agreement is excellent in view of the fact that considerable extrapolation was involved. Most questionable is the value of $Q(n^3F)$ that was extrapolated as indicated previously.

The assumption of (n^1P) to (nF) transfer thus successfully explains the 3^3D excitation function at high pressure. In the same fashion the shift of the peak of the n^1D excitation functions at high pressure toward higher energies may be accounted for.

The fact that the high energy (100 eV to 400 eV) region of the n^3D apparent excitation functions at low pressure is higher relative to the peak values than in the other triplet excitation functions as shown in Fig. 8 might indicate some transfer is still occurring. However, a calculation of transfer of excitation to 3^3D resulted in a decrease of only 10% at 450 eV whereas a decrease of 90% was needed to produce an apparent excitation function of a shape similar to the n^3S and n^3P. The relatively high values at high energy should not therefore be attributed to transfer alone.

TABLE XXII

MEASURED AND CALCULATED 3^3D POPULATION RATES

Electron Energy (eV)	Calculated Population Rate $\frac{10^{16} \text{ atoms}}{\text{amp mm sec}}$				Measured Pop. Rate 10^{16} atoms / amp mm sec
	Direct	^3P Cascade	^3F Cascade	Total	
30	50.4	20.3	104.0	174.7	242.2
33	53.6	21.5	132.4	207.5	257.9
40	42.9	19.0	164.1	226.0	253.4
45	36.5	16.3	179.0	231.8	251.2
50	32.7	13.2	201.9	247.8	264.6
60	25.2	9.4	225.0	259.6	289.3
80	19.8	5.6	255.8	281.2	296.0
100	17.7	3.8	264.0	285.5	305.0
150	13.9	2.5	242.2	258.6	282.6
200	12.3	2.0	220.4	234.7	253.4
250	10.7	1.6	198.4	210.7	231.0
300	10.2	1.5	179.0	190.7	208.6
350	9.7	1.3	171.4	182.4	188.4
400	9.1	1.1	151.9	162.1	174.9
450	8.0	0.9	138.3	147.2	166.0

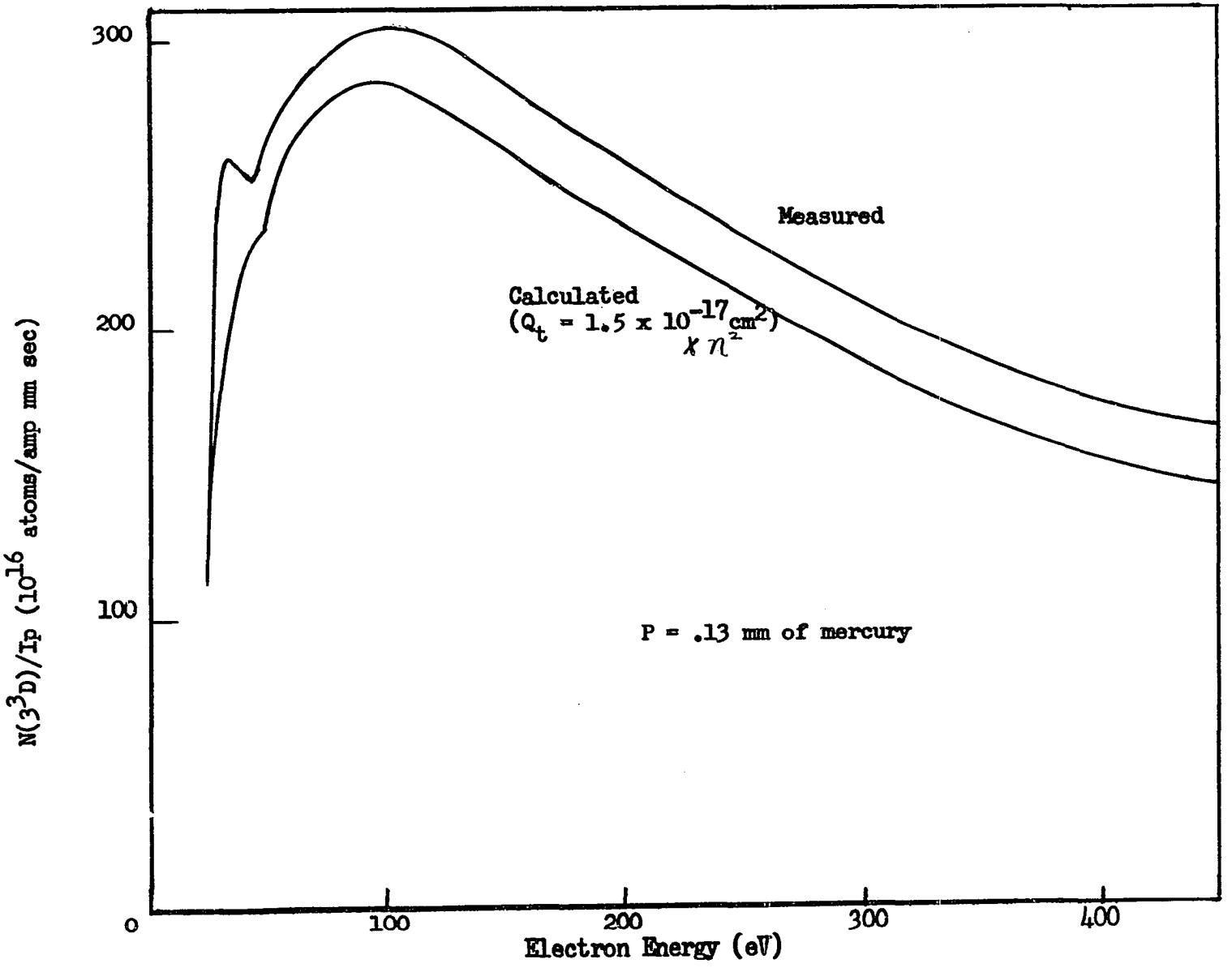


FIGURE 28.—MEASURED AND CALCULATED 3^3D POPULATION RATE

CHAPTER V

SECONDARY PEAKS IN CERTAIN EXCITATION FUNCTIONS AT HIGH PRESSURE

At pressures in excess of 200 microns, a secondary peak appears in the 3^3P, 4^1S, and 4^3S excitation functions as shown by Figs. 29, 30, and 31. In view of the success of the St. John, Fowler transfer theory in explaining secondary peaks in the n^3D excitation functions at high pressure, attempts were made to find a similar transfer mechanism to account for these other secondary peaks. First, it was determined that cascading from neighboring levels, even considering the change in the shape of their excitation functions at high pressure, could not account for the secondary peak in the 3^3P excitation function. Next, transfer of excitation from ^1D to ^3D levels and ^1D to ^3S levels was assumed without success. In order to account for secondary peaks of sufficient magnitude, unreasonably high values of transfer cross section had to be assumed. The assumption of these values resulted in a primary peak in the 3^3P excitation function far larger than that observed. Thus, transfer mechanisms do not seem to explain the secondary peaks.

The fact that the energy of the secondary peak is approximately twice that of the primary peak suggests the possibility of multiple collisions of electrons in the beam. A study of the variation of $I_{PM}(cc)$ for light from the transition from the 3^3P level with I at various energies revealed no marked non-linearity. Therefore, it can be assumed that multiple collisions in the 2.9 mm length of the beam that is viewed are negligible.

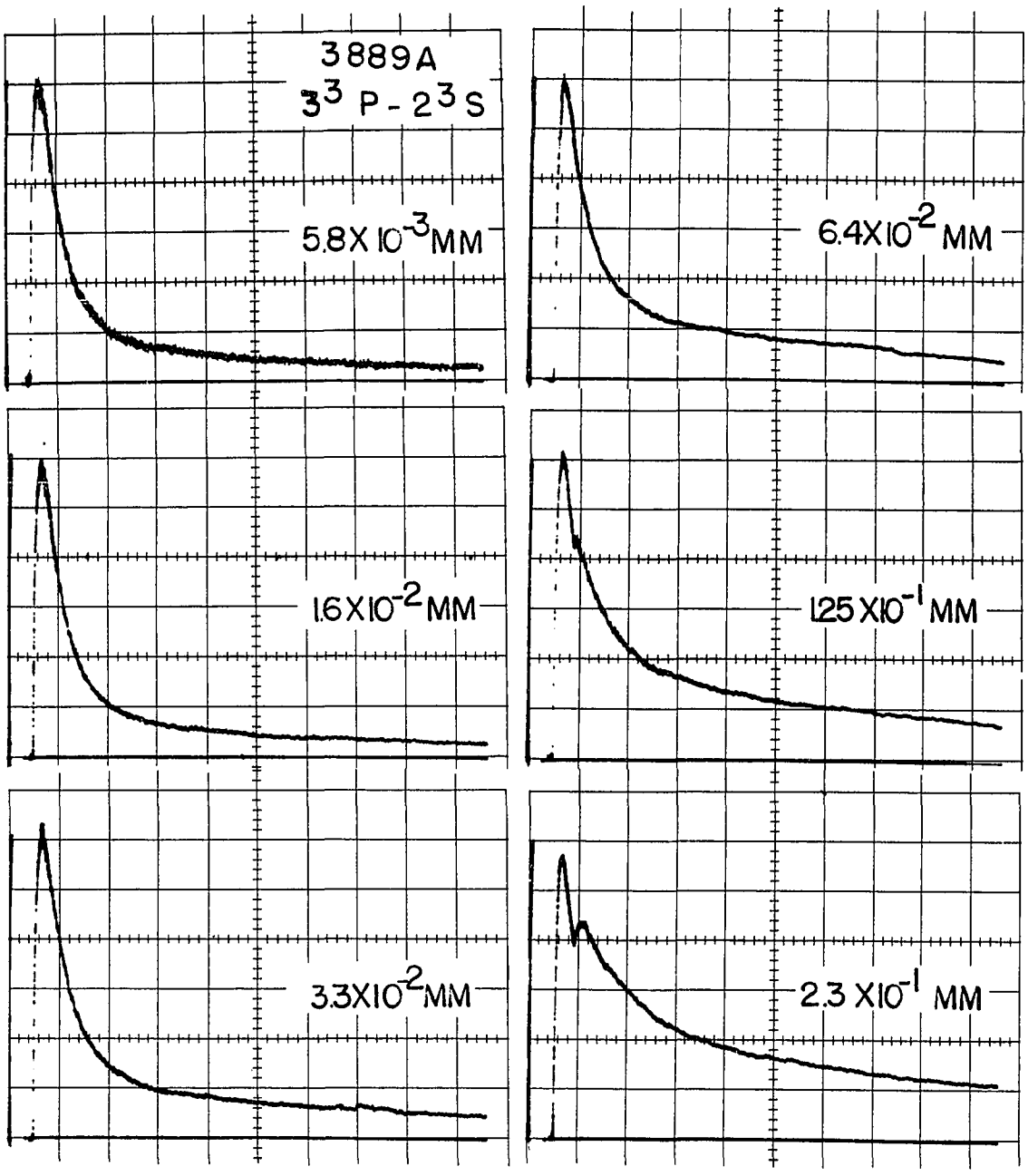


FIGURE 29.--3^3P EXCITATION FUNCTION AT VARIOUS PRESSURES

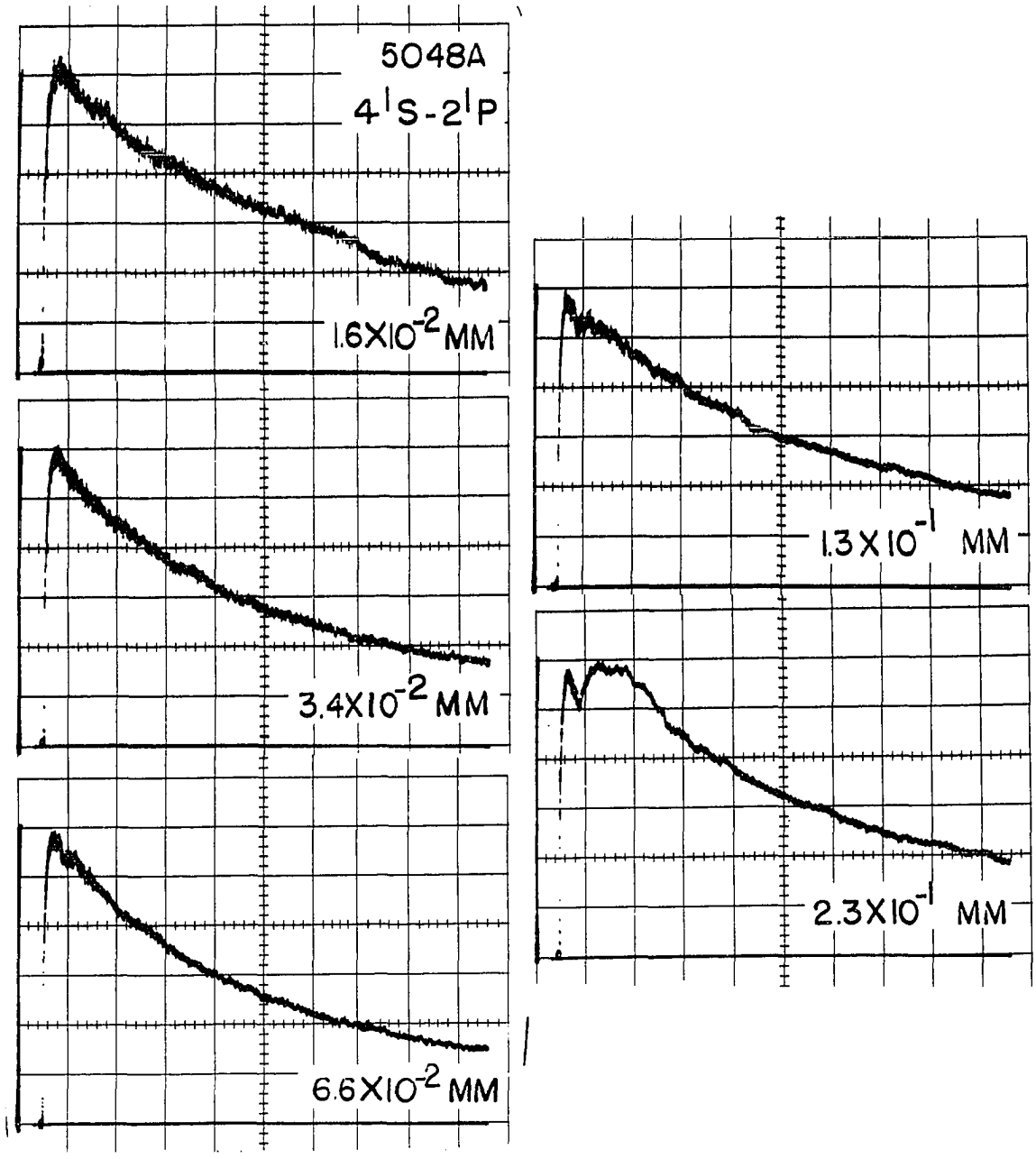


FIGURE 30.--4^1S EXCITATION FUNCTION AT VARIOUS PRESSURES

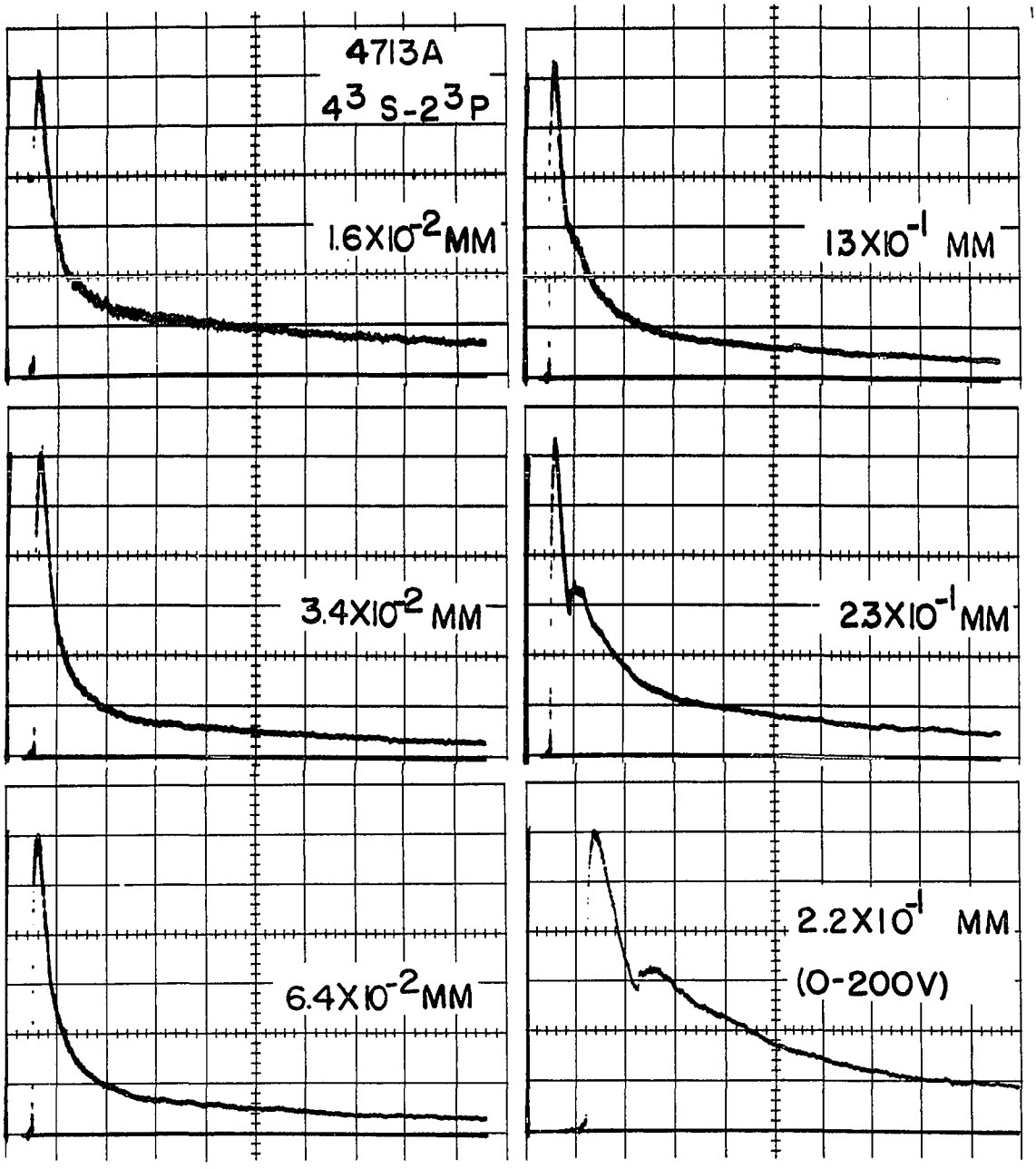


FIGURE 31.--4^3S EXCITATION FUNCTION AT VARIOUS PRESSURES

Consideration must be given to the fact that the distance from the cathode to the viewed portion of the beam is 12.5 mm. This might allow high energy electrons to undergo inelastic collisions with helium atoms, thereby losing some of their energy prior to reaching the viewed portion of the beam. They then would have a higher probability of undergoing subsequent inelastic collisions in the viewed section of the collision chamber due to their having energies closer to those corresponding to the maximum of the excitation function. At low pressures the number of such events would probably be negligible. However, at higher pressures, this might become an appreciable effect.

An approximate total maximum apparent excitation cross section for helium can be estimated in the following way. Estimate the value of the apparent cross section for each energy level by assuming they decrease as $1/n^3$ and extrapolate from the measured values having a given orbital quantum number L. This procedure results in the following estimates for a pressure of 2.3×10^{-1} mm of mercury:

$$Q''(n^1S) \cong 1.4 \times 10^{-17}/n^3 \text{ cm}^2$$

$$Q''(n^1P) \cong 1.1 \times 10^{-16}/n^3 \text{ cm}^2$$

$$Q''(n^1D) \cong 1.2 \times 10^{-17}/n^3 \text{ cm}^2$$

$$Q''(n^3S) \cong 1.9 \times 10^{-17}/n^3 \text{ cm}^2$$

$$Q''(n^3P) \cong 2.5 \times 10^{-17}/n^3 \text{ cm}^2$$

$$Q''(n^3D) \cong 7.7 \times 10^{-18}/n^3 \text{ cm}^2$$

Integrating these quantities over all allowed values of n and summing results in the following approximation for the total apparent maximum excitation cross section for helium

$$Q'' \cong 2 \times 10^{-16} \text{ cm}^2$$

One can then define a mean free path between inelastic collisions for helium by

$$\bar{\lambda} \cong 1/NQ''$$

Since N is obtained from the relation

$$p = NkT$$

it follows that

$$\bar{\lambda} \cong kT/pQ''$$

Substituting the proper values one obtains for a pressure of 2.3×10^{-1} mm

$$\lambda \cong 7 \text{ mm}$$

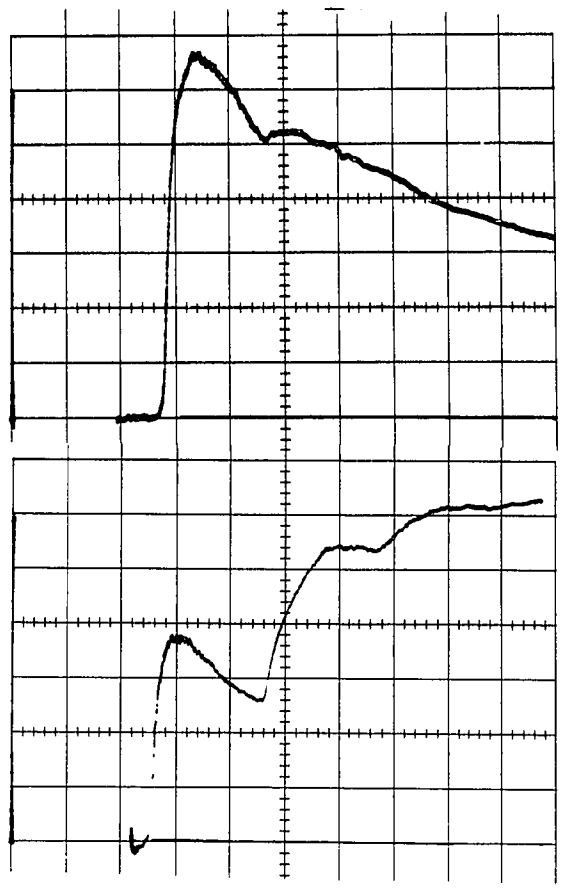
In view of the crudeness of the approximations involved, the most that can be said is that the mean free path is of the same order of magnitude as the distance from the cathode to the viewed portion of the beam. It is conceivable then that at this pressure an appreciable number of high energy electrons will undergo an inelastic collision with a helium atom prior to reaching the viewed portion of the beam and subsequently another collision in that portion. Thus, a fraction of the light examined would have been the result of excitation collisions between helium atoms and electrons with a significantly lower energy than the accelerating energy of the electron gun.

The fact that some apparent cross sections decrease with an increase in pressure, notably $Q''(3^3P)$ as shown in Fig. 7, lends credence to the above analysis. At sufficiently high pressures an appreciable number of electrons could be scattered from the beam by elastic and inelastic collisions resulting in a measured value of

electron beam current, I, that is too high and a value of apparent cross section, Q'', that is too low. This effect would be noticeable only in excitation functions that are not affected by imprisonment or transfer which are effects of a much greater magnitude.

If the above analysis is correct, one would then expect that at still higher pressures more pronounced increases in apparent cross sections and possible additional peaks would occur in the excitation functions for high electron energies. Excitation functions obtained for the 3^3P level at pressures of .198 mm and .6 mm are shown in Fig. 32. They exhibit the expected characteristics. These effects might therefore reasonably be attributed to departures from a monoenergetic electron beam at relatively high helium pressures.

3889 3^3P--2^3S
0.198 mm



3889 3^3P--2^3S
0.6 mm

FIGURE 32.--3^3P EXCITATION FUNCTION AT HIGH PRESSURE

CHAPTER VI

COMPARISON WITH OTHER EXPERIMENTAL WORK

The apparent electron excitation functions of helium have been measured by Lees[6], Thieme[7], Yakhontova[8], McFarland and Soltysik[9], and Heddle and Lucas.[10] Of these Lees, Thieme, and Yakhontova determined absolute cross sections. Additionally Stewart and Gabathuler[11] have determined the peak values of the cross sections of several helium levels. Gabriel and Heddle[1] determined the cross sections for 108 eV electrons for a number of helium levels.

The observations by Thieme, Yakhontova, Heddle and Lucas, Gabriel and Heddle, and Stewart and Gabathuler were at pressures low enough to greatly reduce transfer effects. Of these Thieme and Stewart and Gabathuler, however, did not work at pressures low enough to eliminate imprisonment of resonance radiation and thus their absolute determinations of the 3^1P cross sections are abnormally high. All observers worked at pressures low enough that light emission from ^1S, ^3S, and ^3P states was linear with pressure. All observers cited, including the work reported in this dissertation, observed the excitation chamber in a direction normal to the electron beam. Thus all apparent cross sections determined at low pressures are subject to the same corrections required for polarization and cascade.

Table XXIII shows the peak absolute values of the apparent cross sections of helium levels measured in this work and by Yakhontova, Stewart and Gabathuler, Lees, and Thieme. Some of

TABLE XXIII

COMPARISON OF EXPERIMENTAL APPARENT CROSS SECTIONS

All cross sections are expressed in units of $10^{-20} cm^2$.

Level	Cross Section at Peak					Cross Section at 108 eV	
	This Work	Yakhontova	Stewart and Gabathuler	Lees	Thieme	This Work	Gabriel and Heddle
3^1S	49					31	36
4^1S	24	20	27.5		28	15	16.5
5^1S	9.2	7.7	10.0	5.9	16.5	6.1	7.0
6^1S	4.8		6.1	2.8	9.5	3.0	4.0
3^1P	350		4130	4360	3660	350	457
4^1P	159		950	1270	1080	158	210
3^1D	42					24	25
4^1D	17.6	17.8	24	15.1	32	12	12
5^1D	9.0	8.5	12.2	9.3	18.6	6.2	7.1
6^1D	4.7	5.0	6.9		9.9	3.3	3.0
3^3S	107					10.2	15
4^3S	35	25	37	36	64	3.3	4.4
5^3S	12.3	12.7	17.2	8.6	40	1.17	1.44
3^3P	97	83	105	80	1890	15.3	11
3^3D	31	36	45		42	4.3	25
4^3D	12.0	12.4	18	15.2	23	1.64	4.6
5^3D	6.2	8.5	7.1			0.89	3.0
6^3D	3.9		4.3			0.53	1.5

these experimenters published values for cross sections for excitation of a given line transmitted from a given level. By use of the branching ratio one can readily obtain the cross section for excitation to the upper level involved. The transition probabilities of Gabriel and Heddle were used for determining the branching ratios and thus level cross sections were obtained as displayed in Table XXIII. Stewart and Gabathuler listed both line and level cross sections. Due to the fact that they used branching ratios differing from those produced by the Gabriel and Heddle transition probabilities, their level cross sections show some slight variation from those listed. Table XXIII also shows the values obtained in this work and those of Gabriel and Heddle at an electron energy of 108 eV.

The measurements of Yakhontova are consistent with those reported herein. The ratio of Yakhontova's peak cross sections to ours averages .99 and each lies within the range of .83 to 1.16 with the exception of the 4^3S and 5^3D cross sections. In those cases the factors were .77 and 1.37. This rather good agreement throughout the levels including ^1D and ^3D verifies that the pressures used in both investigations were below those which cause transfer effects. Yakhontova determined the absolute value of the peak cross section of lines from the 3 and 4^1P levels by operating at a gas pressure high enough to cause complete imprisonment (which would yield a value near that of the level cross section) and then determined the line cross sections (5016A and 3965A) by dividing by the appropriate branching factor. Due to a spreading of the beam with increasing imprisonment which is concommitant with increasing pressure, the

measured line intensity will not increase as much as the branching ratio when imprisonment changes from nil to its full value. Thus the line cross sections given by Yakhontova were not converted back to level cross sections and hence are not tabulated in Table XXIII.

Stewart and Gabathuler do not quote directly the pressures used in their determinations of the apparent cross sections, but were well aware of the pressure effects as they gave intensity vs pressure curves. Some of that data was obtained in the 2 micron range and we can assume the sensitivity of their equipment allowed them to obtain the maxima of the apparent cross sections at about that pressure. Their relative consistency with our data for ^1D and ^3D indicates that they were able to minimize the transfer of excitation effects. Their values for 3^1P and 4^1P are very large and indicate an imprisonment effect as one expects at a pressure of 2 microns. Disregarding the ^1P data the ratio of their cross sections to ours averaged 1.26 and varied within the limits of 1.06 to 1.50.

The data of Lees is in serious disagreement with our results for the 3^1P, due to his use of pressures in the 40 micron range. His peak apparent cross sections for the ^1S, ^1D, ^3S, ^3D, and ^3P levels compared to our values by a ratio averaging .86.

The data of Thieme compared to ours shows quite a variety of cross section ratios; his extremely high value for excitation of the 3^1P level is at least in part due to imprisonment effects. His very large value for the 3^3P level defies explanation other than through erroneous calibration procedures. Lees' and Thieme's data were obtained by photographic techniques and hence more subject to errors than the

photoelectric data of the other investigators cited. The magnitudes of Thieme's data will be given no further consideration.

Gabriel and Heddle measured absolute values of the cross sections for 17 helium levels at pressures apparently low for all except the ^3D levels. The ratios of their apparent cross sections to ours averaged 1.12 for ^1S, ^1P, ^1D, ^3S, and ^3P levels, and lay within the range of .76 to 1.37. The ^3D ratio varied up to 3.4 indicating a transfer fill in for the cross sections of Gabriel and Heddle.

A comparison of the shapes of the excitation functions is presented in Tables XXIV and XXV. Each excitation function has been normalized to unity for an electron energy of 100 eV. Included are the data of Yakhontova, Lees, Thieme, McFarland and Soltysik, Heddle and Lucas, and this present work. It can be seen that there is quite good agreement between the shape data presented herein and that of Yakhontova. This is the result of both sets of data being obtained under low pressure conditions. The shapes of the ^1D and ^3D curves of Lees are modified by the ^1P fill in due to his use of relatively high gas pressure. The curves of Thieme are quite similar to those presented herein, a fact derived from the low helium pressures used by him. McFarland and Soltysik obtained their functions with a gas pressure of 10 to 20 microns and thus their curves show some transfer effects. The curves of Heddle and Lucas, while obtained at a pressure of about 1 micron, do not show very good agreement with the curves of the other experimenters.

Frost and Phelps[19] made determinations of cascade contributions.

TABLE XXIV

SHAPE COMPARISON OF EXPERIMENTAL APPARENT EXCITATION FUNCTIONS

	This Work					Yakhontova				Lees				
Level	Peak	60	100	200	400	Peak	60	100	200	Peak	60	100	200	400
3^1S	1.53	1.28	1.00	0.68	0.49									
4^1S	1.55	1.26	1.00	0.66	0.42	1.33	1.08	1.00	0.79					
5^1S	1.45	1.25	1.00	0.68	0.38	1.54	1.23	1.00	0.79	1.55	1.29	1.00	0.73	0.43
6^1S	1.52	1.31	1.00	0.66	0.39					1.38	1.26	1.00	0.52	
3^1P	1.00	0.83	1.00	0.85	0.58	1.00	0.88	1.00	0.85	1.06	0.85	1.00	0.85	0.58
4^1P	1.00	0.76	1.00	0.87	0.60	1.00	0.86	1.00	0.84	1.16	0.94	1.00	0.85	0.60
3^1D	1.73	1.50	1.00	0.51	0.30									
4^1D	1.34	1.32	1.00	0.47	0.28	1.49	1.37	1.00	0.60	1.28	1.13	1.00	0.70	0.47
5^1D	1.34	1.32	1.00	0.47	0.28	1.51	1.40	1.00	0.56	1.13	0.96	1.00	0.72	0.47
6^1D	1.34	1.32	1.00	0.47	0.28	1.63	1.43	1.00	0.51					
3^3S	9.7	2.9	1.00	0.48	0.40									
4^3S	9.7	2.9	1.00	0.48	0.40	10.6	2.6	1.00	0.67	20.8	2.7	1.00		
5^3S	9.7	2.9	1.00	0.48	0.40	12.2	2.7	1.00	0.58	15.5	3.2	1.00		
3^3P	5.7	3.1	1.00	0.34	0.24	8.0	1.75	1.00	0.50	6.3	2.4	1.00	0.40	0.25
3^3D	6.9	2.7	1.00	0.65	0.48	4.0	1.46	1.00	0.63					
4^3D	6.9	2.7	1.00	0.65	0.48	4.9	1.85	1.00	0.69	1.10	1.09	1.00	0.76	0.5
5^3D	6.7	3.0	1.00	0.77	0.50	2.3	1.35	1.00	0.82					
6^3D	6.9	2.7	1.00	0.65	0.48									

TABLE XXV

SHAPE COMPARISON OF EXPERIMENTAL APPARENT EXCITATION FUNCTIONS

	Thieme					McFarland and Soltysik				Heddle and Lucas			
Level	Peak	60	100	200	400	Peak	60	100	200	Peak	60	100	200
3^1S													
4^1S	2.02	1.40	1.00	0.66	0.41					1.6	1.2	1.00	0.77
5^1S	1.69	1.35	1.00	0.61	0.35								
6^1S	2.50	1.61	1.00	0.51	0.35								
3^1P	1.01	0.87	1.00	0.82	0.53	1.03	0.98	1.0	0.59	1.1	1.1	1.00	0.84
4^1P	1.01	0.85	1.00	0.79	0.42								
3^1D						1.08	1.06	1.00	0.63				
4^1D	1.70	1.40	1.00	0.57	0.55	1.40	1.35	1.00	0.44	1.75	1.68	1.00	0.56
5^1D	1.54	1.30	1.00	0.53	0.31	1.55	1.39	1.00	0.47				
6^1D	1.77	1.42	1.00	0.59	0.34								
3^3S													
4^3S	14.6	2.62	1.00	0.18	0.14	14.9	3.6	1.00	0.29	14.0	2.0	1.00	0.77
5^3S	13.5	2.82	1.00	0.24	0.14								
3^3P	10.2	3.0	1.00	0.28	0.12	6.1	2.8	1.00	0.33	12.0	3.9	1.00	0.38
3^3D	4.42	1.95	1.00	0.52	0.38	2.38	1.33	1.00	0.76				
4^3D	4.30	1.78	1.00	0.5	0.28	2.46	1.50	1.00	0.55	12.0	2.75	1.00	0.47
5^3D													
6^3D													

They estimated that no correction was necessary for the ^1S and ^1D curves. They obtained a 10% correction for the 3^1P and 4^1P levels at 100 eV. The triplet curves, at the peak of the excitation function, were populated by cascade as follows: 4^3S, 4%; 3^3P, 49%; 3^3D, 4^3D, 5^3D all 10%.

Gabriel and Heddle determined cascade corrections for electron energies of 108 eV. The 4^1S level population was 2% due to cascading. Higher ^1S level populations were regarded as entirely caused by electron impact. Singlet P populations were assumed free of cascade effects. The 3^1D level was found to have 4% of its population due to cascade, but higher ^1D unaffected by cascade. The triplets were populated by cascade as follows: 4^3S, 23%; 5^3S, 7%; 3^3P, 34%; 3^3D, 4%; 4^3D, 17%; 5^3D, 17%.

CHAPTER VII

COMPARISON WITH THEORY

The theory of excitation of helium atoms by electron impact has been treated rather extensively in the literature. Massey and Mohr[16] calculated the excitation cross sections for the 2^1S, 3^1S, 2^1P, 3^1P, 4^1P, 5^1P, 3^1D, 4^1D, 5^1D, and 4^1F states by the Born approximation and for the 2^3S, 3^3P, 4^3P, and 3^3D states using the Born-Oppenheimer approximation for incident electrons of various energies (60, 100, 200, and 400 eV). Curves for the theoretical excitation functions for the 3^1S, 3^1P, 4^1P, 4^1D, 5^1D, and 2^3S states were also included in this work. Bates et. al.[20] have given a critical analysis of the Born and Born-Oppenheimer approximation along with additional results of cross sections for some of the low-n states of helium. As an improvement over the Born-Oppenheimer approximation, cross sections for the 1^1S to 2^1S, 1^1S to 2^3S, and 1^1S to 2^3P transitions have been calculated by Massey and Moiseiwitsch[21] using the method of EPW. Unpublished calculations by Fox on the excitation cross sections of several ^1S states were quoted in the paper of Gabriel and Heddle[1] and by Seaton.[22] In Table XXVI are listed observed and calculated (Massey and Mohr) excitation cross sections at electron energies of 60, 100, and 200 eV.

The theoretical and observed cross sections of the 3^1S level show good agreement. The calculated cross sections for the ^1S states are subject to a higher degree of uncertainty than those of the other states, because the wave functions of the n^1S states were gotten by

TABLE XXVI

COMPARISON OF OBSERVED AND CALCULATED CROSS SECTIONS

Observed cross sections are corrected for polarization and cascading. All cross sections are expressed in units of $10^{-20}cm^2$.

	60 eV		100 eV		200 eV	
Level	Obs.	Calc.	Obs.	Calc.	Obs.	Calc.
3^1S	38	26	28	15	18.5	11
3^1P	260	340	320	270	290	190
4^1P	112	140	152	110	136	76
3^1D	31		21	4.4	11.1	2.5
4^1D	14.7	3.7	11.6	2.5	5.6	1.3
3^3S	21.5	1.3*	7.6	0.60*	4.1	0.13*
3^3P	42	5.5	13.3	1.1	4.1	0.15
3^3D	9.0	0.13	3.5	0.03	2.6	0.004

* The 3^3S calculated values are extrapolated from 2^3S calculations.

orthogonalization of the Slater-like orbitals. A small change of the effective nuclear charge, for instance, may result in a significant variation of the cross sections. Thus, Massey and Mohr gave 15×10^{-20} cm^2 for the 3^1S cross section at 100 eV, while the same cross section, according to the work of Fox, is 46×10^{-20} cm^2. The value at 100 eV is obtained by assuming the cross section to be inversely proportional to the energy of the colliding electron over this small range of energy. In the light of this, the experimental cross section may be considered to lie within the limits of the theoretical calculations. Figure 33 shows the comparison of the theoretical and experimental excitation functions of 3^1S.

Figure 34 shows the comparison between the theoretical and experimental excitation functions of 3^1P and 4^1P. The discrepancy of voltage below 100 eV is to be expected since the theoretical values were calculated by the use of the Born approximation. Analyses by Altshuler[23] and by Miller and Platzman[24] indicate that the use of approximate helium wave functions may lead to an error in the cross section as large as a factor of two or so. Thus the overall agreement between the observed and calculated excitation cross sections for 3^1P and 4^1P should be considered satisfactory.

The evaluation of the absolute cross sections from the experimental data for the ^1D states is somewhat complicated by the fact that the amount of cascading from the ^1F to ^1D states is not known since no excitation measurements are available for the ^1F states. Approximations are then carried out as described in Chapter III. The absolute cross sections so evaluated for 3, 4, 5, and 6^1D states are

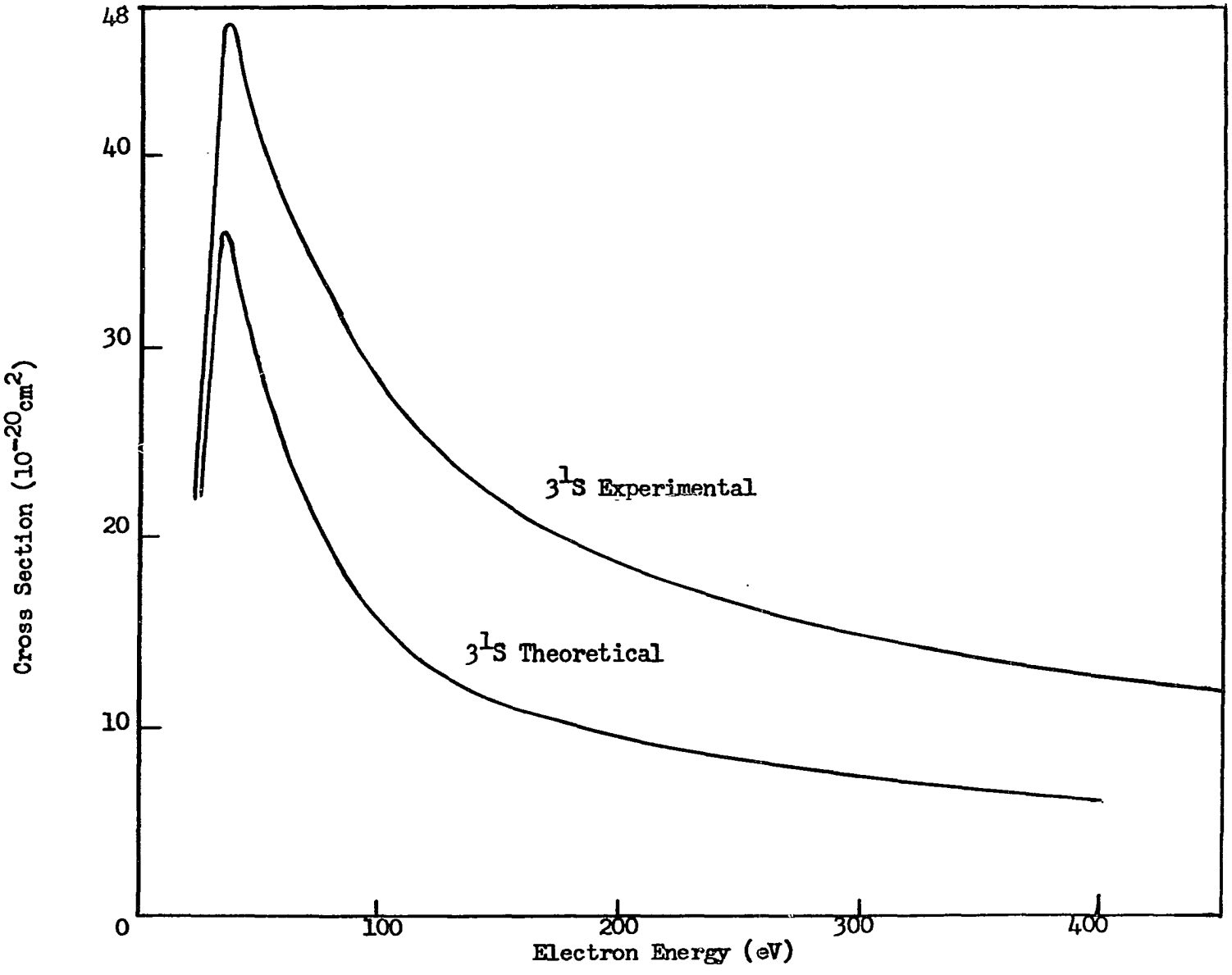


FIGURE 33.—EXPERIMENTAL AND THEORETICAL Q(3^1S) VS ELECTRON ENERGY

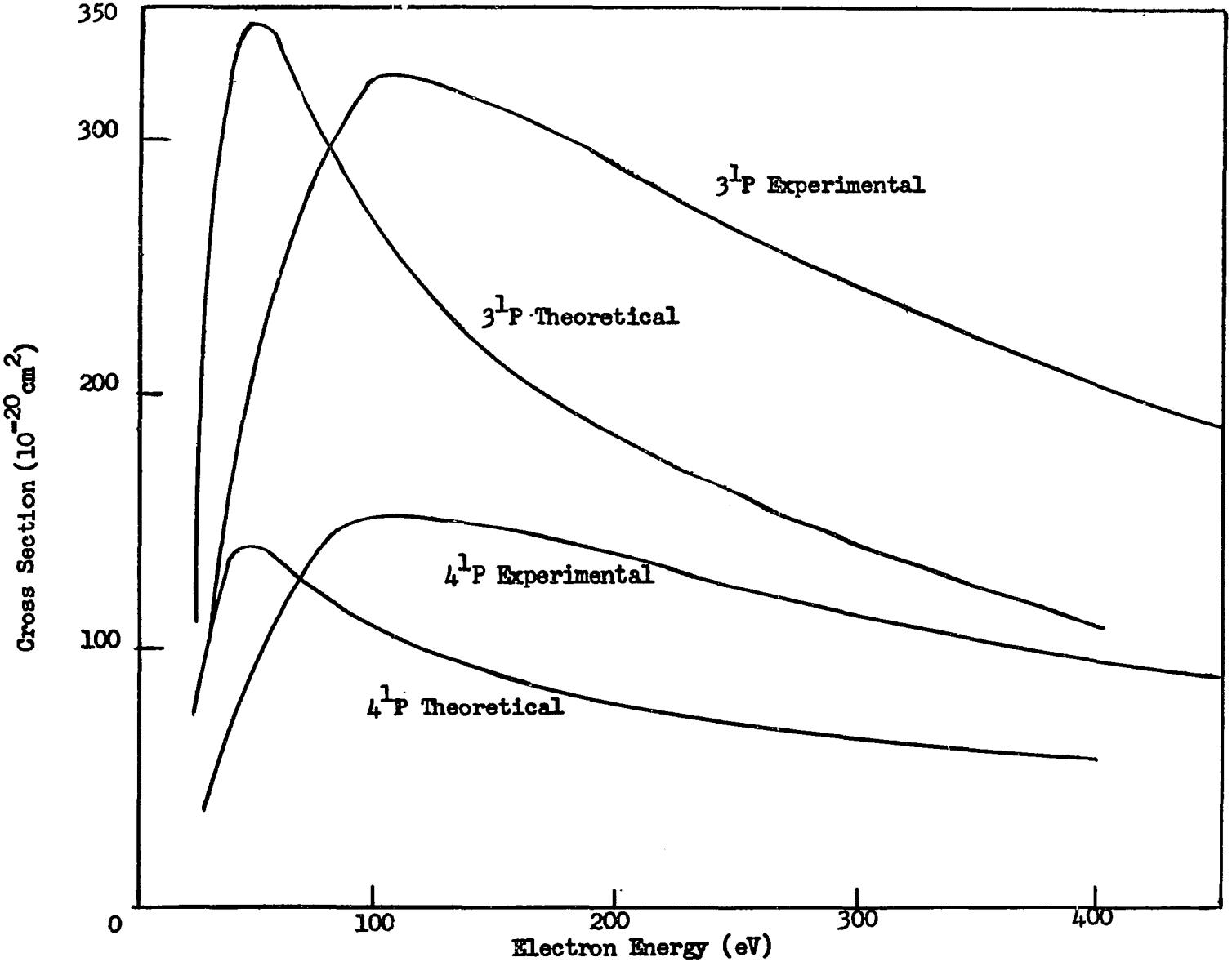


FIGURE 34.—EXPERIMENTAL AND THEORETICAL Q(3^1P) AND Q(4^1P) VS ELECTRON ENERGY

about four times larger than the theoretical values. At first, one might ascribe this discrepancy to the inaccuracy of our estimated populations of the F states. If we were to assume that F to ^1D cascading is entirely responsible for the deviation of the observed Q from the theoretical values, it would be necessary to increase the concentration of atoms in the F states. This in turn would require cross sections for electron excitation of the ^1F states to be 200 to 300 times as large as the theoretical values. The value of $Q(4^1F)$, for example, would have to be about 12×10^{-20} cm^2, a seemingly unreasonable value. Our experimental results for the excitation cross sections of the ^1D states therefore, could not be brought into complete agreement with theory in a consistent manner.

Calculation by Fox as quoted by Seaton[22] gives $Q(3^1D) = 7 \times 10^{-20}$ cm^2 at 108 eV as compared to 4×10^{-20} cm^2 as calculated by Massey and Mohr[16] at 100 eV. The difference between these two values can be taken as an indication of the degree of variation of the theoretical cross section (Born Approximation) which can be expected from the use of different approximate helium wave functions. Seaton has pointed out the calculations by a Born II approximation show that the coupling between 3^1D and 3^1P is not important for the cross section of the 3^1D state. It is very unlikely, then, that the imperfection of the theory could account for the disagreement between the observed and calculated cross sections for 3^1D and 4^1D. Nor is it conceivable that errors in the experimental procedure could have caused the observed values to show this mismatch with the calculated cross sections. The measured apparent cross sections are proportional to the output current of the photomultiplier tube; thus the

relative values of the apparent excitation cross sections should be quite accurate. Of course, the absolute experimental cross sections are subject to the errors of the light intensity calibration as well as the cascade corrections. The amount of cascading populations in the ^1P and ^1D are quite small, i. e., less than 14% of the total populations. Errors in the calibration of the photomultiplier output should affect all the cross sections by a constant factor. This leads to the conclusion that one cannot have simultaneous agreement between theory and experiment for the 3^1P, 4^1P, 3^1D, and 4^1D states.

For the 3^3P and 3^3D states the calculated cross sections are consistently smaller than the observed values. In fact, the discrepancy is too large to be ascribed to the errors in the theory or experiment or a combination of both. In the case of the ^3D states one is again faced with the problem of having to estimate the F to ^3D cascading. If we again assume that the population of the F states is due to direct excitation, calculations show that the contributions of F to ^3D cascading to the population of the n^3D states are less than 1%, i. e., completely negligible.

Finally for the ^3S series, direct comparison between theory and experiment is more difficult since theoretical cross sections are available only for 2^3S while our experimental results cover 3^3S, 4^3S, and 5^3S. In order to make any comparison it is necessary to extrapolate the experimental data with the assumptions that (i) the shape of excitation functions for all the n^3S states is identical, and (ii) the peak values of these functions follow the relation $n^{-\alpha}$ or $(n^*)^{-3}$ as was assumed by Phelps and Frost[19] and by Gabriel and Heddle.[1]

Here, n* is the effective quantum number such that the energy of the state is equal to a negative constant divided by $(n^*)^2$. The extrapolation procedure yielded experimental values of $Q(2^3S)$ equal to 180, 69, and 39 x 10^{-20} cm^2 at 60, 100, and 200 eV respectively for the $n^{-\alpha}$ relations, where $\alpha = 4.0$. Values of 140, 51, and 30 x 10^{-20} cm^2 were obtained for the $(n^*)^{-3}$ relationship where $n^* = n - .30$. These are to be compared with the theoretical values of 5, 2.4, and .5 x 10^{-20} cm^2 calculated by the Born-Oppenheimer approximation. Massey and Moiseiwitsch[21] have shown that when the distortion of the plane wave is taken into consideration, the calculated cross sections become much smaller at low voltages. Thus it is seen that the experimental cross sections for the ^3S series are about 30 times the theoretical values. A comparison of the mismatch of theory and experiment of the ^3S family with that of the ^3P and ^3D can best be made at the n = 3 level. Since no theoretical cross sections are available for the 3^3S state they were extrapolated from n = 2 to n = 3 by use of the $(n^*)^{-3}$ relationship. These figures are to be found in Table XXVI. They are used only to provide an estimate of the theoretical values and to draw conclusions of a qualitative nature.

An examination of Table XXVI reveals that the fraction of the observed cross section accounted for by theory is much smaller for the 3^3D state than for the 3^3S and 3^3P states. However, a more important consideration would seem to be that of the magnitude of the unaccounted for cross sections, i. e., Q(obs.) - Q(theory). This value is of the same order of magnitude at a given electron energy for the three triplet states under comparison. Thus, the mechanism

producing the excessive population in the triplet states does not preferentially populate any one state more than the others.

CHAPTER VIII

CONCLUSIONS

The electron excitation cross sections for 18 excited states of helium have been determined by measuring the intensities of the radiation originated from these excited states at low pressure. Corrections have been made to allow for the cascading and polarization effects. The agreement between the observed and theoretical cross sections for the 3^1P, 4^1P, and 3^1S states is satisfactory. The experimental cross sections for 3^1D and 4^1D are about four times larger than the theoretical values. For the ^3S, ^3P, and ^3D states the experimental results far exceed (by a factor of ten or more) the calculated cross sections.

The discrepancy in the cross sections of the triplet series with the calculated values is far too large to be explained by experimental uncertainty. Nor can one reasonably expect the Born-Oppenheimer approximation to produce cross sections which are ten to a hundred times too small at electron energies above 60 or 100 eV. This is particularly true in view of the fact that the ^1P and ^1S cross sections calculated by the Born approximation do agree with the experimental values. Furthermore, calculations by Massey and Moiseiwitsch[21] show that the excitation cross sections obtained from the Born-Oppenheimer approximation and from the EPW method approach each other at electron energies above 50 eV. One does not expect the use of more refined methods of calculation will change the theoretical cross sections (above 50 eV) significantly. In the case of 3^1D and

4^1D, although the disagreement between theory and experiment is less severe, it is very unlikely that the cumulative errors of the theoretical calculation and the experimental work, including the associated analysis of the excitation data, could account for the deviation of a factor of four.

The explanation which seems most plausible is that the observed population of the triplet states (and possibly, to some extent, of the ^1D states) is produced mainly by processes other than direct excitation. Results of the measurements of the life-time of the triplet states by Holtzberlein and Fowler[25] also point toward the same conclusion. Of course, the mechanism or mechanisms with which the triplet states are populated must have the correct linear behavior with respect to pressure and electron beam current.

Changes in the magnitude of the excitation cross section for n^1P states as pressure increases can be accounted for by imprisonment of resonance radiation. Changes in the shape and magnitude of the ^1D and ^3D excitation functions are sucessfully accounted for by transfer of excitation according to the St. John, Fowler theory.[3] The secondary peaks appearing in the n^1S, n^3S, and n^3P excitation functions at high pressure seem to be explained by departures from the monoenergetic character of the electron beam at these pressures.

LIST OF REFERENCES

1. A. H. Gabriel and D. W. O. Heddle, Proc. Roy. Soc. A258, 124 (1960)

2. R. M. St. John, C. J. Bronco, and R. G. Fowler, J. Opt. Soc. Am. 50, 28 (1960)

3. R. M. St. John and R. G. Fowler, Phys. Rev. 122, 1813 (1961)

4. C. C. Lin and R. M. St. John, Phys. Rev. 128, 1749 (1962)

5. C. C. Lin and R. G. Fowler, Ann. Phys. (New York) 15, 461 (1961)

6. J. H. Lees, Proc. Roy. Soc. (London) A137, 173 (1932)

7. O. Thieme, Z. Physik 78, 412 (1932)

8. V. E. Yakhontova, Vestnik Leningrad Univ., Ser. Fiz. i Khim. 14, 27 (1959) (Translation 951 by Atomic Energy Research Establishment, Harwell, Berkshire, England

9. R. H. McFarland and E. A. Soltysik, Phys. Rev. 127, 2090 (1962); 128, 1758 (1962)

10. D. W. O. Heddle and C. B. Lucas, Proc. Roy. Soc. (London) A271, 129 (1963)

11. D. T. Stewart and E. Gabathuler, Proc. Phys. Soc. (London) 74, 472 (1959)

12. R. M. St. John, C. C. Lin, R. L. Stanton, H. D. West, J. P. Sweeney, and E. A. Rinehart, Rev. Sci. Instr. 33, 1089 (1962)

13. R. D. Larrabee, J. Opt. Soc. Am. 49, 619 (1959)

14. F. K. Richtmeyer and E. H. Kennard, Introduction to Modern Physics, 4th ed., (McGraw-Hill Book Co., New York, 1947), Chapt. V

15. I. C. Percival and M. J. Seaton, Phil. Trans. Roy. Soc. (London) A251, 113 (1958)

16. H. S. W. Massey and C. B. O. Mohr, Proc. Roy. Soc. (London) A227, 38 (1954); A258, 147 (1960)

17. J. H. Lees and H. W. B. Skinner, Proc. Roy. Soc. (London) A137, 186 (1932)

18. E. Wigner, Nachr. Ges. Wiss. Gottingen, p.375 (1927)

19. L. S. Frost and A. V. Phelps, Westinghouse (Pittsburgh) Research Report 6-94439-6-R3 (1957)

20. D. R. Bates, A. Fundaminsky, J. W. Leach, H. S. W. Massey, Phil. Trans. Roy. Soc. (London) A243, 93 (1950)

21. H. S. W. Massey and B. L. Moiseiwitsch, Proc. Roy. Soc. (London) A227, 38 (1954); A258, 147 (1960)

22. M. J. Seaton, "The Theory of Excitation and Ionization by Electron Impact", Atomic and Molecular Processes, edited by D. R. Bates (Academic Press, New York, 1962)

23. S. Altshuler, Phys. Rev. 87, 992 (1952); 89, 1093 (1953)

24. W. F. Miller and R. L. Platzman, Proc. Phys. Soc. (London) A70, 229 (1957)

25. T. M. Holtzberlein and R. G. Fowler, Paper B-1, 16th Annual Gaseous Electronics Conference (Pittsburgh, October 1963)